293A

PROCEEDINGS OF

ICE SCOUR AND ARCTIC MARINE PIPELINES

WORKSHOP

13th INTERNATIONAL SYMPOSIUM ON OKHOTSK SEA & SEA ICE

Mombetsu, Hokkaido, Japan.

February 1-4, 1998

PROCEEDINGS OF
ICE SCOUR AND ARCTIC MARINE PIPELINES WORKSHOP

held at

13th INTERNATIONAL SYMPOSIUM ON OKHOTSK SEA & SEA ICE
Mombetsu, Hokkaido, Japan. February 1-4, 1998

Sponsored by:
Minerals Management Service, US Dept. of Interior
Geological Survey of Canada
BP Exploration Inc.
and Exxon Neftegas

Organised by:

C-CORE, Memorial University
St. John's, Newfoundland, Canada, A1B 3X5
Phone: +1 709 737 8354 Fax: +1 709 737 4706

Sakhalin Oil & Gas Institute
18 Karl Marx St., Sakhalin, Okha, 694460 Russia
Phone: 011 872 140 4220 Fax: 011 872 140 4204

and Okhotsk Sea and Cold Ocean Research Association
Okhotsk Sea Ice Science Research Co.
25-2, Motomombetsu, Mombetsu 094 Japan
Phone: +81-1582-3-1100 Fax:: +81-1582-3-1514 /

Proceedings published by C-CORE, November 1998

Preface

C-CORE and the Sakhalin Oil & Gas Institute (SOGI) jointly organized this workshop, with the assistance of OSCORA, to review ice scour effects relevant to the safe design and operation of marine pipelines offshore Canada, Alaska and the Russian Federation, including Sakhalin Island and Baydaratskaya Bay.

The general aims of the workshop were to exchange information through the review of progress in understanding the mechanics of ice keel scour, the ability to model the scouring process and the application of models to the issue of pipeline burial and protection.

The workshop was held jointly with the 13th International Symposium on Okhotsk & Sea Ice (organized by The Okhotsk Sea & Cold Ocean Research Association (OSCORA) and International Association for the Physical Sciences of the Ocean (IAPSO)) in Mombetsu Hokkaido, Japan from 1 to 5 February 1998.

The workshop attendance was open to all symposium attendees and involved up to 50 participants. Invited presentations were given by representatives from oil & gas industries, regulatory authorities, research institutes and consultants from both the Russian Federation, NATO and Asian countries.

The workshop was directed by Professor Andrew Palmer of Cambridge University, Dr Jack Clark of C-CORE and Dr. S.M Bogdanchikov of JSC Rosneft-SMNG. C-CORE, SOGI and OSCORA had committees to organize the workshop. The C-CORE committee was chaired by Dr. Jack Clark, and included Ms. Whittick and Drs. Phillips and Woodworth-Lynas. The SOGI committee was chaired by Dr. S.M Bogdanchikov (General Director of JSC Rosneft-SMNG) and included Dr. Astafiev and other representatives of SOGI and SMNG. The OSCORA-Scour committee was chaired by Dr. Hiroshi Saeki and Dr. Hiromitsu Kitagawa (Hokkaido University).

The workshop was sponsored by:
Minerals Management Service, US Dept. of Interior
Geological Survey of Canada
BP Exploration Inc.
and Exxon Neftegas

To receive further information on the Ice Scour and Arctic Marine Pipelines Workshop, please contact:

Dr. Ryan Phillips
C-CORE, Memorial University
St. John's, Newfoundland, Canada, A1B 3X5
Phone: +1 709 737 8354 Fax: +1 709 737 4706
E-mail: ryanp@morgan.ucs.mun.ca

TABLE OF CONTENTS

ICE SCOUR & ARCTIC MARINE PIPELINE WORKSHOP
13th INTERNATIONAL SYMPOSIUM ON OKHOTSK SEA & SEA ICE
Mombetsu, Japan. February 1-4, 1998

WORKSHOP SCHEDULE

Monday 2 February, 15:00 Chairs: Andrew Palmer & Dr Saeki

Opening Comments by A Palmer

Clark, J., Phillips, R and Paulin MJ.
Ice scour research for safe design of pipelines: 1978-1998

Palmer, A.
Alternative paths for determination of minimum burial depth to safeguard pipelines

Tuesday 3 February, 9.00 Chairs: Ryan Phillips & Dr Kitagawa

Smith. C.E., Hinnah, D.W. and Walker, J.
Offshore pipeline integrity: the key to pollution free operations

Croasdale, K.R.
Review of strength of first-year ice features and driving forces relating to ice scour

Woodworth-Lynas, C.M.T.
Sub-scour soil deformations and the development of ideas from field work in the last decade.

Beketsky, S
Method of ice ridge age definition

Tuesday 3 February, 13.00 Chairs: Mike Paulin & Dr Hirayama

Beketsky, S
Sakhalin ice gouge measurements through stamuka drilling

Blasco, S.M., Shearer, J.M. and Myers, R.
Seabed scouring by sea ice: scouring process and impact rates: Canadian Beaufort shelf

Stepanov, I.V., Timofeyev, O.Y., Klepikov, A.V. and Malek V.N.
An approach to optimisation of the burial depth of underwater pipelines on Arctic offshore

Kioka, S, Terai, Y., Otsuka, N., Honda, H. and Saeki H.
Mechanical model of ice gouging on sloping sandy beach

Wednesday 4 February 1997, 9.00 Chairs: Chris Woodworth-Lynas & Dr Saeki

Stepanov, IV
Statistical analysis of the shape characteristics of hummocks in Baydaratskaya Bay

Foriero, A
Steady state ice scouring of the seabed

Discussion: Leaders Andrew Palmer & Ryan Phillips

Poster presentations only:

Beloshapkov, A., Marchenko, A. and Dlugach, A.
Seabed exaration by ice formations

Grass, J.
Ice scours and ice ridges of Lake Erie, Ontario, Canada.

ICE SCOUR & ARCTIC MARINE PIPELINE WORKSHOP

13th INTERNATIONAL SYMPOSIUM ON OKHOTSK SEA & SEA ICE
Mombetsu, Japan. February 1-4, 1998

REGISTERED PARTICIPANTS LIST

Masaaki Aota
Hokkaido University
Sea Ice Research Laboratory, 6-4-10
Minamigaoka
Mombetsu Hokkaido 094
Japan
Tel: +81 1582 3 3722
Fax: +81 1582 3 5319
Email aota@pop.lowtem.hokudai.ac.jp

S P Beketsky
Sakhalinmorneftegaz-Exxon
820 Gessner #529
Houston Texas
USA 77024
Tel: 713 935 6018
Fax: 713 935 6057
Email

Jacques Benoit,
AGRA Earth & Environmental Japan
6-1,3-Chome
Kitakyuhoji-Machi, Chuo-ku
Osaka 541-0057 Japan
Tel: +81-6-244-3600
Fax: +81-6-244-3605
Email jbenoit@agraee.com

Steve Blasco
GSC Atlantic
Bedford Institute of Oceanography
Dartmouth Nova Scotia
Canada B2Y 4A2
Tel: 902 426 3932
Fax: 902 426 4104
Email blasco@agc.bio.ns.ca

Edward C Clukey
Exxon Production Research Co.
P.O. Box 2189
Houston Texas
USA
Tel: 713 965 7316/7251
Fax: 713 966 6423
Email Ed.C.Clukey@exxon.sprint.com

Amy Faranski,
Exxon Production Research Co.
P.O. Box 2189
Houston Texas
USA
Tel: 713 965 4436
Fax: 713 966 6423
Email Amy.S.Faranski@exxon.sprint.com

Adolfo Foriero
Universite Laval
Pavillon Adrien Pouliot
Ste. Foy Quebec
Canada
Tel: 418 656 2089 /2163
Fax: 418 656 2928
Email adolfo.foriero@gci.ulaval.ca

Richard Goff
BP Exploration Inc
c/o Intec Engineering,
15600 JFK Blvd.
Houston Texas
USA 77032
Tel: 281 987 0800
Fax: 281 590 5955
Email goffrd@bp.com

Soshi Hamaoka
Okhotsk Sea & Cold Ocean Research Association
25-2 Motomombetsu,
Mombetsu Hokkaido 094
Japan
Tel: +81 1582 3 1100
Fax: +81 1582 3 1514
Email hamaoka@ohotuku26.or.jp

Dennis W Hinnah
Minerals Management Service
Department of Interior,
949 East 36th Ave, Suite 308
Anchorage Alaska
USA 99508-4363
Tel: 907 271 6065
Fax: 907 271 6504
Email

Ken-ichi Hirayama
Graduate School of Engineering
Iwate University
4-chome 3-5 Ueda, Morioka 020
Japan
Tel 019-621-6447,
Fax 019-621-6460
E-mail hirayama@msv.iwate-u.ac.jp

Hiromitsu Kitagawa
Graduate School of Engineering
Hokkaido University
N13 W8 Kita-ku, Sapporo 060 Japan
Tel 011-706-7246,
Fax 011-706 -7249
E-mail kit@eng.hokudai.ac.jp

Andrew Palmer
Cambridge University Engineering Department
Trumpington Street, Cambridge
UK CB2 1PZ
Tel: +44 1223 332718
Fax: +44 1223 332662
Email acp24@eng.cam.ac.uk

Mike Paulin
C-CORE
Memorial University
St. John's Newfoundland
Canada A1B 3X5
Tel: 709 737 8352
Fax: 709 737 4706
Email mpaulin@engr.mun.ca

Ryan Phillips
C-CORE
Memorial University
St. John's Newfoundland
Canada A1B 3X5
Tel: 709 737 8371
Fax: 709 737 4706
Email ryanp@morgan.ucs.mun.ca

Dan Rice
Joint Pipeline Coordinators Office
Department of Natural Resources
Anchorage Alaska
USA
Tel: 907 272 0690
Fax: 907 271 2646
Email drice@pipeline.state.ak.us

Hiroshi Saeki
Graduate School of Engineering
Hokkaido University
N13 W8 Kita-ku, Sapporo 060 Japan
Tel 011-706-6183,
Fax 011-706 -7249
E-mail

Kunio Shirasawa
Hokkaido University
Sea Ice Research Laboratory, 6-4-10 Minamigaoka
Mombetsu Hokkaido 094, Japan
Tel: +81 1582 3 3722
Fax: +81 1582 3 5319
Email kunio@pop.lowtem.hokudai.ac.jp

Charles E Smith
Minerals Management Service
Technology Assessment Branch, DOI,
381 Elden Street, Mail Stop 4700
Herndon Virginia
USA 22070-4817
Tel: 703 787 1561/1559
Fax: 703 787 1555
Email smith@smtp.mms.gov

Igor V Stepanov
Arctic & Antarctic Research Institute
State Research Centre of Russian
Federation, 38 Bering Street
St Petersburg, Russia 199397
Tel: +7 812 352 1003
Fax: +7 812 352 2688 / 1557
Email aaricoop@aari.nw.ru

Greg Swank,
State Pipeline Coordinator's Office
411 West 4th Avenue
Anchorage, Alaska 99501-2343
Tel: (907) 271-4412
Fax: (907) 272-0690
Email: gswank@pipeline.state.ak.us

Peggy Tsang,
Counsellor (Science & Technology)
Canadian Embassy
7-3-38 Akasaka, Minato-ku
Tokyo, Japan, 107-8503
Tel: +81 3 5412 6200 xtn, 3325
Fax: +81 3 5412 6254
Email: peggy.tsang@toyo05.x400.gc.ca

Albert Wang
Exxon Neftegas
Exxon Production Research Co., P.O.
Box 2189
Houston Texas
USA 77252-2189
Tel: 713 965 7335
Fax: 713 966 6194
Email Albert.T.Wang@exxon.sprint.com

John Watson
Exxon Neftegas
Exxon Production Research Co.,
P.O. Box 2189, Houston Texas
USA 77252-2189
Tel: 713 965 7335
Fax: 713 966 6194
Email

Chris Woodworth-Lynas
Petra International
Cupids
Newfoundland
Canada A0A 2B0
Tel: 709 528 4856
Fax: 709 528 3056
Email petra@nf.sympatico.ca

Ice Scour Research for the Safe Design of Pipelines: 1978-1998

Jack I. Clark, Ryan Phillips, and Mike Paulin
C-CORE, Memorial University of Newfoundland, St John's, NF, Canada

INTRODUCTION

Ice scouring of the seabed is a widespread feature of most of the coastal regions of northern continents. It is a phenomenon which occurs when ice (pressure ridge or iceberg) moves while in contact with the seabed. The scour may take the form of a long linear furrow following a relatively straight line or it may be erratic in its path, covering only a few tens of metres or many tens of kilometres. In open waters, such as the east coast of Canada as far south as the southern tip of the Grand Banks, (and sometimes beyond) and in the northern Norwegian Sea, ice scour is normally associated with glacial ice in the form of icebergs. In northern oceans, such as the Beaufort Sea and the Barents Sea, most of the ice scours are caused by deep keels formed by pressure ridges that impact the seabed. Ice scours are also caused by multi-year ice, ice islands or icebergs in these regions.

Ice scour is of economic significance due to the likelihood of disruption of seabed structures. Phenomenological studies of iceberg scouring by C-CORE have provided the framework for more quantitative analyses wherein the stress and displacement fields below scouring icebergs have been investigated. These studies include excavation of relic ice scours in western Canada where well-preserved iceberg scour features from glacial Lake Agassiz have been found. These studies have provided confirmation of subscour deformations associated with scouring, and have indicated a failure mechanism. In addition, observations have been made of ice scour tracks for relatively small "icebergs" across the St. Lawrence tidal flats near Montmagny, Quebec and in the Bay of Fundy. The observations have led to the experimental modelling of iceberg processes in the laboratory and the centrifuge in order to determine the stress and displacement fields below a scouring iceberg. The data from laboratory centrifuge testing is being used to validate and calibrate numerical models as well as to provide site specific design parameters. All of the work is focused to the development an engineering model that will include an adaptation of an existing pipeline/soil interaction model.

The purpose of this paper is to introduce the research that has been undertaken by C-CORE to determine the forces and soil displacements that can be expected under a seabed that is being scoured by various ice and seabed interaction processes.

1978 - 1990

Research on iceberg scours at C-CORE started in 1978. Gustajtis (1979) presents a comprehensive review of what was known at that time and a number of observations on speculative aspects of the ice scour process. At the same time, the Atlantic Geoscience Centre (AGC) and a number of oil companies were carrying out research on ice scours off the east coast of Canada. Clark *et al.* (1990) and Clark *et al.* (1994) present an overview of the development of the C-CORE research program through the following phases from 1978 to the early 1990s:

1. The collection of phenomenological data
2. Analyses of side scan sonar mosaics
3. Direct observations of scours from manned submersibles
4. Initiation of studies of relict scours in the Canadian Arctic and Lake Agassiz, Manitoba
5. Direct observation of small-scale iceberg scour events by the St. Lawrence River
6. Laboratory modelling of the scour process

The early work included offshore mapping and statistical analysis of iceberg scour marks along the Atlantic Canadian continental shelf. This work culminated in a large, industry-sponsored field project, the Dynamics of Iceberg Grounding and Scouring (DIGS) experiment, jointly managed by C-CORE, Geonautics Ltd. and the Bedford Institute of Oceanography. DIGS is described in the accompanying paper by Woodworth-Lynas (1998). The first compelling evidence of large sub - scour soil movement was obtained from onshore field studies of relict iceberg scours exposed on the former seabed of glacial Lake Agassiz in southeastern Manitoba, (Woodworth-Lynas,1998). Sub - scour displacements as large as 3.5 m were deduced from measured offsets of remnant bedding in the strong overconsolidated clay. Other evidence of sub-scour deformations in the geologic record are presented in that paper.

Field programs investigated soil deformation beneath modern small scale scours formed by pan ice during spring breakup on the tidal flats of the St. Lawrence estuary near Montmagny, Quebec and at Cobequid Bay, Nova Scotia, Poorooshasb and Clark (1990). The scour features studied were typically 0.5 to 1.0 m in width, and ranged in depth from about 0.15 to 0.2 m. At Cobequid Bay, cohesive sediment layers were deflected vertically downward under the scours down to a depth approximately 0.5 m beneath the trough of a typical feature.

Laboratory studies using the scour tank facilities at the Memorial University of Newfoundland included model test series conducted in very soft silt and sand respectively, Clark *et al.* (1990) and Clark *et al.* (1994). The first set of tests in silt were performed at two different scour cut depths of 40 and 70 mm.. Below the shallower scour, soil displacements were recorded to a maximum depth of about 200 mm.. Whereas apparent remoulding of the soil occurred to a depth equal to twice the scour depth below the deeper feature. The sand tests were conducted at specified relative densities between 0 and 50 percent. Two different scour cut depths, 40 and 75 mm, were investigated. Soil displacements were measured to depths below the initial surface as great as 3.5 times the depth of scouring, and the horizontal component of displacement was dominant. A change in the attack angle of the model iceberg from 30 to 15 degrees also produced a noticeable increase in the amount of disturbance beneath the scour.

PRESSURE RIDGE ICE SCOUR EXPERIMENT: PRISE

PRISE is a continuing interdisciplinary, internationally-funded program of interrelated, focused studies directed towards the protection of offshore oil and gas pipelines from the effects of sea ice and iceberg seabed scour. The ultimate goal of PRISE is to *develop the capability to design pipelines and other seabed installations in regions scoured by ice, taking into account the soil deformations and stress changes which may be caused during a scour event.* The need for this

capability was identified during a round-table discussion with several oil companies and the federal government in 1990 during an international workshop on ice scour held in Calgary, Clark (1990).

PRISE has involved a wide range of sponsors and participants, as listed below in the acknowledgements. The results of this program are mainly proprietary to the sponsors. A summary of reports from the PRISE program are listed below and identified numerically as superscripts in the following text. A series of reports from the Norwegian Geotechnical Institute on pipeline considerations for relic scours were also made available to PRISE through a reciprocal agreement with the Norwegian Research Council. These NGI reports are listed below. Papers and theses describing certain aspects of the PRISE program are also shown. PRISE is divided into five phases:

Phase 1: PRISE Planning and Extreme Gouge Dating Project Feasibility Study

Planning for PRISE was completed in early 1992[1-2], and resulted in definition of an executive plan for the 5 phases of the project[3].

The Extreme Gouge Dating Project (EGDP) dealt with the probability of occurrence of deeply-penetrating ice scour events. The objective of EGDP was to verify a radiometric technique that could be used to determine the absolute age of seabed sediments filling very deep scour mark troughs. By determining the age of extreme features, the return period can be calculated. With this knowledge, risk of future extreme scour events can be estimated. The EGDP feasibility study[5] was completed in spring 1992.

Phase 2: Extreme Gouge Dating Project

A field program was mounted in the Alaskan Beaufort Sea in summer 1992 to support the objectives of EGDP. The objectives were to make detailed seafloor maps of deep scour marks and collect cores for radiometric dating. This work[6] was only partially successful because of severe ice problems and the availability of very limited time on the survey vessel. Further work on verifying the radiometric technique was put on hold by the funding participants in favour of progressing with Phase 3.

Phase 3: Centrifuge and Numerical Modelling, Pipeline Design Guidelines

A preliminary series of 9 initial centrifuge model tests of ice scour in soft clay was carried out on the Cambridge University geotechnical centrifuge in 1992, Lach (1996). Data from these tests provided the first indications of sub-scour soil and pipeline movements and provided invaluable guidance in designing subsequent test series. Preliminary development of finite element models of ice/soil interaction was carried out at the same time, (Yang *et al.*, 1996). Both of these pieces of work were funded by a grant from the Natural Sciences and Engineering Research Council (NSERC) Canada and were completed in November 1993.

Phase 3a began at C-CORE in December 1993 and was completed in March 1995. It involved the analysis of results from a comprehensive suite of 10 centrifuge model tests of ice scour[7]. This work modelled the scour process in soils that approximate natural seabed situations where pipelines are planned, such as in offshore Sakhalin Island, Russia. The objectives were achieved: (1) to model 20 scour events in clay, sand and layered clay/sand soils, (2) to describe and quantify the general cases for each soil type and to highlight the similarities and differences in the responses of the

different soils to the same ice keel loads, and (3) to verify physical model results against field data from modern and relic scour marks. The effects of five parameters were assessed[8], including soil type, soil condition, attack angle, scour depth and scour width.

Woodworth-Lynas *et al.* (1995) present the preliminary findings of the investigation of soil structures that form as the result of ice keel scour-induced soil deformation produced by these centrifuge models of ice keel scour. From the models four classes of structures were identified (lateral berm piles; sand boils; sub-scour shear failure mechanisms; low angle thrusts) and compared with similar structures of large-scale, naturally-occurring scour marks. The remarkable correlations between modelled and observed structures indicated that the models replicated accurately the scouring process, and strengthened confidence in the interpretation of soil behaviour phenomena, such as vertical and horizontal loads and pore pressure changes, that cannot be observed in the field.

Phase 3b began in the fall of 1994 and was completed in late 1995[9]. It involved the adaptation of a soil/pipe interaction engineering model, through finite element analyses and interpretation of the Phase 3a centrifuge model tests. This portion of Phase 3 consisted of 6 tasks: (1) evaluation of an xisting finite element (FE) ice scour model, (2) verification of the FE model by comparing results with physical and centrifuge model results and to existing field data, (3) determination of scour-induced soil deformations, (4) adaptation of the existing engineering model for soil/pipe interaction analysis to the ice scour problem, (5) calibration and validation of the engineering model against physical and centrifuge model data, (6) recommendations for soil measurements during a full-scale scour event (Phase 4). Woodworth-Lynas *et al.* (1996) and Nixon *et al.* (1996) describe the resulting model.

Phase 3c was completed in April 1997[12]. It involved the centrifuge modelling[10] of 9 more extreme ice scour events in stiffer clays, stiff silts and medium dense sands with penetration depths of 3-5 m. Some of these tests were focussed towards specific pipeline projects at Northstar, offshore Alaska and Sakhalin Island, offshore Russia. The Phase 3b finite element analyses were also reviewed[11] by experts who recommended strategies for improving future analyses.

Phase 3d[15] confirmed the magnitude and extent of lateral sub-scour deformations expected under ice scours in dilatant materials through 4 tasks: 1) direct field observations[13], 2) physical model simulations[14], 3) numerical model simulations[15] and 4) development of an indigenous knowledge workshop[15]. Task 3 also included the implementation of some of finite element analysis strategies recommended during the Phase 3c review.

Current and Possible Future Activities

C-CORE organised the Ice Scour and Arctic Marine Pipeline Workshop to which this paper was presented. This workshop was held at the time of the 13th International Symposium on the Okhotsk Sea and Sea Ice workshop in January 1998 in Mombetsu, Hokkaido, Japan. This workshop reviewed progress in the technical understanding of ice scour and identified tasks for further consideration and action. The workshop attendance was balanced with about 50 representatives from regulatory authorities, industry, consultants and research organisations.

The results of the PRISE program are now finding application in specific site studies for individual PRISE members. C-CORE is now developing a complementary JFP to develop a framework for risk assessment of ice damage to seabed facilities. This JFP will incorporate the results of the PRISE program with considerations of environmental loads and ice keel information. This JFP will be used to identify key areas for further research.

In the future, the engineering model should be validated against the results of observations and measurements from a real, full-scale ice scour event. The field-verified model, including pipeline design guidelines, can then be introduced to industry and government as a design tool that will enable the safe engineering of offshore pipelines in areas subject to seasonal ice scour. This validation may involve PRISE phases 4 and 5, which have not yet been undertaken.

Phase 4: Full-Scale Ice Scour Event

No data have ever been collected on ice/soil interaction forces and movements during a full-scale ice scour event. These data are crucial for verification and calibration of the proposed engineering model. Conceptualization by C-CORE of a field program for monitoring a full-scale event was completed in 1992.

Phase 5: Burial and Monitoring of Experimental Pipeline

Experimental pipelines in on-land permafrost areas where production lines are planned have been installed and monitored at several sites to provide data for the final design. It is anticipated that similar installations of instrumented pipelines in regions affected by ice scour could provide useful information. The PRISE team is continually identifying opportunities to monitor an actual pipeline located in an area subject to frequent ice scour.

ACKNOWLEDGMENTS

C-CORE gratefully acknowledges the participation and sponsorship of PRISE by the following organisations:

ARCO Alaska Inc.
BP Alaska
Chevron
Exxon Production Research Company
Gulf Canada Resources
Minerals Management Service
Mobil Research and Development Corporation
Mobil Oil Canada Properties
National Energy Board (Canada)
Norwegian Research Council
Petro-Canada
Union Texas Petroleum
Natural Sciences & Engineering Research Council, Canada

C-CORE also gratefully acknowledges the participation in PRISE of these other organisations

Andrew Palmer and Associates Ltd.
Concordia University
Environmental Science and Engineering, Inc.
Golder Associates,
Norwegian Geotechnical Institute
University of Birmingham
Atlantic Geoscience Centre,
US Geological Survey
Nixon Geotech Ltd.
Woodward-Clyde Consultants
University of Laval

PRISE REPORT SUMMARY

1. PRISE - The Pressure Ridge Ice Scour Experiment: A Joint Industry Program.
2. Workshop Proceedings, June 13-14, 1991 (St. John's).
3. Phase I - Planning, Final Report February 1992.
4. Ice Scour Bibliography, compiled February 18, 1992.
5. Extreme Gouge Dating Project - Feasibility Study - Phase I (ESE/C-CORE), April, 1992.
6. Phase II Progress Report, March 1993.
7. Phase 3a: Centrifuge Modelling of Ice Keel Scour, Data Reports, 10#
8. Phase 3a: Centrifuge Modelling of Ice Keel Scour, Final Report. April 1995.
9. Phase 3b: Engineering Model Application, Final Report. August 1995.
10. Phase 3c: Extreme Ice Scour Event - Modelling and Interpretation, Centrifuge Test Reports, 9#
11. Phase 3c: Extreme Ice Scour Event - Modelling and Interpretation, Review & Development of Finite Element Modelling. 97-C20.
12. Phase 3c: Extreme Ice Scour Event - Modelling and Interpretation, Final Report. 97-C34.
13. Phase 3d: Safety and Integrity of Arctic Marine Pipelines – Results of Field Study, 97-C30.
14. Phase 3d: Safety and Integrity of Arctic Marine Pipelines – Centrifuge Test Reports, 2#
15. Phase 3d: Safety and Integrity of Arctic Marine Pipelines – Final Report, 98-C15.

NORWEGIAN GEOTECHNICAL INSTITUTE REPORTS

1. Quality Plan 524234 - PRISE, November 1, 1992.
2. Estimating impact pressure of submarine slides on pipelines (Report 524234-1).
3. Relic scour study (Report 524234-2).
4. Site investigation and laboratory testing techniques for offshore pipelines (Report 524234-3).
5. Free span problems related to offshore pipelines (Report 524234-4).
6. Freely-suspended pipeline spans and construction techniques (Report 524234-5).

REFERENCES

Canadian Seabed Research (1992) Scour Infill Study for EGDP Site Selection in the Canadian Beaufort Sea. Report to Geological Survey of Canada.

Clark J.I. (1990) Workshop on ice scouring and design of offshore pipelines, Calgary, AB, April 1990. Sponsored by Canada Oil and Gas Lands Administration & C-CORE.

Clark J.I., M.J Paulin and F. Poorooshasb (1990) Pipeline Stability in an Ice-scoured seabed. 1st European Offshore Mechanics Symposium (EUROMs 90) Trondheim Norway.

Clark J.I., M.J. Paulin, P.R Lach, Q.S. Yang and H. Poorooshasb (1994) Development of a design methodology for pipelines in ice scoured seabeds. OMAE '94. Proc. . International Conference on Offshore Mechanics and Arctic Engineering, 13th, Houston, TX, 1994. Vol. 5 pp.107-125.

Gustajtis K.A (1979) Iceberg scouring on the Labrador shelf, Saglek Bank. C-CORE Report 79-13.

Hodgson G.J, J.H. Lever, Woodworth-Lynas C.M.T and C.FM. Lewis (editors) 1988. The Dynamics of Iceberg Grounding and Reperitive Mapping of the Eastern Canadian Continental Shelf. Environmental Studies Research Funds Report No 094, Ottawa, ON, 318p.

Lach, P.R. (1996). Centrifuge Modelling of Ice Scour. Ph.D thesis. Faculty of Engineering & Applied Science, Memorial University of Newfoundland

Lach, P.R., J.I. Clark and F. Poorooshasb (1993) Centrifuge Modelling of Ice Scour.. Proc. Fourth

Canadian Marine Geotechnical Conference, St. John's, NF, June 27-30, Vol 1: 357-374.

Nixon, D.F., A. Palmer and R. Phillips (1996) Simulations for buried pipeline deformations beneath ice scour. 15th International Conference on Offshore Mechanics and Arctic Engineering, Florence, Italy, June 16-20.

Poorooshasb F. and J.I .Clark (1990) On small scale ice scour modelling, In Clark (1990), p193-236.

Woodworth-Lynas C.M.T. (1998) Sub-scour deformations and the development of ideas from field work in the last decade. Proceedings of Ice Scour and Arctic Marine Pipeline Workshop, 13th Okhotsk Sea & Sea Ice Symposium, Hokkaido, Japan, February 1998.

Woodworth-Lynas C.M.T, R. Phillips, J.I Clark, F. Hynes and X. Xiao (1995) Verification of Centrifuge Model Results Against Field Data: Results from the Pressure Ridge Ice Scour Experiment (PRISE). Second International Conference on Development of the Russian Arctic Offshore, St. Petersburg, Russia, September 18-22. (Reprint in this volume).

Woodworth-Lynas C.M.T., D.F. Nixon, R. Phillips and A. Palmer (1996) Subgouge deformations and the security of Arctic marine pipelines. Offshore Technology Conference, Houston, Texas, May 1996.

Yang, Q.S., H.B. Poorooshasb, and P.R. Lach (1996) Centrifuge modelling and numerical simulation of ice scour. Soils and Foundations, Vol. 36, No 1, pp. 85-96.

Yang, Q.S., H.B. Poorooshasb, P.R. Lach and J.I. Clark (1994) Comparisons of physical and numerical models of ice scour. Proceedings of Eighth International Conference on Computer Methods and Advances in Geomechanics, (Siriwardane and Zaman, eds.): Morgantown, West Virginia, May 22-28 1994, Vol. II: 1795-1801.

Alternative Paths For Determination Of Minimum Burial Depth To Safeguard Pipelines Against Ice Gouging

Andrew Palmer
University Engineering Department, Cambridge, England

ABSTRACT

The designer of a marine pipeline in a shallow sea in the Arctic has to define a trenching depth that will reduce to a very small level the risk of ice gouging damage that will lead to a leak. The logical path to that decision requires the assembly of various kinds of data, all of them with some degree of uncertainty, and complemented by analytical models. The significance of subgouge deformation has now been recognised.

The paper explores different decision paths. The traditional path starts from gouge depth observations, and continues to extreme gouge statistics, which has to be supplemented by some model of subgouge deformation and pipeline response. The paper argues for a more direct path, which starts from subgouge deformation, and considers how that might be accomplished.

INTRODUCTION

Ice gouges are a sign and warning of a potential hazard to subsea systems such as pipelines and wellheads. The engineering objective of ice gouge studies is to enable the design engineer to make rational decisions about protection.

Protection is based on trenching to a secure depth, because it is usually impracticable to make the system can be made strong enough to resist the forces that a ice might apply. A straightforward calculation [1] indicates that the ice force required to cut one of the large gouges frequently seen in the Beaufort Sea is more than 10 MN. That is an order of magnitude larger than the forces sometimes accidentally applied to marine pipelines by ships' anchors, and those forces almost invariably cause severe damage which take the pipeline beyond a limit state in which operation cannot be continue.

The gouges themselves are in a sense irrelevant to the pipeline engineer except as an indicator of the presence of grounded ice and an important clue about how deeply it cuts. The engineer has to focus on the damage that the ice might cause to a pipeline, rather than on the visible gouge. Indeed, it might be possible to arrive at a rational decision about a safe trenching depth without actually having complete information about an extreme gouge depth. This is obvious, but occasionally forgotten in concentration on the gouges themselves.

The old paradigm supposed that a pipeline is not safe if the ice can contact it, but safe if it is buried deeply enough for the ice to cross over it without touching. If that were correct, the design task would be to establish the maximum depth to which an ice mass might cut a gouge, possibly with some statistical element and some degree of acceptance of risk, and then to bury the pipeline below the extreme gouge depth. This parallels the concept of the 100-year design wave, widely applied in offshore structural engineering, under which a structure is designed to resist a hypothetical wave, which estimated to occur once in 100 years and is supposed to represent an acceptable exceedance risk.

It is now seen that this paradigm is deficient. Subgouge deformations extend some way below a gouging mass. At least in some instances substantial deformations extend to more than twice the gouge depth [2]. This may not be true in all soils, and much research remains to be done on the influence of soil type and density. Subgouge deformations have been observed in 1-g model tests (starting with the work of Poorooshasb [3]), in centrifuge tests [2], and in field investigations of relic gouges [4].

A pipeline trenched below the maximum gouge depth is therefore not necessarily safe. Opinion has shifted significantly: whereas at the time of the 1989 Calgary symposium the consensus view was that subgouge deformations had only secondary importance, most engineers concerned with this problem now recognise that subgouge deformations are central to decisions about trench depth.

Ultimately, the pipeline engineer has to make a decision about a design trench depth. He uses statistical inputs and probabilistic arguments to guide him towards that decision, but he cannot give the trenching contractor a statistical distribution. He has to give the contractor a hard number, though he will of course have to take account of trenching tolerances.

The purpose of this paper is to explore different routes towards the decision.

DECISIONS BASED ON OBSERVATIONS OF GOUGE DEPTH

The traditional approach is founded on measurements of gouge depths. A survey observes gouge depth and breadth statistics along the intended pipeline route. The analyst fits a probability distribution to the observed statistics, decides on an acceptable exceedance probability, and determines the extreme gouge depth that corresponds to that probability.

This is a rational procedure as far as it goes, but it is based on the old paradigm that neglects subgouge deformation. It is now agreed that subgouge deformation cannot be neglected, and the model has to be extended by a model of subgouge deformation. The model might be very simple (eg. "subgouge deformations capable of damaging a pipeline extend not further than twice the gouge depth"), or it might be much more sophisticated, both in terms of geotechnical response and in terms of pipeline structural mechanics.

A complication is the effect of infill, which distorts the interpretation of gouge statistics. At any moment, the observed geometry of a gouged seabed is a snapshot of a family of gouges, some new, some partly modified by wave-induced sediment transport or by later gouging, some about to be erased, and some already invisible. In shallow water, seabed sediment transport is an extremely effective erasure mechanism [5]. Large waves are much more effective than small waves: sediment transport rate is roughly proportional to (wave height)$^{3/2}$ [6]. Most gouge measurements are made in the open-water season of late summer, and often storms between breakup and measurement will have modified much of the evidence of gouging in the previous ice season.

It is accepted that gouges in shallow water (5 m) are less deep than in intermediate depths (20 m), and that this is because large ice masses capable of cutting deep gouges are not formed in shallow water, and that they cannot drift in from deeper water because they ground and come to a stop. There seems no reason to disbelieve this. However, the effect may be exaggerated, because in shallow water even modest sea states cause so much sediment transport that gouges are erased. A significant wave height H_s of 1.8 m with a 5.3 s period is generated by a 30 knot (force 7) wind blowing over a 20 nm (37 km) fetch for 3.5 hours or more, from the Sverdrup-Munk-Bretschneider model (see, for example, Komar [7]). Meteorological data for the Beaufort Sea suggest that such storms are not infrequent. In 5 m of water these waves mobilise any seabed soil finer than coarse gravel (D 20 mm), and in 10 m the same waves mobilise any soil finer than very fine gravel (D 3 mm): this calculation is based on the Sleath model [8].

There are obviously more sophisticated models of wave generation, sediment transport and infilll rate, but these simple ideas are robust enough to lead to a clear conclusion. An observer should not expect to see extensive gouging in shallow water, even though gouging does actually occur, unless he makes measurements between the formation of the gouge and the first storm in the open-water season.

Assembling the different factors that influence observed gouge depths, and adding the components of a model that relates observed gouge depth to subguge disturbance, suggests the decision model schematised in a flow diagram in Figure 1 below.

A variant of this approach is to centre the analysis on ice keel depth statistics [9], which can be assembled from measurements by upward-looking sonar on the seabed, or from submarines, or from correlations with sail height statistics measured by radar. In this context, unfortunately, the use of keel statistics introduces a further complication, because the bottom of a grounded keel of an ice mass does not gouge at the same depth as it would if the ice were floating freely. That is because the vertical reaction between the bottom and the ice is of the same order of magnitude as the horizontal gouging force: this is predicted theoretically [1], and has been confirmed in centrifuge models [2]. A simple calculation shows that the vertical reaction is large enough to lift the ice significantly. It will also tilt the ice, just as grounding destabilises and tilts a stranded ship [10]. Accordingly, a decision tree based on keel statistics adds another level of uncertainty.

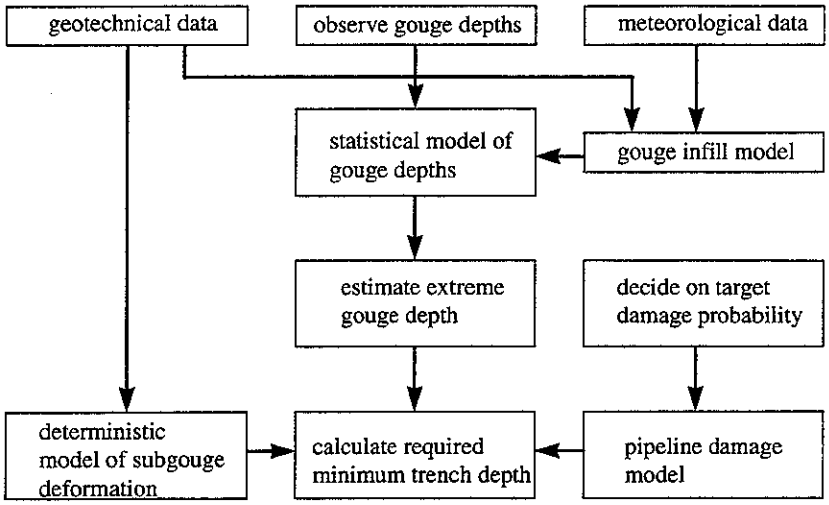

Figure 1 Decision tree based on observations of gouge depth

DECISIONS BASED ON OBSERVATIONS OF SUBGOUGE DEFORMATION

An alternative approach is more direct. The pipeline engineer is never interested in the observed gouge depth for its own sake, but only as an indirect - and potentially misleading - clue to the subgouge deformation beneath. It is the depth that the soil is repeatedly remoulded to that is important. If technology can be developed to detect that depth reliably, gouges themselves become irrelevant.

At least three possibilities are known. The first concept is based on the fact that remoulding alters the mechanical state of a seabed soil. This idea is developed in more detail in a separate paper (Palmer [11]). If the soil has been formed by natural sedimentation, and thereafter has remained undisturbed, each level has been loaded in one-dimensional 'normal' consolidation (in the rather artificial terminology of soil mechanics). If soil that was initially normally consolidated later comes to be repeatedly remoulded, as a result of climate change and/or change of sealevel, then the soil reaches the critical state [12], at which repeated remoulding no longer tends to induce a change of pore pressure or a change of voids ratio. A soil in the critical state responds to loading in a different way to the same soil in the normally consolidated state. In particular, the changes of pore pressure are quite different: whereas the normally-consolidated soil responds to shear deformation by a marked increase in pore pressure, the soil in the critical state does not change its pore pressure.

This suggests that it ought to be possible to detect the maximum gouging depth that corresponds to contemporary ice climate by direct geotechnical measurements, through the coincidence between the maximum gouging depth and a break in mechanical properties between remoulded and unremoulded normally-consolidated soil. A standard site investigation technique is the cone penetrometer test(CPT), which drives a standardised cone-shaped metal point into the soil (see, for example, Meigh [13]). A CPT measures the cone resistance (the force on the cone itself), the sleeve resistance (the force on a cylindrical section just behind the cone), and the pore pressure induced on the cone. Semi-empirical correlations can be used to relate the soil type and condition to the cone resistance and the ratio between sleeve force and cone force. A break at the maximum gouging depth ought then to be marked by an increase in pore pressure and an increase in cone resistance. It should be possible to distinguish it from a discontinuity in the type of soil, by correlation with sub-bottom profiling or borehole logs. A useful feature of this option is that good geotechnical data are needed in any event, because they are essential to sound decisions about trenching.

A second idea is to detect chemical differences between gouged and ungouged soil. Nuclear weapons testing from the 1940s to the 1960s created a wide distribution of long-lived radioactive isotopes, and extraordinarily sensitive methods are available to detect and measure them. The isotopes will have contaminated the surface layer of the seabed, and will then have been mixed into bed by repeated gouging. It may then be possible to detect the maximum gouge depth by a discontinuity in radiochemical measurements on cores.

The related idea of radiochemical dating of individual gouges was tried as part of the PRISE gouge research project [14]. It was unsuccessful, but largely for practical reasons associated with the very limited ship time available. It seems to be worth revisiting.

There are other unexplored and more tentative possibilities. Biological activity is a worthwhile indicator that distinguishes between sediments that are mobilised by storms and those that are deep enough to be stable over a long period, but it is not known to have been explored in the Arctic. Chemical solution and redeposition processes create links between carbonate sand particles in the sub-tropics, and form a very sharp indicator of seabed mobility [6], but in cold seas are probably too slow to have observable effects.

If subgouge deformation could be observed in the field, it would open a much more direct path to a decision. This is illustrated in Figure 2.

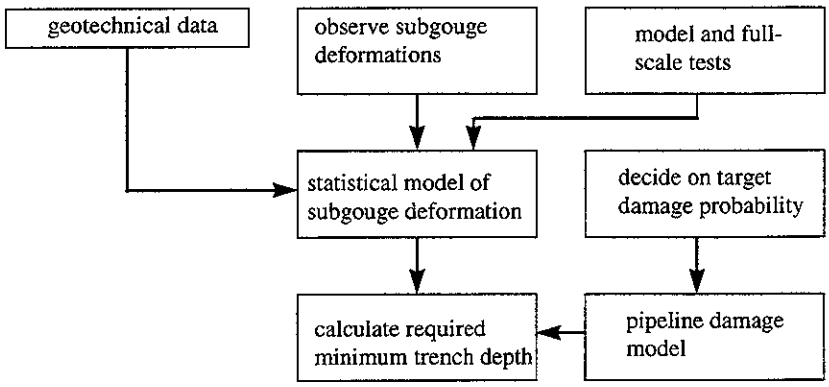

Figure 2 Decision tree based on observations of subgouge deformation

The advantages would clearly be very great. In particular, all the uncertainties associated with infill would be eliminated, so the method would be more reliable in shallow water.

RELATION TO PIPELINE DAMAGE MODEL

The objective is to avoid unacceptable damage to a pipeline. It is helpful to adopt a limit state philosophy, and to concentrate on conditions that might threaten continued operation or security. Thinking of a hierarchy of damage levels in response to a gouging incident, the following can be distinguished:

Level 1 the pipeline is deformed elastically;
Level 2 the pipeline yields, and begins to deform plastically;
Level 3 the pipeline wall wrinkles or becomes severely ovalised;
Level 4 the pipeline leaks;
Level 5 the pipeline is torn apart.

Level 1 is of no consequence, though it might lead to a technical violation of the requirements of some older codes (which limit allowable stress to a defined fraction of yield stress). Level 2 not in itself a limit state, and much research has been carried out to demonstrate that. Modern codes allow yield, provided that the pipe material and the welds have adequate ductility, provided that the strain is not excessive [15,16], and provided that yield does not trigger harmful secondary effects.

Level 3 creates a slight restriction to flow, and may make it impracticable to run some kinds of pigs through the pipeline, so that it may be a serviceability limit state. It may also create a condition in which low-cycle fatigue later shifts the state to level 4. The operator is concerned about level 3 from the point of view of operation, but the wider community is not.

Level 4, on the other hand, is obviously damaging to the environment and of much proper concern to regulators and the public at large, and it would have harmful knock-on consequences to the industry. The pipeline engineer has to find a way through the uncertainties so that the design has an extremely low possibility of leading to level 4. Some of that uncertainty relates to the pipeline itself. Broadly, however, pipeline structural mechanics is better understood than the soil mechanics of gouging, and the variability of pipeline response is coming to be much better understood as a result of research on reliability-based codes [17]. The pipeline itself therefore contributes relatively little to the overall burden of uncertainty.

CONCLUSION

The pipeline engineer has to make a definite decision on trenching depth, and to found that decision on a mass of statistical evidence. Much of that evidence is somewhat uncertain. If the decision path is unduly complex, there is a risk that the multiplication of uncertainties will lead to a final number that has unacceptably wide confidence limits. The paper suggests that one way to avoid that outcome is to look for more direct paths, and to move attention away from gouges themselves and towards the possibility of direct detection of extreme gouge depths from the geotechnical record.

ACKNOWLEDGEMENT

This work is supported by the Jafar Foundation. The author thanks Richard Goff, Mike Jefferies, Derick Nixon, Ryan Phillips and Chris Woodworth-Lynas for helpful discussions.

REFERENCES

1 Palmer, A.C., Konuk, I, Comfort, G. and Been, K. Ice gouging and the safety of marine pipelines. Proceedings, Twenty-second Offshore Technology Conference, Houston, 3, 235-244, OTC6371 (1990).

2 Woodworth-Lynas, C.M.L., Nixon, J.D., Phillips, R. and Palmer, A.C. Subgouge deformation and the safety of Arctic marine pipelines. Proceedings, Twenty-eighth Annual Offshore Technology Conference, Houston, 3, 235-244, paper OTC6371 (1996).

3 Poorooshasb, F., Clark J.I. and Woodworth-Lynas, C.M.Y. Small-scale modelling of iceberg scouring of the seabed. Proceedings, Tenth International Conference on Port and Ocean Engineering under Arctic Conditions, Lulea, 1, 133-145 (1989).

4 Woodworth-Lynas, C.M.L. and Guigné, J.Y. Iceberg scours in the geological record: examples from glacial Lake Agassiz. Glaciomarine environments: processes and sediments. Geological Society, Special Publications 53, 217-233 (1990).

5 Niedoroda, A.W. and Palmer, A.C. Subsea trench infill, Proceedings, Eighteenth Annual Offshore Technology Conference, Houston, OTC 5340, 4, 445-452 (1986).

6 Palmer, A.C. A flaw in the conventional approach to stability design of pipelines. Proceedings, Offshore Pipeline Technology Conference, Amsterdam (1996).

7 Komar, P.D. Beach processes and sedimentation. Prentice-Hall (1976).

8 Sleath, J.F.A. Sea Bed Mechanics. Wiley Interscience (1984).

9 Wadhams, P. The prediction of extreme keel depths from sea ice profiles. Cold Regions Science and Technology, 6, 257-266 (1983).

10 Rawson, K.J. and Tupper, E.C. Basic ship theory. Longmans (1976).

11 Palmer, A.C. Geotechnical evidence of ice scour as a guide to pipeline burial depth. Canadian Geotechnical Journal, 34, 1002-1003 (1998).

12 Schofield, A.N. and Wroth, C.P. Critical state soil mechanics. McGraw-Hill (1968).

13 Meigh, A.C. Cone penetration testing. Construction Industry Research and Information association, Butterworths (1987).

14 Niedoroda, A.W., Wong, G.T.F. and Woodworth-Lynas, C.M.T. Extreme goige dating project, feasibility study - Phase 1. ESE/C-CORE report, ESE project no. 3925010-0100-3120. (1992).

15 Klewer, F.J., Palmer, A.C. and Kyriakides, S. Limit state design of high-temperature pipelines. Proceedings, Offshore Mechanics and Arctic Engineering Conference, Houston (1994).

16 Rules for submarine pipeline systems. Det norske Veritas, Høvik (1996).

17 Mørk, K.J., Kollberg, L., and Bjørnsen, T. Limit state design in DnV'96 rules for submarine pipeline systems: background and project experience. Proceedings, Thirty-first Annual Offshore Technology Conference, Houston, 4, 333-340 (1998).

Offshore Pipeline Integrity: The Key to Pollution-Free Operations

by

Charles E. Smith[1], Dennis W. Hinnah[2] and Jeffery Walker[3]

ABSTRACT

The Arctic poses many engineering challenges to the development of offshore oil and gas operations, especially relative to the design, installation and operations of offshore pipelines. In addition to the usual engineering considerations such as operating procedures, corrosion control, and inspection that are necessary to ensure the integrity of offshore pipelines in general, Arctic offshore pipelines face additional constraints due to the ice cover, ice features interacting with the sea floor, and the presence of permafrost. A large body of information exist relative to the design, installation operation, damage assessment and repair of offshore pipelines in general. However, due to the lack of major offshore Arctic oil and gas developments, far less effort has been put forth for offshore Arctic pipelines. This paper will review some of the major regulatory concerns relative to these issues for Arctic pipelines, the applicability of current integrity assessment and repair techniques, and results of major research initiatives undertaken to address these concerns.

INTRODUCTION

Development of commercial oil and gas discoveries will require subsea pipelines from the production facility to shore. Arctic offshore pipelines are technically feasible, but due to many engineering and environmental constraints, their cost could control the economical feasibility of the project. It is felt that the necessary state-of-the-art equipment is currently available for the safe and reliable installation of Arctic offshore pipelines. There are more than 600 miles of onshore pipelines on the U.S. North Slope, which demonstrates the capability to design, construct, and operate pipelines under Arctic conditions.

The factors that will affect the commercial viability of Arctic offshore pipelines include ice scouring (gouging), permafrost, seasonal ice cover, strudel scour, and other oceanographic and environmental considerations (i.e. currents, soil transport, etc). It has been said that "timing" may be the key to a successful installation. For example, delays in construction due to bowhead whale migration and changes in ice conditions may extend a project many years beyond its original deadline. The following will review the regulatory responsibilities as well as the technical considerations involved in the installation and operation of an Arctic offshore pipeline.

1. Research Program Manager, Technology Assessment and Research Program, Engineering and Research Branch, Minerals Management Service, 381 Elden Street, Herndon, Virginia 20170-4817
2. Petroleum Engineer, Field Operations, Minerals Management Services, Alaska OCS Region, 946 E. 36th Avenue, Anchorage, Alaska 99508-4302
3. Supervisor for Field Operations, Minerals Management Service, Alaska OCS Region, 946 E. 36th Avenue, Anchorage, Alaska 99508-4302

Regulatory Authorities

The U.S. Department of the Interior, Minerals Management Service (MMS); U.S. Department of Transportation, Office of Pipeline Safety (OPS); and the State of Alaska, Department of Natural Resources-Joint Pipeline Office (JPO) have regulatory authorities for offshore pipelines in the U.S. Arctic. The MMS and the OPS administer Federal pipeline responsibilities through a 1996 Memorandum of Understanding, which delineates each agency's jurisdiction. Generally, the MMS is responsible for pipelines upstream of the sales/transfer point (i.e., trunk lines connecting production facilities); the OPS regulates transportation pipelines from production facilities to shore. The State JPO issues rights-of-way for pipelines across State submerged lands. The MMS also issues rights-of-way or rights-of-use and easements for pipelines that cross the Federal Outer Continental Shelf (OCS).

The regulatory regimes of these three entities generally are the same and address the various aspect of quality assurance related to pipeline integrity including design, construction, installation, maintenance, repair, inspection, operation, spill prevention and safety, as well as environmental protection. Pressure testing of pipelines is required following installation to ensure integrity. Shutdown valves are required at both ends of the pipeline to ensure that the pipeline can be isolated in the event of damage or a leak. Pressure sensors that activate automatic shutdown valves are required to ensure that in the event of a detectable leak, the pipeline is automatically shut in to prevent continued flow. Inspection and monitoring of the pipeline (visual and smart pigs) are required to identify internal and external damage (corrosion, erosion, etc.) to the pipeline or changes in the pipeline configuration (settlement) that may indicated potential problems. Quality assurance programs are used to maintain and repair the pipeline to design criteria. These agencies also have approval, inspection, and oversight responsibilities for pipeline construction and operation and enforcement authorities to shut down the pipeline in the event of noncompliance or potential problems with safe operation of the pipeline.

Design Considerations for Offshore Arctic Pipelines

There are many unique considerations for subsea Arctic pipelines. Permafrost, strudel scour, and ice gouging (including sub-gouge soil deformation) usually are considered the more significant forces acting on the subsea portion of the pipeline and will be the focus of this review. The effects of ice on a support structure for the pipeline shore approach or on the offshore production facility in which the pipeline riser would be housed are also important consideration; depending on the location and water depth of the structure, ice loads will vary based on the type of ice conditions existing (land fast, pack ice, shear zone). The capability to design structures in the Arctic to resist ice forces has been demonstrated by the Endicott production facility and the numerous exploratory drilling structures that have been successfully used in the U.S. and the Canadian Beaufort Sea. Other major design considerations, such as external and internal corrosion, coastal erosion, and seismicity are not unique to the Beaufort; technology has been demonstrated for pipelines in other offshore areas to address these types of concerns and is not reviewed in this paper.

Permafrost and strudel scour are unique factors that must be accommodated in the design of an offshore pipeline in the U.S. Arctic and pose a different potential for pipeline failure compared to ice gouging. Unlike ice gouging, permafrost and strudel scour do not generally impose significant loads directly on the pipeline. Long-term heat loss can thaw permafrost, resulting in differential settlement (Fig. 1) while strudel scour can erode sediment from under the pipeline, resulting in long spans of pipeline being unsupported (Fig. 2). In both cases, neither the cause nor resulting failure would be instantaneous compared to damage or rupture caused by ice gouging, however, the potential exists for possible long term damage. In many cases, the pipeline route would be selected to avoid these types of conditions. In the event the pipeline route did cross these types of conditions, designing pipelines to prevent or accommodate differential settlement from permafrost thaw, or to accommodate unsupported spans, is within current engineering capability. In addition, monitoring, and inspection practices also would be able to detect changes in a pipeline configuration and allow for remedial action in advance of potential failure.

Onshore permafrost is well preserved, continuous, and extends from near the surface to considerable depth. Subsea permafrost, on the other hand, is discontinuous and the depth to the surface of the permafrost is variable, generally becoming deeper with water depth. Subsea permafrost is a more significant problem for the shore approach (where the permafrost is closer to the surface) than the offshore segment of the pipeline. The degree of differential settlement depends in part on the extent and nature of permafrost. The nature and the extent of "ice" in the soil also is critical; significant differential settlement is a concern only if the soils are thaw-unable. If widespread, the pipeline may settle uniformly, which is not a major problem. Site-specific surveys along a proposed pipeline route can determine the permafrost character of the subsoil and the potential for significant subsidence and differential settlement.

The principles of heat loss and permafrost thaw are well understood and have been applied in designing onshore pipelines. These same principles also have been well demonstrated in designing exploration and long-term development and production wells that involve flowing higher temperature fluids through casing set through permafrost. Depending on the thickness of the permafrost near the shore approach, the pipeline can be buried below the thaw unstable layer of permafrost into a competent thaw-stable layer. Insulation of the pipeline, refrigeration, and/or cooling the oil are the primary methods to protect against a significant differential settlement due to permafrost thaw. Pile-supported pipelines, backfilling a trench with thaw-stable materials, and higher strength pipe that can accommodate greater bending stresses are also options.

Strudel scour results by over-ice flooding from the spring river runoff. The hydraulic head and velocity of the water cause the water to flow through cracks in the sea ice, which can produce linear and circular strudel scours or depressions in the sea floor and can leave extended lengths of pipeline unsupported should they be buried in the location of the scour. In the Beaufort Sea, the areas affected by strudel sour have only been observed near the mouths of major rivers. Typical strudel depths are on the order of 3 to 20 feet with diameters of 30 to 40 ft and are found within 3 to 4 miles of the coast. In a majority of cases, the pipeline route can be located to avoid strudel scour. Where strudel scour may be present, designing pipelines to withstand unsupported lengths on the order of tens of

feet is within current technology. In such cases, there are also remedial and preventive actions that can be used to minimize the risk and effect of strudel scour on subsea pipelines. Dykes and slotting to redirect overflow away from the pipeline are potential forms of mitigation. Annual visual surveys following the breakup period can identify exposed pipeline, which can be reburied.

Ice gouging /scouring (Fig. 3 and 4), which can impose near instantaneous loading on a pipeline, is by far the most significant force to address in the offshore Arctic. Ice gouging can impose loads that are orders of magnitude greater than other loads impacting a pipeline. Unlike loads resulting from differential settlement (permafrost thaw) or unsupported spans resulting from strudel scour, which can be accommodated by the pipeline design, it may not be possible to design unprotected pipelines to resist the direct loads of significant ice gouging. In such cases, trenching/burial is the obvious mechanism to protect a subsea pipeline from ice gouging. Trench depth must be sufficient to avoid direct contact by the ice keel and the associated forces transferred through the soil (Fig. 5). Burial can provide additional protection but for extreme scour depths can be very costly. The type of ice (a multi year ice keel vs. a first-year rubble pile) and the type of soil (consolidated lays vs. unconsolidated sands) affect the depth and magnitude of forces that would act on a subsea pipeline. In the early 1980's, when there was considerable exploration ongoing in the U.S. and Canadian Beaufort Sea, significant research, both laboratory and fieldwork, was conducted on the effect of ice gouging on subsea pipelines; such loads can now be quantified for pipeline design with adequate site specific field data.

Ice gouging in the Beaufort Sea generally is concentrated along the stamukhi zone, generally between the 18 to 30 meter isobath. Inshore of the stamukhi zone (water depths less than 18 m), ice gouging is much less severe and has low frequency of occurrence and shallow gouge depths (generally less than 3ft). Offshore of the stamukhi zone, water depth increases and the number of ice keels large enough to reach the bottom decreases. In the U.S. Beaufort ice gouges generally are oriented east-west, consistent with the prevailing wind and surface current directions. The Beaufort Sea does not have large "ice islands," similar to the Grand Banks or other Arctic areas, and which can cause more significant gouging.

Where possible, an offshore pipeline would most likely come to shore by the most direct and shortest path. If a direct onshore landfall was not available or practicable near the offshore platform, the offshore segment would likely parallel the shoreline shoreward of the stamukhi zone. This avoids the area of highest ice-gouge intensity and depths as well as areas of potential strudel scour. The bottom founded and landfast-ice zones provide the maximum opportunity for installation and repair during the winter season. Trenching capabilities in these water depths currently are available.

In the event a pipeline, originating in deeper water, was planned to cross the stamukhi zone, the total length of pipeline within this zone would be limited (low exposure variable) and could still be trenched and buried at sufficient depth to avoid gouging forces. Similarly, that portion of the pipeline outside the stamukhi zone may be susceptible to deeper gouges from individual iceberg events; but the pipeline can still be trenched below predicted gouge depth. The combined probabilities of an ice gouge event exceeding the burial depth is very small.

Oil-Spill Response Considerations

A potential pipeline oil spill, should one occur, would be limited in volume. Spill volumes would be on the order of several hundreds of barrels as compared to the potential tens of thousands of barrels from a well blowout or the hundreds of thousands of barrels from a tanker spill. Potential spill volume is mainly controlled by three things: leak-detection capability, pipeline diameter, and length.

Generally, leak-detection systems can measure leaks less than 1 percent of the total flow volume. For leak rates at and above the threshold, response times for detecting the leak and shutting in the pipeline are on the order of minutes; resulting spill volumes would be on the order of a few tens of barrels. For leak rates that are less than the threshold, the leak could go undetected until visual inspection or a discrepancy in mass balance between production and sales was identified. Leak rates of several hundreds of barrels per day are expected to be detected from within a few hours to days. Pinhole leaks of a few barrels could continue for extended periods and could possibly not be discovered until breakup. In both cases, the volume of oil is on the order of magnitude of a few hundred barrels. Following shut in of the pipeline, the remaining capacity of the pipeline also is subject to leaking. However, not all the oil would "drain." Some oil will "drain" due to expansion of the oil due to pressure loss in the pipeline-on the order of a few tens of barrels. Additional oil would continue to "drain" until seawater intake eventually came into equilibrium with the oil. Undulation of the pipeline caused by natural variations in the seabed would cause high and low points, so that only the portion of the damage pipeline between the two highest points would "drain".

Oil-spill-cleanup technology under arctic conditions can be found elsewhere, however the same response strategies are applicable for a pipeline spill. Because the most likely routing of the pipeline will be in the landfast-ice zone (shoreward of the stamukhi zone), where ice conditions are stable for extended periods, oil spill cleanup capabilities will be enhanced. In this area, under-ice retention of oil (on the of 1,000 bbl per acre of ice), restricted movement (currents are insufficient to move the oil encapsulated by the rough ice bottom), encapsulation of oil into growing new ice, and the surfacing of oil during the early stages of breakup provide multiple and long-term opportunities to clean up a spill using mechanical response techniques. Such efforts can be labor intensive but effective and efficient, particularly given the small volumes of oil involved. In the event the spill occurred or was not detected until late in the spring and ice had deteriorated to a point that over-ice mechanical response was not possible, in situ burning would remain a viable option; oil that is encapsulated under the ice and surfaces later does not weather and still is susceptible to in situ burning. Again, given the limited spill volumes associated with a pipeline spill, a spill during the winter and early spring can be cleaned up before open water transport and spreading occurred.

Pipelines originating in deeper water beyond the stamukhi zone have potential for spills occurring in or beyond the shear zone where ice conditions could be more dynamic. Depending on the ice conditions, mechanical recovery could be limited. In situ burning could be used under some conditions (provided oil can be contained by natural or man made barriers such as fire proof boom, and the oil hasn't weathered or emulsified). If ice conditions were to dynamic to initiate a recovery

action or in situ burning, the oil could be tracked pending development of suitable ice conditions to initiate a response or until the oil disperses naturally.

Response planning must provide for logistics and transportation of equipment and personnel to the spill site. Response strategies will involve prestaging of equipment at the production platform, mobilization of offsite resources, and prestaged equipment along the pipeline route. Helicopter-deployable equipment has been an important component of response preparedness due to logistical constraints and will play a major role for open-water response planning, in particular for facilities that are located farther away from the shore. Response times for over-ice conditions are not as "vital" but also will involve a combination of over-ice vehicle (rollagon, hovercraft, trucks) and helicopter-supported response. In general, response times for the pipeline spills will continue to be on the order of a few hours.

Technology Assessment and Research (TA&R) Program

The MMS supports an active research program to understand the engineering constraints for offshore operations, especially as related to the structural integrity of structures and pipelines, the prevention of pollution, and the technologies necessary to clean up an oil spill should one occur. In essence, the program provide an independent assessment of the status of OCS technologies and, where deemed necessary, investigates technology gaps and provides leadership in reaching solutions.

The TA&R Program has funded a variety of projects and major international workshops to develop a better understanding of the engineering constraints for operating in the ice-infested Arctic:

- International Workshop on Sea Ice Mechanics are Arctic Modeling;
- Pressure Ridge Ice Scour Experiment;
- Management of Human Error in Operations of Offshore Facilities;
- Methodology for Risk-Based Optimization of Pipeline Integrity Maintenance Activities;
- Sea Ice Mechanics;
- Offshore Earthquake Monitoring and Analysis;
- Arctic Undersea Inspection of Pipeline and Structures;
- International Workshop on Damage to Underwater Pipelines;
- International Workshop on Offshore Pipeline Safety; and
- Rapid Leak Detection for Sea floor Pipelines.

Perhaps the most illuminating research effort ongoing since the late 1980's is the Pressure Ridge Ice Scour Experiment (PRISE). PRISE is a large government and joint-industry project that has been conducted through the Center for Cold Ocean Resources Engineering (C-CORE) Memorial University of Newfoundland, Canada. Major elements of this program included:

- The Extreme Gouge Dating Program to develop data on the ages and depths of extreme ice gouges to determine their frequency of occurrence and to plan offshore pipeline routes;

- Conduct centrifuge model tests to develop an engineering model to design Arctic marine pipelines to withstand soil deformations caused by ice scouring events;
- Conduct numerical modeling efforts using advanced finite element computer codes to characterize the stress and strain distributions under ice gouging conditions; and
- Initiate a field testing program to confirm the validity of the centrifuge and numerical modeling techniques.

Because of this work, site-specific field data on frequency and depth of ice gouging is being collected and will be used to quantify the likely effects of ice gouging loads to ensure adequate pipeline design. PRISE is currently developing design guidelines that industry may employ to construct Arctic pipelines. PRISE was designed to increase knowledge of the scouring process and specifically of subscour deformation processes. This integrated, multi disciplinary approach has progressed from the selection and development of theoretical and numerical models and the corroboration of these models with results of small-scale, high-gravity centrifuge model data as well as the validation of model results with full-scale observations. The result of the program will be an industry-accepted design tool (a field-verified finite-element model) complete with a set of specific design guidelines.

The International Workshop on Sea Ice Mechanics and Arctic Modeling was held in Anchorage, Alaska, on April 25-28, 1995, and focused on the current state of practice and future research needs relative to Arctic offshore oil and gas operations and presented results of the U.S. Navy's Office of Naval Research Sea Ice Mechanics Initiative (SIMI) Program. The workshop provided information on the measurement of sea-ice stress, ice motion, ice-thickness distribution, keel depths, ice and keel strength, ice-friction coefficients and fracture properties, meteorological parameters and currents obtained as part of the SIMI Program.

An ongoing study on the management of human and organizational error in operations of offshore facilities seeks to develop and verify engineering reliability analysis procedures to allow quantitative evaluation of alternatives from management of human and organizational errors in the operation of offshore facilities. Human error accounts for 80-90% of the failures of marine systems. Recent examples include the Piper Alpha platform explosion in the North Sea and the Exxon Valdez tanker grounding in Prince William Sound, Alaska. Traditional engineering approaches used in the design, construction and operation of marine systems have largely ignored this aspect. If the marine safety record is to be improved, then this aspect must be addressed by engineers. This is particularly true of existing marine systems, where there have been dramatically increased pressures for environmentally safe and economically sound operations. It is also very important in the development of new innovative marine systems (such as very deep-water platforms, Arctic and deepwater pipelines and floating structures), where experience does not exist to ensure proper management of potential human factors. This study will offer information on how to control human and organizational error sources.

The MMS is part of a joint industry program (JIP) through the Center for Engineering Research in Canada directed at optimizing pipeline integrity maintenance activities using a risk-based approach.

The goal of this JIP is to develop models and software tools for estimating risk levels associated with individual pipelines or individual segments within a pipeline system. The models and tools developed will allow risk reductions associated with various inspection and maintenance activities to be quantified, thus providing a basis for comparing alternatives. The overall framework will include an approach to evaluate potential risk-reduction benefits against associated costs, thus allowing optimal decisions to be made regarding the choice of an integrity maintenance strategy.

The potential economic benefits to pipeline operators of using a risk-based approach are significant. On one hand, any small reduction in failure rates resulting from better maintenance planning would reduce the potentially high cost of failure, this is especially true for Arctic Pipelines. On the other hand, if excessive conservatism in repair strategies can be identified and eliminated, costly premature maintenance activities may be avoided.

The MMS sponsored a major international workshop on pipeline safety in New Orleans in December of 1991. The overall purpose was to discuss current practice, progress, desirable future activities and key future directions in the field of offshore design and management, as well as safe practice in the offshore pipeline industry. It was also designed to bring together the various parties active in the field of offshore pipelines, to form a written record of the major issues at the present time, and to provide definition of areas for management and research focus, to include Arctic Pipelines.

The international steering committee identified eight special topics as being of particular importance, and which are still valued today:

- Design, analysis and installation issues for integrity of Arctic and shallow water pipeline;
- Evaluation of system integrity, limit state design issues and reliability assessment;
- Internal monitoring (pigging, coupons, nondestructive testing, etc.);
- External surveillance (drivers, remotely operated vehicles, acoustic location, etc.);
- Routine operation & maintenance issues (including corrosion control and leak detection);
- Abnormal operation, emergency and storm response;
- Repair & rehabilitation problems; and
- Deepwater considerations-design, inspection, repair and rehabilitation.

In February 1995, the MMS also sponsored the International Workshop on Damage to Underwater Pipelines. This workshop was held in order to provide a forum for collaboration among professionals working in this field, and to bring together the various activeparties active parties to provide definition of areas for management and research focus, and to form a written record of the major issues at that point in time. The overall purpose was to discuss current practice, share progress, identify desirable future activities and agree on key future directions in the offshore and underwater pipeline industry. It addressed such concerns as:

- Regulatory issues;
- Operating and other types of damage;
- Reliability design for new and existing pipelines;
- Repair considerations; and
- Response to abnormal situations.

Outstanding Technical Issues

Major advances have been made over the last few years relative to the design and installation of a Arctic offshore pipeline. However, a few outstanding technical issues still need to be resolved, especially for site-specific installations:

- Burial depth of a pipeline;
- Methods to determine and characterize subsea permafrost;
- Methods to determine and characterize subsea sediment type;
- Coastline processes as they effect landfall and type of shore line approach;
- Pipeline corrosion; and
- Effects of seismic activity on pipeline performance.

Burial depth of offshore pipelines is an issue of concern for the pipeline's protection. The concern is site-specific, i.e., the same depth is not necessary throughout the length of the pipeline. The site-specific depths are determined by:

- The length, depth, and frequency of ice gouges;
- The ice strength (presence of multi-year ice);
- The sea floor soil type,;
- Presence of permafrost; and
- Ice content of soil.

Cost-effective methods to detect subsea permafrost must be determined. Once the permafrost is located, reasons for its presence must be answered. Seabed mean temperature and salinity information is needed to explain the presence of permafrost along with the conditions of occurrence and the duration of seasonal seabed freeze-up. An explanation for its presence could help answer other unknowns such as its physical and chemical characteristics and potential for subsidence. Subsidence is the biggest concern to pipeline burial in subsea permafrost. How and when the permafrost will thaw and subside (due to the flow of warn fluids through the pipeline) are unanswered questions.

The problem of characterizing the sediments in a cost-effective manner is similar to the problems already discussed above under permafrost. Some over consolidated sediments offer more protection to the pipelines from gouging, and allow for a greater degree in the sidewall slope and stability of the trench. The technical capability exists to trench in over consolidated sediments and they are, therefore, a favorable option. The effect of seasonal seabed freezing on soil conditions also needs to be explored.

Improvements to existing methods such as coring, logging and seismic, as well as development of novel methods, are needed to obtain data for characteristic mapping of soil conditions along the pipeline route. Mapping of ice scours, ice reconnaissance, soil types, and permafrost presence, along with sit-specific surveys (such as borehole sampling) can help to understand the technical issues involved.

Coastline processes, as they affect landfall and type of shoreline approach, is an important issue because the offshore pipeline must usually cross a potentially unstable beach. Site-specific shoreline erosion histories and shoreline transgression and regression histories should be used to design the proper shoreline approach. This information is necessary because of the expense of shore line approaches, however, it is noted that some of these problems could be resolved by using directional drilling techniques.

Corrosion could jeopardizes the life of an Arctic offshore pipelines. The pipeline warmth and the high oxygen content of the water may increase corrosion rates. Contact with sediments in reducing conditions may cause pitting. An understanding of corrosion as it is affected by such Arctic conditions as ice contact and the aurora borealis needs to be researched. Ice contact and the aurora borealis are not current technical barriers to pipelines, but a better understanding of both is needed.

The effect of earthquake activity on pipelines need to be better understood for the design of pipelines in seismically active areas, especially relative to faulting, etc. Site-specific seismic information is needed over time to provide a historical data base for design.

Research Needs

In order to increase our confidence in offshore Arctic pipelines, additional research on the following topics are recommended.

- Better understanding of ice gouging and infilling by looking at site-specific gouge lengths, depths, and frequencies;
- Better understanding of the factors that control properties, distribution, and detection of subsea permafrost;
- Better understanding of the properties, distribution, and detection of sea floor sediments; their effect on trenching; and their stability after trenching;
- Better understanding of coastline processes and the factors that effect erosion; and
- Better understanding of seismic activity and its potential effect on pipelines.

Conclusion

Arctic offshore oil and gas deposits are potentially one of the major undeveloped petroleum resources remaining. The capability to drill exploratory well in water depths up to 200 feet in the Arctic has been proven. Production in these areas have been negated more by the lack of commercial, economical discoveries than by technology. Considering the current state-of-practice, it is felt that the technology exist to successfully design, install and maintain an Arctic offshore pipeline systems. The information gained as activities are extended into deepwater and more hostile ice conditions, combined with extensive research, should provide a solid technological base for future operation. Hence, this vital resource, if developed expeditiously, economically, and in an environmentally sound manner, can represent a significant source of energy for the future.

References

Bellassai, S.J. "Comments of the National Research Council Marine Board Committee Report: Improving the Safety of Marine Pipelines," International Workshop on Damage to Underwater Pipelines, New Orleans, Louisiana, February 1995.

British Petroleum Exploration. 1977. "Northstar Development Project, Pipeline Right-of-Way Lease Application (Revised)," Anchorage, Alaska, January 3, 1997.

Code of Federal Regulations, Title 30, Chapter II, "Subchapters B and C, Parts 250 to 290." The Office of Federal Register, National Archives and Records Administration, Revised as of July 1, 1995.

Comfort, G. and K. Been, "Analysis of Subscour Stresses and Probability of Ice Scour-Induced Damage for buried Submarine Pipelines, Summary Report," Abstract prepared by Fleet Technology Ltd., Kanata, Ontario, and Golder Associates Ltd., Calgary, Alberta, March 1990.

Committee on Assessment of Safety of OCS Activities, Marine Board, Assembly of Engineering, National Research Council, and the National Research Council, Safety and Offshore Oil, National Academy Press, Washington, D.C., 1981.

Craig, J.D. K., Sherwood, and P.P. Johnson. "Geologic Report for the Beaufort Sea Planning Area, Alaska: Regional Geology, Petroleum Geology, Environmental Geology," Minerals Management Service, Anchorage, Alaska, December 1985.

INTEC Engineering, Inc., "Ice keel Protection, Northstar Development Project, Preliminary Engineering," INTEC Project No. H-660.2, Technical Note TN410 Rev. 1, Contractor report submitted by INTEC Engineering Inc. to British Petroleum Exploration (Alaska), September 1996.

INTEC Engineering Inc., "Pigging, Valving and Leak Detection, Northstar Development Project, Preliminary Engineering," INTEC Project No. H-660-2, Technical Note TN340 Rev. 1, Contractor report submitted by INTEC Engineering Inc. to British Petroleum Exploration, September 1996.

Johnson, T.L., "Strudel Scour: An Arctic Seafloor Scouring Process," Abstract included in the Civil Engineering in the Arctic Offshore Proceedings, American Society of Civil Engineers, New York, New York, pp. 744-753, 1995.

Lanan, G.A., INTEC Engineering Inc.; A.W. Niedoroda, R.J. Brown, and Associates; and W.F. Weeks, Cold Regions Research and Engineering Laboratory, "Ice Gouge Hazard Analysis," Paper presented at the 18th Annual Offshore Technology Conference in Houston, Texas, May 5-8, 1986.

MBC Applied Environmental Sciences, "A synthesis of Environmental Information on Causeways in the Nearshore Beaufort Sea, Alaska," Prepared by MBC Applied Environmental Sciences, Costa Mesa, California, for Minerals Management Service, Anchorage, Alaska, Workshop Proceedings, April 17-20, 1989.

McKeehan, D.S., INTEC Engineering, "Arctic Marine Pipelines," MMS Arctic Synthesis Meeting, Anchorage, Alaska, June 1995.

Nessim, M.A. and M.J. Stephens, "Optimization of Pipelines Integrity Maintenance Based on Quantitative Risk Analysis," Abstract prepared by Centre for Frontier Engineering Research Inc., Edmonton, Alberta, 1995.

Palmer, A.C., Andrew Palmer and Associates; I. Konuk, Canada Oil and Gas Lands Administration; G. Comfort, Fleet Technology Ltd.; and K. Been, Golder Associates, "Ice Gouging and the Safety of Marine Pipelines," Paper presented at the 22nd Annual Offshore Technical Conference in Houston, Texas, May 7-10, 1990.

PFL Inc., Offshore and Arctic Technology, "Arctic Offshore Pipeline Systems, A Reference Manual," Abstract prepared by PFL Inc., Offshore and Arctic Technology, Calgary, Alberta, 1990.

R.F. Busby Associates, "Arctic Undersea Inspection of Pipelines and Structures," Contractor report submitted by Busby Associates, Inc., Arlington, Virginia, to the Arctic Program funded by Minerals Management Service, June 1983.

Vaudrey and Associates, Inc., "Potential Hazards to Shore Approaches of Arctic Pipelines in the Alaskan Chukchi and Beaufort Seas," Prepared by Vaudrey and Associates, Inc., Van Luis Obispo, California, for U.S. Naval Civil Engineering Laboratory, Port Hueneme, California, August 1991.

"Proceedings of the International Workshop on Pipeline Safety," sponsored by the Minerals Management Service, New Orleans, Louisiana, December 1991.

"Proceedings of the International Workshop on Damage to Underwater Pipelines," sponsored by the Minerals Management Service, New Orleans, Louisiana, February 1995.

"Proceedings of the Sea Ice Mechanics and Arctic Modeling Workshop," sponsored by the Mineral Management Service and U.S. Navy Office of Naval Research, Anchorage, Alaska, 1995.

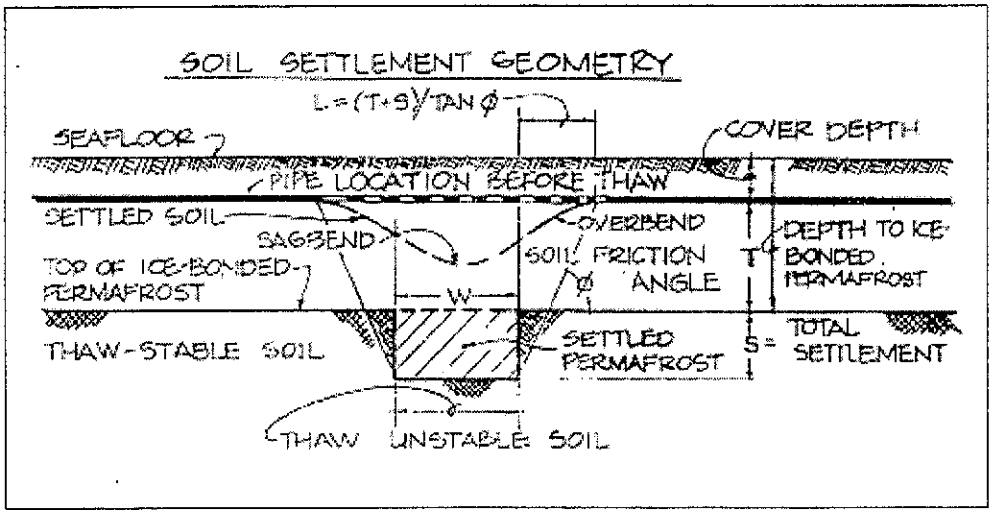

Figure 1- Differential settlement due to permafrost thaw

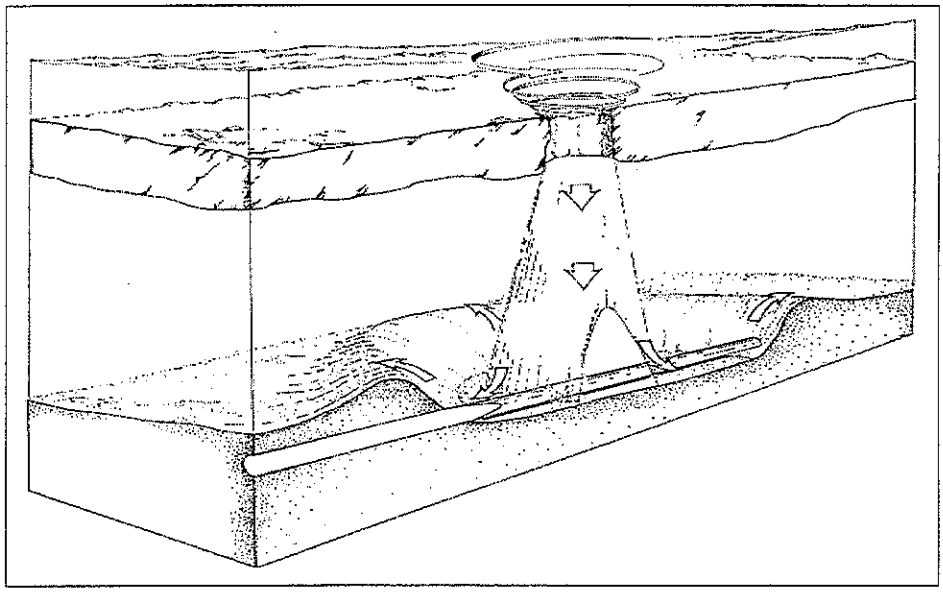

Figure 2-Pipeline span created by strudel scour

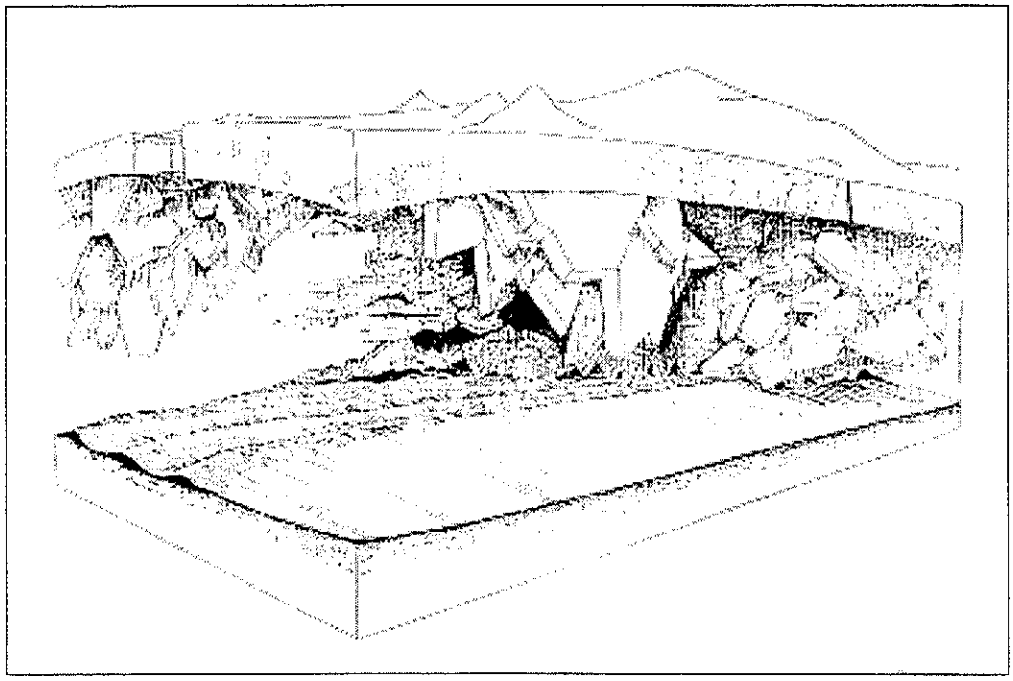

Figure 3-Ice ridging result in deep keels that can scour the seafloor

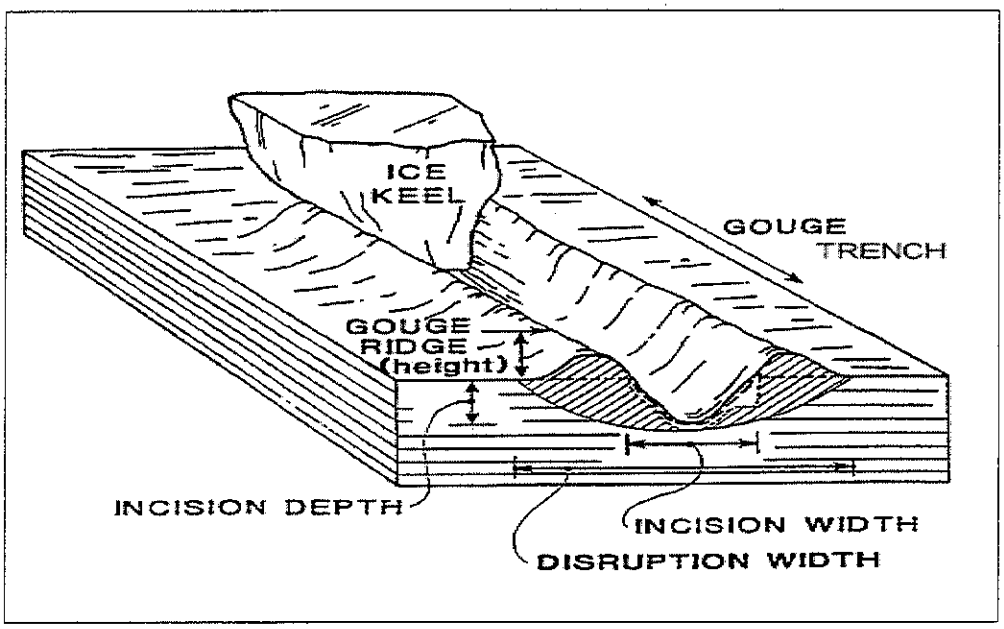

Figure 4- Ice gouge/scour terminology

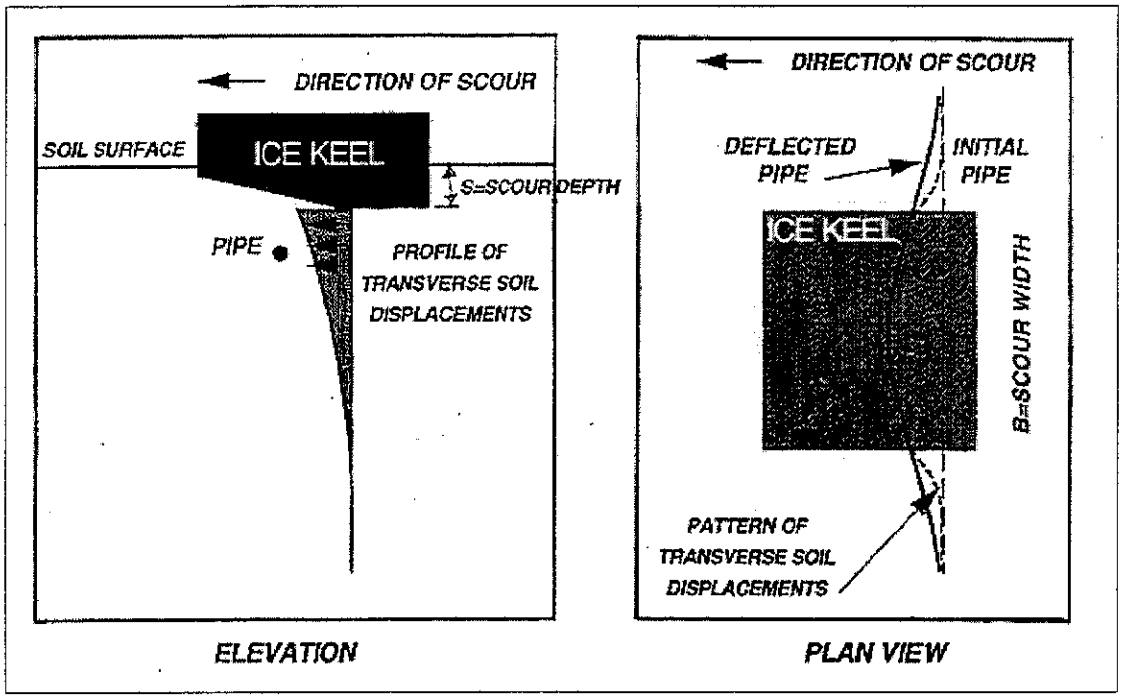

Figure 5-Geometry of an ice scour illustrating transverse soil displacement

Review of Strength of First Year Ice Features and Driving Forces Relating to Ice Scour

K. R. Croasdale
K.R. Croasdale & Associates Ltd., Calgary, Alberta, Canada

ABSTRACT

Offshore Platforms in the Sakhalin region need to be designed to withstand the forces imposed by first year ice features such as deep pressure ridges and refloated Stamukha. In calculating ice forces, it has been useful to consider three possible limits to the ice loads. In the first limit, the ice fails local to the structure as it is pushed into it by large driving forces. The ice load cannot be any higher that this limit which is termed the "limit stress load". To calculate the limit stress load it is necessary to understand the strength of the ice feature in the appropriate failure mode. In recent years, research has been underway to better quantify the strength of first year ridges especially their keels. It is also the strength of the ridge keels which will limit ice scour depths and the loads imposed on subsea pipelines and other seabed facilities.

This paper describes the research relating to the strength of first year ridge keels and the current methods to calculate ice forces. Application of this work to subsea facilities is discussed and load ranges given.

Ice forces can also be limited by the driving forces on the ice feature and/or its momentum. In both these limits, the ice is brought to rest before the full limit stress load is attained. These limits may have relevance to ice scour processes and they are described in the paper.

REFERENCES

Bruneau, S.E., G.B. Crocker, R.F. McKenna, K.R. Croasdale, M. Metge, R. Ritch and J.S. Weaver (1998). Development of techniques for measuring *in situ* ice rubble shear strength. Proceedings of 14th International IAHR Ice Symposium, Vol. 2, Potstam NY.

Bruneau, S.E ., McKenna, R.F., Croasdale, K.R., Crocker, G.B., King, A.D. (1996) *In situ* direct shear of ice rubble in first year ridge keels. 49th Canadian Geotechnical Conference: Frontiers of Geotechnology. Preprints, St. John's, NF, 1996 pp.269-278

Sub-Scour Soil Deformations and the Development of Ideas from Field Work in the Last Decade

C.M.T. Woodworth-Lynas
PETRA International, Cupids, Newfoundland, Canada A0A 2B0

INTRODUCTION

The modern day phenomenon of scour by seasonal ice and icebergs in the earth's polar and sub-polar oceans is well known, and a very extensive literature exists (for example see the bibliography by Goodwin *et al.* 1985) documenting occurrence of scour marks, modern scouring rates and the process of scouring (e.g. Geonautics Limited, 1985; Hodgson *et al.* 1988; Lewis and Woodworth-Lynas, 1990; Woodworth-Lynas *et al.* 1991). In large polar to temperate freshwater bodies such as Great Slave Lake and Lake Erie present-day scouring by seasonally-occurring ice generally takes place during the spring breakup (Weber, 1958; Grass, 1984, 1985). The planform pattern of relict scour marks visible on the present day land surface has been reported from large areas of Canada and the northern United States that were formerly occupied by glacial lakes of the Quaternary period, such as Lake Agassiz (Horberg, 1951; Clayton *et al.* 1975; Dredge, 1982; Mollard, 1983) Lake Ojibway (Dionne, 1977) and Lake Iroquois (Gilbert *et al.* 1992) and similar patterns, created by icebergs during deglaciation, also have been identified on the modern lake floor of Lake Superior (Berkson and Clay, 1973).

Until the mid-1980's it was generally believed that the influence of a scouring ice keel on the seabed was essentially restricted to horizontal bulldozing. This mechanism clears material to either side into two co-linear mounds, or berms, as the keel moves forward creating a trough, or scour mark, at the trailing edge of the keel. From this point of view there would be little or no sub-scour soil movement, and consequently that oil and gas pipelines buried just below the depth of scour would experience little or no stress or strain. These ideas were generally supported by the published results of small-scale physical model studies of ice keel scour conducted at ambient (1g) gravity. The use of aluminum or steel for the model keels helped reinforce the notion that ice keels could be thought of as rigid indenters that ploughed through a yielding seabed.

These views began to change in 1985 as a result of the Dynamics of Iceberg Grounding and Scouring (DIGS) experiment (Hodgson *et al.* 1988), a landmark field study during which icebergs were closely monitored as they ran aground on the silty sea floor of the Labrador continental shelf of eastern Canada. Data retrieved from accelerometer packages placed on the grounding icebergs allowed the first ever direct measurement of grounding forces. Complete above and below water 3-dimensional profiling of the icebergs meant that the grounding forces could also be modeled and verified against the actual measurements. Thus the complex physics of ice/seabed interaction were measured and understood. Physical model studies, often guided by the results from DIGS, helped to expand knowledge of ice keel-induced subscour soil behaviour (e.g. Abdelnour and Graham, 1984; Been, 1990; Golder Associates Ltd. 1989; Paulin, 1992; Poorooshasb, 1989). The Pressure Ridge Ice Scour Experiment (PRISE), a very extensive series of physical model studies conducted in a geotechnical centrifuge at accelerations of 75 to 200g, has greatly expanded our knowledge of scour-induced failure mechanisms in a variety of different soil types and conditions, Clark *et al.* (1998)

The Development of Ideas from the Results of Field Work

Surface Morphology of Scour Marks

From a small 3-person submersible the morphologies of newly-created scour marks in fine-grained soils were documented for the first time during the Dynamics of Iceberg Grounding and Scouring (DIGS) experiment. Scour mark troughs, between the two berm ridges, were found to be generally flat-bottomed. The troughs were characterized by the presence of ridge-and-groove microtopography, developed parallel to the scour mark axis, with amplitudes up to 30 cm (Woodworth-Lynas *et al.* 1991). These features formed at the trailing edge of the keel where scoured soil was moulded by clastic material (pebbles, cobbles and boulders) embedded in the ice and by open ice fissures, as they passed over the newly exposed soil. In places along the inner berm margins ridges and grooves were developed at an angle to the scour mark axis reflecting combined forward and lateral displacement of material towards the berm as the iceberg moved forwards. In places on the floor of the trough between the berms voids, up to 1 m deep and 2 m wide, truncated the ridges and grooves. Voids were created following the dissolution of small (a few m^3) masses of debris-laden ice that were mechanically broken off from the base of the keel and then pressed into the seabed by the scouring iceberg. Initially low areas within the scour mark trough may preserve seafloor that has not been affected by ice/seabed interaction. In these regions deposition of bulldozed sediment from the surcharge at the leading edge of the keel partially filled the narrow spaces beneath the keel in areas of initially low seabed elevation.

Scour mark berms consisted of *in situ* fractured but intact blocks of material on the inner flanks, and disarticulated blocks 1-2 m high along the berm crest. The outer berm slopes generally consisted of pieces of larger blocks spalled from the berm crest resting in relatively finely comminuted, reworked material. The reworked material originated in the leading edge surcharge before being displaced to either side of the keel. Scour mark berms had irregular topography ranging in height from a few centimetres to as much as 6 m above the seabed. Isolated, irregularly-shaped mounds resting on undisturbed seafloor beyond the outer berm were pieces of cohesive sediment that may have originated at the berm crest as overhangs, and which subsequently collapsed.

Thus DIGS showed that bulldozing, although important, wasn't the only mechanism at work during ice/seabed interaction. The side berms showed clear evidence that the material of which they were comprised had been initially compacted, presumably beneath the keel, and then displaced both horizontally and vertically upwards to form remarkable block-like topography. In one scour mark trough conical mud boils suggested that sub-scour liquefaction had occurred (unpublished data). There was also strong evidence that ice blocks had been broken out of the keel and subsequently pressed into the seabed as the rest of the keel passed over. Together these observations hinted strongly that sub-scour deformations and stresses were quite significant. They also showed that the concept of the keel as a rigid indenter was untenable: the keel was modified by the seabed during scouring, presumably to a stable condition that allowed the creation of scour marks that typically maintain constant morphology over several kilometres.

Sub-surface Soil Structures of Scour Marks

During the DIGS experiment standard acoustic geophysical surveys of the seabed were carried out. However, these kinds of survey cannot unequivocally resolve sub-scour soil structure (e.g. Gilbert,

1990). Sediment cores may be taken from scour marks but the scour-induced structures that they may sample cannot be adequately quantified in terms of large-scale, sub-scour soil deformation mechanisms (Fischbein, 1987). Ideally, an exposed cross-section through a single scour mark should reveal details of scour-induced soil structure thus indicating deformation mechanisms that cannot otherwise be defined. The only places in the world where sub-scour soil deformations may be observed directly is in areas where ancient scour marks are now exposed on land. Fortunately, there are places where scour marks of glacial age (10,000 years) are perfectly preserved at the present land surface.

Complete cross-sections of scour marks have been described from only four localities worldwide. Three of these localities comprise glaciolacustrine environments, and one (in Norway) records a glacial outburst flood that inundated partially exposed marine sediments (Longva and Thoresen, 1991). From Scotland, Thomas and Connell (1985) described a 10-m long grounding structure, at least 2 m deep, from Wisconsinan-age (Weichselian) glaciolacustrine sediments. They observed small scale reverse faults below the inner margins of the trough and showed "downfolded" strata extending to at least 1.3 m below the trough (Figure 1). They interpreted the structures to be the result of ice/sediment interaction during a grounding event caused by a slow lowering of water level, with no horizontal keel movement: processes that are not typical of most ice scour marks. This feature is analogous to modern "scour pockets" created by grounding icebergs during annual breakout floods (Fahnestock and Bradley, 1973).

Eyles and Clark (1988) described a well-preserved scour mark, approximately 9 m wide and 2.5 m deep, at Scarborough Bluffs, Ontario. They interpreted the scour mark, incised into delta front sandy lake sediments, to have been made by a pressure ridge keel in water depths of 20 m about 60 000 years ago. They described thrust and normal faults, load casts and folds below and on either side of the scour mark trough (Figure 1), and suggested that sediments had been affected by shearing up to 2 m below the scour mark trough during the scouring event.

In Norway, Longva and Bakkejord (1990) reported on excavations of two iceberg scour marks and an iceberg pit that were formed during a Holocene glacial outburst flood in the Romerike area about 9,200 years ago (Longva and Thoresen, 1991). Excavated sections across the scour marks revealed evidence of folding, faulting and sediment liquefaction (Figure 1). Deformation in sub-scour sediments occurred to approximately three times the depth of scour mark incision (Oddvar Longva, pers. comm. 1986).

From the clay soils of former glacial Lake Agassiz, Woodworth-Lynas and Guigné (1990) described scour marks 50 - 65 m wide, 2 - 2.5 m deep and 0.5 - 8.5 km in length. In the soils beneath the trough of one scour mark (Figure 2) they documented normal faults with dip-slip displacements of at least 3.5 m. These faults were thought to have been the result of bearing capacity failure of the clay sediment beneath the scouring keel (Poorooshasb *et al.* 1989). The faults propagated to depths beyond 5.5 m below the deepest part of the scour mark trough (Woodworth-Lynas, 1992). Sub-horizontal thrust faults occurred beneath the scour mark berms (Woodworth-Lynas and Guigné, 1990), and a horizontal fault, 4-5 m below the trough and connecting two apparent bearing capacity failure surfaces, was evidence that significant horizontal shear had occurred to at least this depth during scour.

Preliminary studies of a deep scour mark have been carried out by the author, Nicholas Eyles (University of Toronto) and Carolyn Eyles (McMaster University). The feature is developed in layered granular and cohesive soils exposed in a cliff section of sands and clays at Scarborough, Ontario. The scour mark is a steep-sided, U-shaped trough 10 m wide and 4 m deep with asymmetric berms of excavated diamict material (Figure 3). The trough is filled with a massive muddy sand that probably was deposited during a single storm event. Scour-induced deformation has caused downward displacement of the lower diamict sequence boundary into underlying deltaic sands. Downward displacement has affected at least the top 2 m of underlying sand, and sub-scour deformation can be traced to at least 4.5 m below the deepest part of the scour mark trough.

Engineering Significance of Field Work

Field studies of modern scour mark morphologies on the sea floor and of sub-scour soil structures beneath ancient features on land have been instrumental in focusing the attention of industry and of regulators on a need to understand the forces and deformation mechanisms experienced by different soils during scour events. The results of this considerable body of field work have been used both to constrain and to verify the results of subsequent centrifuge modeling and analytical modeling of the scouring process that has taken place at C-CORE in the last 7 years (see Clark *et al.,* 1998 and Palmer, 1998 in these proceedings). The results of these modeling studies are being used to assist in the design of offshore pipelines that must withstand scouring forces.

Bibliography

Abdelnour, R. and B. Graham. 1984. Small scale tests of sea bottom ice scouring. In, International Association for Hydraulic Research (IAHR), 7th International Symposium on Ice, Hamburg, August 27-31: 267-279.

Been, K. 1990. Mechanisms of failure and soil deformation during scouring. In, Workshop on Ice Scouring and the Design of Offshore Pipelines. Calgary, April 18-19: 179-191.

Berkson, J.M. and C.S. Clay. 1973. Microphysiography and possible iceberg grooves on the floor of western Lake Superior. Geological Society of America Bulletin, 84 (4): 1315-1328.

Clark, J.I., M.J. Paulin and R. Phillips 1998. Ice scour research for safe design of pipelines: 1978-1998. Proceedings of Ice Scour and Arctic Marine Pipelines Workshop, Hokkaido, Japan. Published by C-CORE, November 1998.

Clayton, L., W.M. Laird, R.W. Klassen and W.D. Kupsch. 1975. Intersecting minor lineations on Lake Agassiz plain. Journal of Geology, 73: 652-656.

Dionne, J.C. 1977. Relict iceberg furrows on the floor of glacial Lake Ojibway, Quebec and Ontario. Maritime Sediments, 13 (2): 79-81.

Dredge, L.A. 1982. Relict ice scour marks and late phases of Lake Agassiz in northernmost Manitoba. Canadian Journal of Earth Sciences, 19: 1079-1087.

Eyles, N. and B.M. Clark. 1988. Storm-influenced deltas and ice scouring in a late Pleistocene glacial lake. Geological Society of America Bulletin, 100: 793-809.

Fahnestock, R.K. and W.C. Bradley. 1973. Knik and Matanuska rivers, Alaska: a contrast in braiding. In, Fluvial Geomorphology (M. Morisawa, ed.), Proceedings of the Fourth Annual

Geomorphology Symposium, Binghampton, New York, Sept. 27-28: 220-250.
Fischbein, S.A. 1987. Analysis and interpretation of ice-deformed sediments from Harrison Bay, Alaska. M.Sc. thesis, California State University, Hayward, 107p.
Geonautics Limited. 1985. Design of an iceberg scour repetitive mapping network for the Canadian east coast. Environmental Studies Revolving Funds Report No. 043, Ottawa: 50p.
Gilbert, G.R. 1990. Scour shape and sub-scour disturbance studies from the Canadian Beaufort Sea. Proceedings of an invited workshop, Ice Scouring and the Design of Offshore Pipelines, April 18-19th, Calgary, Alberta. Canada Oil and Gas Lands Administration and Centre for Cold Ocean Resources Engineering.
Gilbert, R., K.J. Handford and J. Shaw. 1992. Ice scours in the sediments of glacial Lake Iroquois, Prince Edward County, eastern Ontario. Géographie physique et Quaternaire, 46 (2): 189-194.
Golder Associates Ltd. 1989. Indentor testing to verify ice/soil/pipe interaction models. Phase I. January 1989. Report to Gulf Canada Resources Ltd. Proprietary Joint Industry Project: 42p (2 appendices).
Goodwin, C.R., J.C. Finley and L.M. Howard. 1985. Ice scour bibliography. Environmental Studies Revolving Funds Report No. 010, Ottawa: 99p.
Grass, J. 1985. Lake Erie cable crossing - ice scour study. In, Workshop on Ice Scouring, 15 - 19 February, 1982, National Research Council of Canada Associate committee on geotechnical research, Technical memorandum No. 136: 1-10.
Grass, J.D. 1984. Ice scour and ice ridging studies in Lake Erie. IAHR Ice Symposium, Hamburg: 33-43.
Hodgson, G.J., J.H. Lever, C.M.T. Woodworth-Lynas and C.F.M. Lewis (editors). 1988. The dynamics of iceberg grounding and scouring (DIGS) experiment and repetitive mapping of the eastern Canadian continental shelf. Environmental Studies Research Funds Report No. 094, Ottawa: 316p.
Horberg, L. 1951. Intersecting minor ridges and periglacial features in the Lake Agassiz basin, North Dakota. Journal of Geology, 59 (1), 1-18.
Lewis, C.F.M. and C.M.T. Woodworth-Lynas. 1990. Ice scour. In, Geology of the continental margin of eastern Canada, Geology of Canada, No.2 (M.J. Keen and G.L. Williams, eds.). Geological Survey of Canada: 785-792.
Longva, O. and K.J. Bakkejord. 1990. Iceberg deformation and erosion in soft sediments, southeast Norway. Marine Geology, 92: 87-104.
Longva, O. and M.K. Thoresen. 1991. Iceberg scours, iceberg gravity craters and current erosion marks from a gigantic Preboreal flood in southeastern Norway. Boreas, 20 (1): 47-62.
Mollard, J.D. 1983. The origin of reticulate and orbicular patterns on the floor of the Lake Agassiz basin. Geological Association of Canada Special Paper No. 26: 355-374.
Palmer. A. 1998. Alternative Paths For Determination Of Minimum Burial Depth To Safeguard Pipelines Against Ice Gouging Proceedings of Ice Scour and Arctic Marine Pipelines Workshop, Hokkaido, Japan. Published by C-CORE, November 1998.
Paulin, M.J. 1992. Physical model analysis of iceberg scour in dry sand and submerged sand. M.Eng. thesis, Memorial University of Newfoundland: 183p.
Poorooshasb, F. 1989. Large scale laboratory tests of seabed scour. Contract report for Fleet Technology Ltd. C-CORE contract Number 89-C15. *Published as*: Analysis of subscour stresses and probability of ice scour-induced damage for buried submarine pipelines, Volume

IV, Large scale laboratory test of seabed scour. Canada Oil and Gas Lands Administration, January 1990: 168p.

Thomas, G.S.P. and R.J. Connell. 1985. Iceberg drop, dump, and grounding structures from Pleistocene glacio-lacustrine sediments, Scotland. Journal of Sedimentary Petrology, 55 (2): 243-249.

Weber, J.N. 1958. Recent grooving in lake bottom sediments at Great Slave Lake, Northwest Territories. Journal of Sedimentary Petrology, 28 (3): 333-341.

Woodworth-Lynas, C.M.T. 1992. The geology of ice scour. Ph.D. thesis, University of Wales: 269p.

Woodworth-Lynas, C.M.T. and J.Y. Guigné. 1990. Iceberg scours in the geological record: examples from glacial Lake Agassiz. In, Glacimarine environments: processes and sediments (J.A. Dowdeswell and J.D. Scourse, eds.). Geological Society Special Publication No. 53: 217-233.

Woodworth-Lynas, C.M.T., H.W. Josenhans, J.V. Barrie, C.F.M. Lewis and D.R. Parrott. 1991. The physical processes of seabed disturbance during iceberg grounding and scouring. wide and 4 m deep with asymmetric berms.

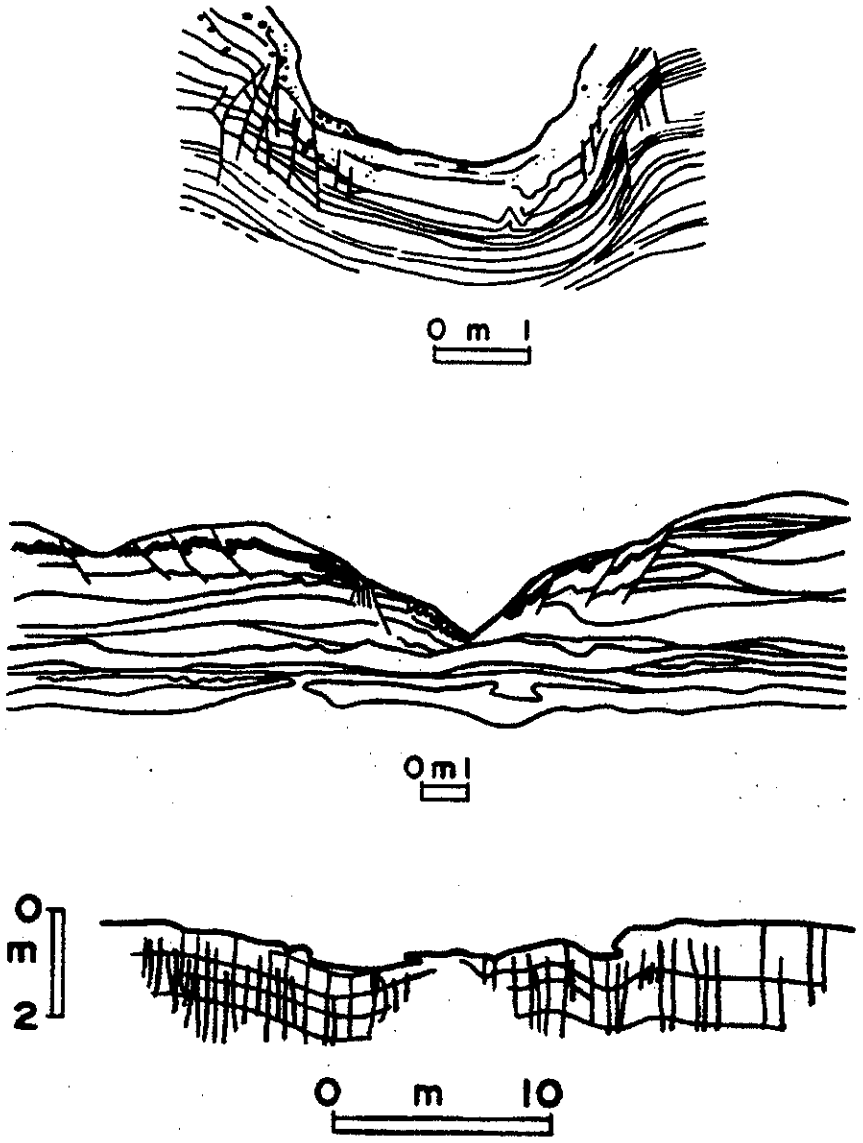

Figure 1.

Top: Cross-section of a 10m long iceberg grounding structure developed in laminated silts, sands and gravelly sands, from a quarry north of Aberdeen, Scotland. Adapted from Figure 6 of Thomas Connell (1985)
Centre: Cross-section of a 9m wide scour mark trough in delta-front sands, Scarborough Bluffs, Ontario. Adapted from Figure 10a of Eyles and Clark (1988).
Bottom: Cross-section of a 30m wide scour mark in laminated glacimarine clay, Romerike, southeast Norway. Adapted from Figure 6 of Longva and Bakkejord (1990).

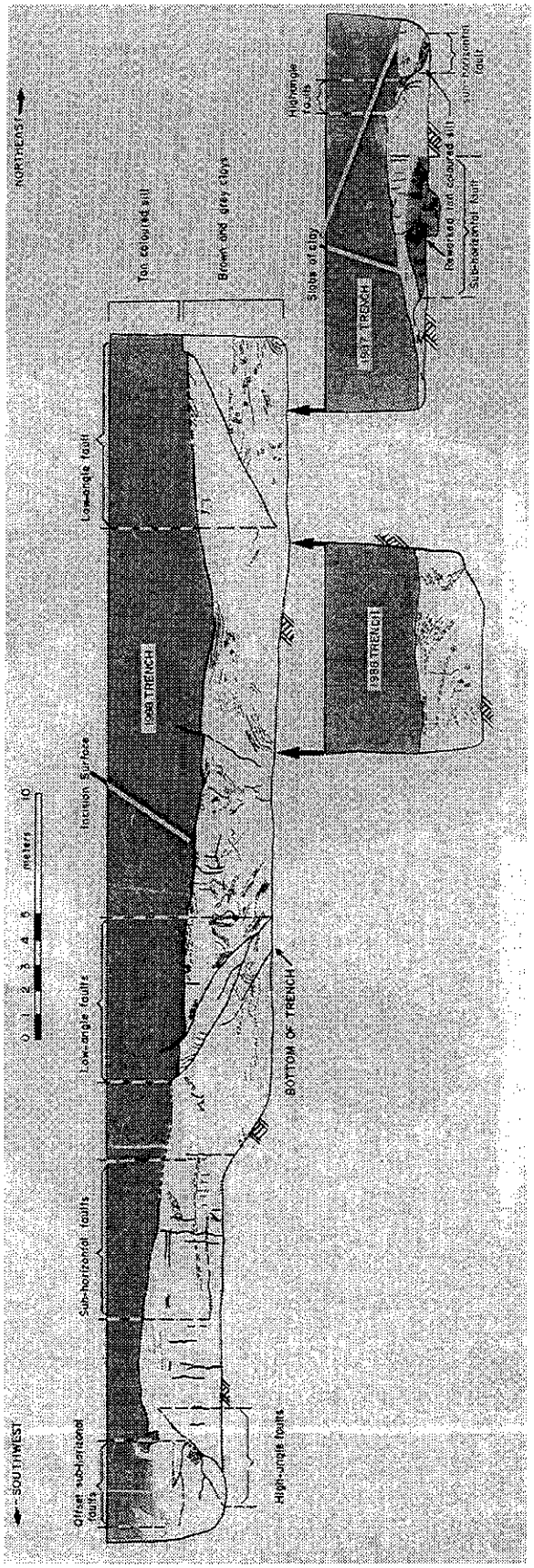

Figure 2.

Cross-section through a scour mark in clay soils of former glacial Lake Agassiz showing the scour mark incision surface (sub-horizontal line), sub-scour faults (heavy solid lines) and deforming bedding (curved lines), No vertical exaggeration.

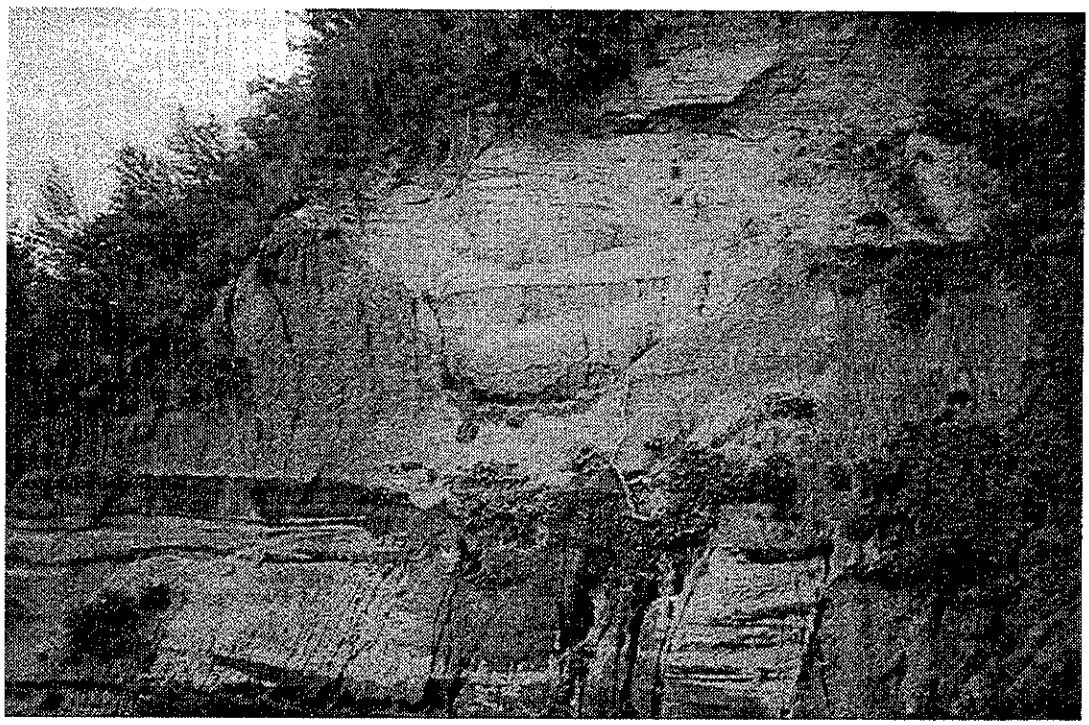

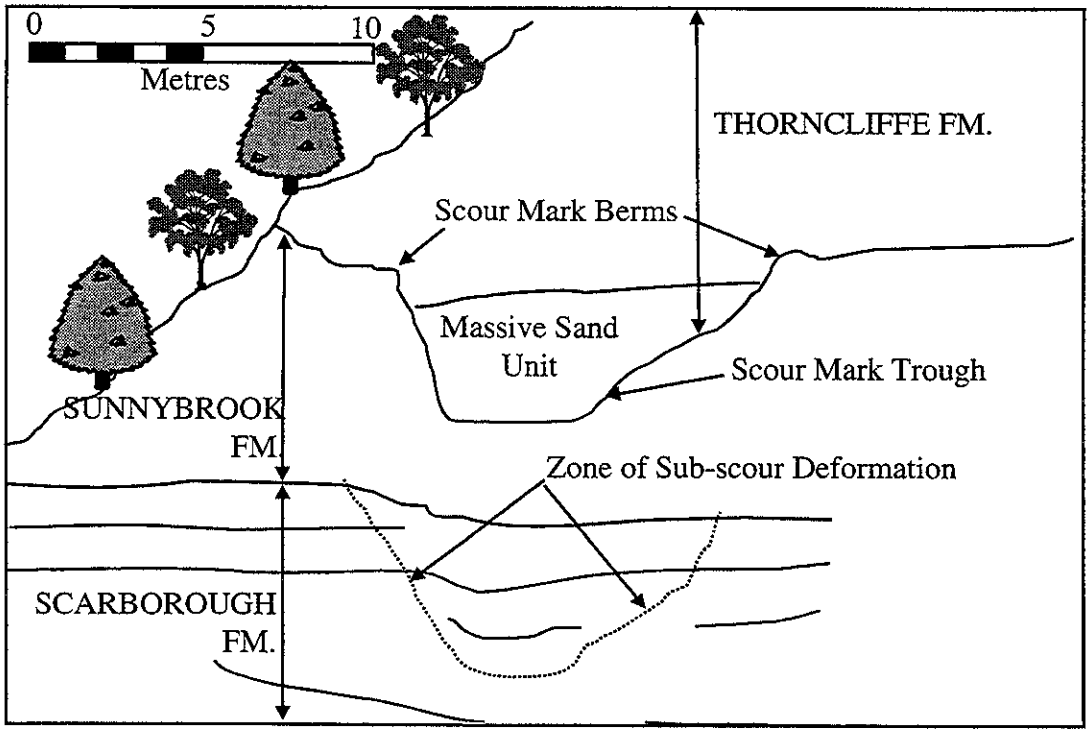

Figure 3. Deeply incised scour mark in layered granular and cohesive soils exposed in a cliff section at Scarborough, Ontari. The scour mark is a steep-sided, U-shaped trough 10m wide and 4m deep with asymmetric berms.

Method Of Ice Ridge Age Definition

Sergei Beketsky
Sakhallinmorneftegaz – Exxon, 820 Gessner, suite 529, Houston, Texas 77024, USA
Tel (713) 935-6018, Fax: (713) 935-6057

INTRODUCTION

The main hazard for hydrotechnical facilites in the offshore of northern Sakhalin are drifting hummocks or ice ridges.

The age of an ice ridge is very important for the study of drifting ice ridges and their inner structure analysis. Based on the survey data (Beketsky *et al.*, 1997) the age of an ice ridge affects its porosity, consolidated layer thickness, its physical/mechanical parameters and its integrated strength. All these parameters are important for the asssesment of an ice load on the hydrotechnical structures and offshore pipelines.

To determine an ice ridge age the author proposes the method which is based on determination of time period for thickness increase of level non-rafted ice around an ice ridge and comparing it to the thickness of ice blocks forming an ice ridge. It is assumed that an ice ridge drifts together with an ice floe, from which it was formed. The main calculation parameter is the sum of the air temperatures $\Delta\Sigma t_c$ for calculating period.

The ice ridge age has been estimated based on the method proposed by the author. The age of the studied ice ridges, which is a function of the ice increase time Δh_L, based on the correlation between the ice thickness increase and sum of the degree-days for north-east Sakhalin, has been determined.

DEVELOPMENT OF AN ICE RIDGE AGE CALCULATING METHOD

Main critical calculating parameter is determination of the correlation between ice thickness increase for particular area and sum of air temperatures Σt_c for calculated period.

The polar weather station observation data obtained by different authors suggest that the most common for the Arctic seas are empirical formula, which is the analytical expression of the correlation curves between the ice thickness and the sum of the degree-days, which has parabolic shape and can be appoximated by the equation:

$$h_L = a.(\Sigma t_c)^b \qquad (1)$$

Where:
h_L - the ice thickness; Σt_c - the sum of the degree-days; a,b – empirical coefficients.

The meaning of accuracy of the method for the ice thickness calculation is the difference between the calculated and the real ice thickness. The accuracy of the recommended method shall be in the range of +/- 5-10%.

To obtain the calculating formula for the correlation of the ice thickness from the sum of the degree-days the ice thickness increase has been monitored. The ice thickness measurement was performed every 5 days on the stationary profile at 11 points on the distance of 10 meters. At the same time the air temperature was measured by a termograph. Later the average ice thickness in the profile and number of the degree-days during the ice thickness measurement have been calculated.

An approximation of received data has allowed us to obtain the correlation between the ice thickness and sum of the degree days which has parabolic shape:

$$h_L = 3.1\ (\Sigma t_c)^{0.47} \qquad (2)$$

Maximum deviation between field data and calculated parameters is not more than 8% (Fig. 1), which is an agreement with accuracy condition of this calculating method.

ESTIMATION OF AN ICE RIDGE AGE USING PROPOSED METHOD

Using the method proposed by the author the estimation of the studied ice ridge age during springtime in the NE Sakhalin shelf has been done. As it was mentioned earlier this method is based on the difference between the thicknesses of the level non-rafted ice around an ice ridge and ice blocks forming ice ridge. Figure 2 presents schematic view of the level ice thickness increase near an ice ridge. The measurements of the level non-rafted ice thickness near an ice ridge and ice blocks thickness of an ice ridge have been done according to this scheme. Average thickness of level non-rafted ice near the (h_L) was 90cm, average ice block thickness forming an ice ridge (h_o) was 60cm.

1. Calculate the degree-days for h_L - 90cm and h_o = 60 cm.

For this purpose we use the correlation received earlier (2) for the ice thickness increase depending on the sum of the degree-days for the NE Sakhalin shelf. Thus Σt_c = 1293 and 546 degree days respectively (see Fig. 2).

2. Find the difference of these sums: Σt_c = 746.5 degree-days.

3. Find the average daily air temperature for February based on the meteostation data B. Shantar which is –19.3°C.

4. Determine the ice ridge age, which is the function of the ice thickness increase time Δh_L - 30cm. For this purpose the $\Delta\Sigma t_c$ shall be divided by average daily air temperature –19.3°C.

The result is 39 days.

Therefore, the age of the surveyed ice ridges is approximately 1-1.5 month, which corresponds to the ice ridge floe drift time from Shantar islands to the NE Sakhalin shelf and also the general ice drift direction for this area. Irregular distribution of ice ridges and ice rubbles as well has high

occurrence of the ice ridges on the surface has confirmed that these ice ridges by their type of development belong to 2nd type (Beketsky and Astafiev, 1997), ie, have been formed to the north of the Schmidt peninsula in the drift boundary area.

Computated age of the studied ice ridges was confirmed by the salinity study results of the ice blocks forming ice ridges. Salinity value ranges from 3 to 4.5%, which corresponds to one-month old marine ice of this region.

REFERENCES

1. Beketsky, SP, Astafiev, VN and Bogdanchikov SM, 1997, "Technique of determination of design parameters of hummocks", Proceedings of the 14th International Conference on Port and Ocean Engineering under Arctic Conditions, Yokohama, Japan, Vol. IV, pp 239-244.

2. Beketsky SP, 1996, "Morphology and strength of hummocks and grounded hummocks in the Sea of Okhotsk", Synop. Of thesis of Ph.D of Geogr, S-Petersburg: Arctic and Antarctic Institute, pp 1-25(in Russian)

3. Beketsky SP and Astafiev, VN, 1997, "Morphology of hummocks in the Sea of Okhotsk", The Twelfth International Symposium on Okhotsk Sea and Sea Ice, Mombetsu, Hokkaido, Japan, pp 42-48.

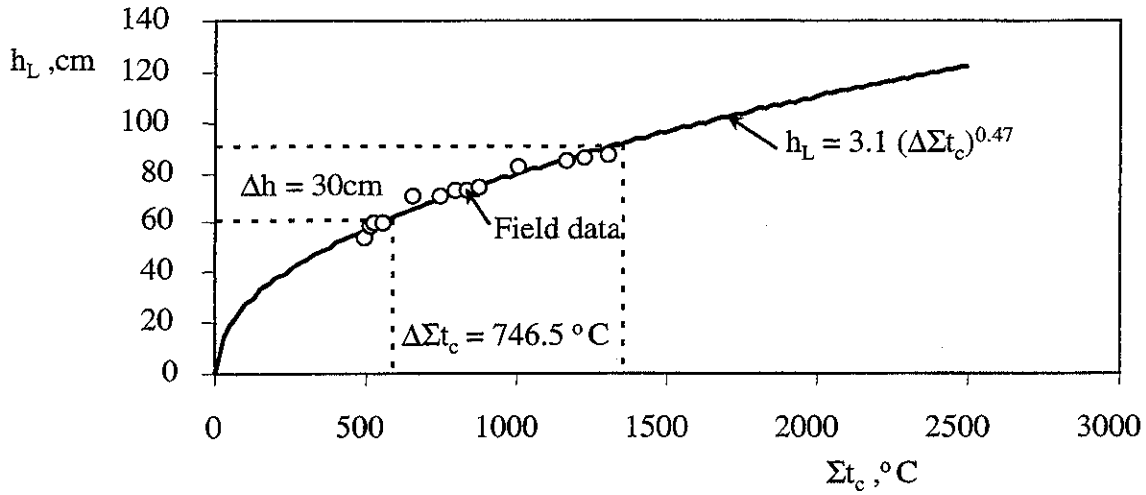

Figure 1. Correlation between the ice thickness increase and the sum of degree-days

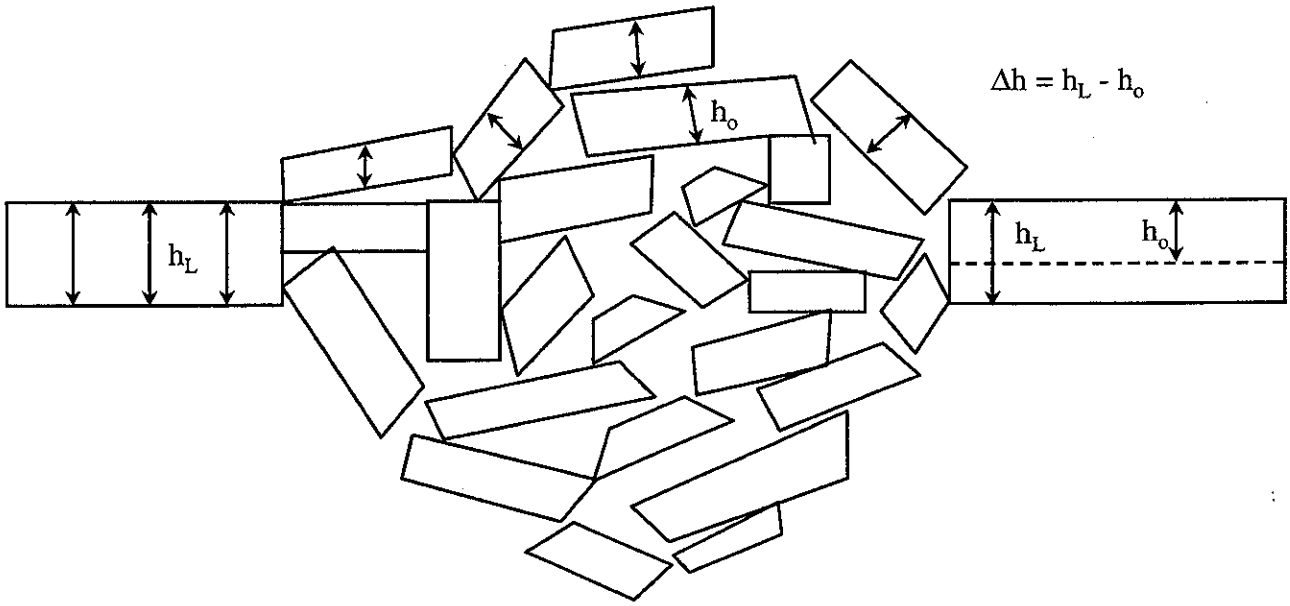

Figure 2. Scheme for definition of level ice thickness increase near an ice ridge

Sakhalin Ice Gouge Measurements through Stamukha Drilling

Sergei Beketsky
Sakhalinmorneftegas – Exxon, 820 Gessner, suite 529, Houston, Texas 77024, USA
Tel: (713) 935-6018, Fax: (713) 935-6057

INTRODUCTION

Development of oil and gas resources in the freezing seas requires an integrated approach for the ice survey. Typical feature of the ice cover megastructure in the Sakhalin area is the presence of stamukhas. During their development these ice features strongly impact the sea floor, creating static and dynamic loads on the offshore pipelines. Therefore, one of the issue of the offshore pipeline design is to determine the probable depth of ice ridge impact at different water depth in the studied area.

Since early 1970's the ice gouges caused by the ice ridges have been recorded by the sonars (Weeks et al, 1983, Lewis et al, 1996, Lewis and Blasco, 1990).

In such hydrodynamic area as offshore of North Sakhalin this method of ice gouge survey is not appropriate due to their rapid fill up. Loose soil, strong currents and frequent storms are contributing factors to this fill up.

From 1985 to 1990 under author's supervision the study of ice gouge depth has been conducted, through thermal dynamic drilling of stamukhas in three regions: Sakhalin Bay, North Bay and NE coast of Sakhalin (Fig. 1). Survey methods have been developed by the author.

WORK PROCEDURE

To determine stamukhas penetration into the sea floor the visual survey, geodetic work and thermal drilling have been performed.

1. Visual Observation. Based on the ice survey data the zones of the maximum stamukhas concentration and survey objects are identified. The presence of the tidal scouring also is recorded, which serves as an indicator of the stamukha. Then the visual work is performed along with photography or drawing of the upper (above water) part of a stamukha. Analyses of probable direction of an ice ridge impact during the seafloor penetration and a point of possible contact of stamukha with the seafloor are performed.

2. Geodetic work. The scope of the work includes the installation of a pole in the middle of a stamukha to be able to tie it up to the governmental geodetic points. It serves as a reference point to tie up later the water depth measuring points around stamukha and it is used for generating the topographic map of the upper part of the ice ridge.

The sea level fluctation was measured using the temporary water measuring point. The drilling of the ice and hydrography work was done following the plotting of the water depth measuring points. Determination of the final sea depth around stamukha is done based on the water measuring point data. The absolute markers of the thermal drilled wellheads as well as the configuration and location of the tidal scouring are identified during the topographic survey of the upper part of stamukha. The data of the depth measuring are plotted on the bathymetry map using the scale 1:500, 1:200, with 0.25m isobath spacing. The direction of a gouge is determined from the bathymetry data, as well as its geometrical parameters and a site seafloor slope.

The topographical plan is generated during the topographic survey of the upper part using 1:500 and 1:200 scales indicating tidal scouring location, thermal drill profiles with absolute markers of wellheads. Topography survey data are critical for determination of the ice ridge surface area and its upper part volume.

3. Thermal drilling. The thermal drilling is used for acquiring detailed seafloor relief directly underneath of a stamukha. Thermal drilling is performed on the perpendicular profiles, the distance between boreholes is determined based on the stamukha's dimension but it shall not exceed 10m. The spacing between boreholes becomes smaller at the point of contact of a stamukha with the seafloor. During the entire drilling time the detailed documentation of the well has been generated. The following parameters were recorded: the drilling rate which depends on the relative ice strength, identification of dense and loose layers including voids, thickness of the consolidated layer (an ice layer without voids at the water level). Upon drilling completion of each borehole the soils samples were taken to determine its physical and mechanical parameters, also the water level in the well was measured.

4. Processing and analysis of the received data. The well columns are plotted based on the field data. The ice feature sections are generated from the well data and topographic maps. Dimensions of the upper, consolidated and lower parts of the ice ridges are determined based on the well columns plotted from the drilling data. Porosity of the entire stamukha is calculated, as well as the porosity of the upper and lower parts, the porosity of the consolidated layer is set as 0 (Beketsky, Truskov, 1995).

   Dimensions of the ice ridges are determined by the topographic maps: width, length, elongation coefficient (ratio between width and length of stamukha) (Borodachev et al, 1990). The section shape and slope angles of the upper and lower parts of the ice ridges are determined from the plotted sections. Sail heights and keep depth of a stamukha are presented relative to the average multi-year level. The gouge parameters are calculated based on the analyses of entire work scope data, including if possible a diving survey of the seafloor such as: number of gouges, their direction, length, width and depth.

RESULTS OF THE STUDY

The table presents the morphological characteristics of the studied stamukhas.

Based on the data of this study it was concluded that the area of most probable impact of the ice ridges is located between two isobath 21-23m. The parameters of ice gouges were as follows: length 20-75m, width 10-30m, depth 0.4-2.13m.

Based on the thermal drilling data and topography survey data the author has generated models of an ice hummock, an ice ridge and a stamukha for north Sakhalin shelf of Sea of Okhotsk. For the first time these generated models have been published by the author in his article (Bekesky, 1996). These models describe all key ridge properties, including ridge geometry (lateral dimensions, ridge sail heights, sail shape, keel depth, etc) and physical characteristics (porosity, consolidated layer thickness, ice ridge strength, etc).

These models can be used in the calculation of an ice ridge impact on the soil. They can also be used for planning and conducting laboratory and ice-basin tests and carrying out computer simulations.

REFERENCES

1. Beketsky SP, Truskov PA, 1995, "Internal Structure of Ice Pressure Ridges in the Sea of Okhotsk." The 13th POAC-95 conf., Murmansk, Russia, vol 1, pp 109-111.

2. Beketsky SP, 1996, "Morphology and strength of hummocks and grounded hummocks in the Sea of Okhotsk", Synop. of thesis of Ph.D of Geogr., S-Petersburg: Arctic and Antarctic Institute, pp.1-25 (in Russian)

3. Borodachev, V.E.., Beketsky S.P., Truskov P.A. and Polomoshnov A.M., 1990, "About Morphological Hummock Characteristics" Proc. Arctic and Antarctic Res. Inst., Leningrad, vol.418, pp.116-128 (in Russian)

4. Lewis C.F.M., Parrott D.R., Simpkin P.G. and Buckley J.T., 1986, "Ice scour and seabed engineering", Proc. Workshop Ice Scour Research, 1985, Environmental Research Revolving Funds, Report 48.

5. Lewis CFM and Blasco SM, 1990 "Character and Distribution of Sea-Ice and Iceberg Scours". Proc Workshop on Ice Scouring and the Design of Offshore Pipelines, Canadian Lands Administration, Calgary, Alta., pp 96-101.

6. Weeks W.F., Barnes W.P., Rearic D.M. and Reimnitz E., 1983, "Statistical aspects of ice gouging on the Alaskan shelf of the Beaufort Sea.", Report 83-21, US Army CRREL, Hanover, NH.

Table - The morphological parameters of stamukhas and ice gouges

Study area	Dates of the study	Average water depth, m	Dimensions of stamkhas			Ice gouge parameter		
			Maximum sail height, m	Length m	Width m	Length m	Width m	Depth m
Odoptu	03,1985	14,5	4.05	39	18	75	30	2.0
Odoptu	3-4,1985	11.5	3.32	52	30	-	-	1.1
Odoptu	04,1985	12.6	3.89	50	27	-	-	1.8
Sakhalin Bay	02,1986	6.2	10.59	83	44	45	26	2.0
Sakhalin Bay	02,1986	10.0	7.97	150	40	42	25	2.13
Sakhalin Bay	02,1986	7.5	6.64	89	60	-	-	1.17
Sakhalin Bay	02.1986	6.2	6.41	67	42	56	20	1.64
Sakhalin Bay	2-3,1986	6.6	6.73	58	44	20	20	1.37
Sakhalin Bay	03,1986	6.4	8.57	112	30	38	20	1.39
Sakhalin Bay	03.1986	6.6	5.95	97	48	-	-	0.5
Odoptu	03,1987	6.0	6.27	50	37	-	-	0.5
Odoptu	03.1987	7.0	2.1	18	16	-	-	0.5
Odoptu	03,1987	9.61	4.39	102	51	-	-	1.0
North Bay	03,1989	9.0	4.63	24	22	-	-	-
North Bay	03,1989	9.0	9.1	70	20	-	-	-
Odoptu	03,1990	13.07	6.52	47	38	-	-	0.3
Odoptu	03,1990	15.88	6.2	40	36	-	-	0.5
Odoptu	03,1990	14,62	6.0	48	32	-	-	0.4

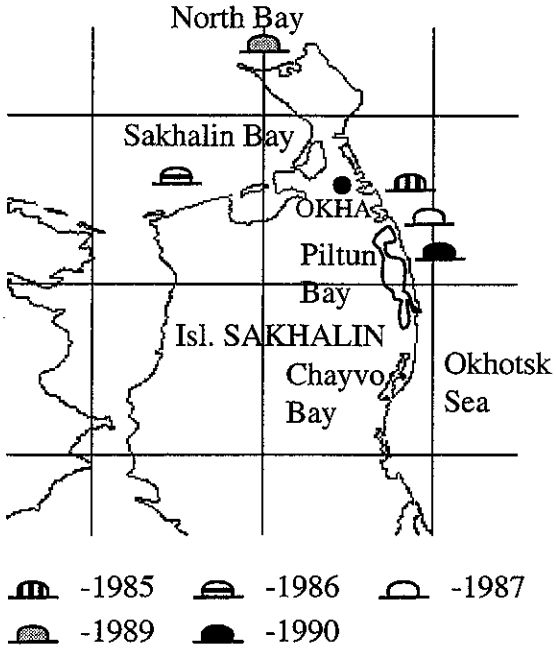

Figure 1. Stamukha thermal drilling sites for the ice gouge study

Seabed Scouring by Sea-Ice: Scouring Process and Impact Rates: Canadian Beaufort Shelf

S.M. Blasco[1], J.M. Shearer[2] and R. Myers[3]

1. Geological Survey of Canada, Dartmouth, Nova Scotia, Canada
2. J.M. Shearer Consulting, Ottawa, Ontario, Canada
3. Canadian Seabed Research Ltd., Porters Lake, Nova Scotia, Canada

Abstract

From 1974 to 1990, transects of the seabed of the Canadian Beaufort Shelf were mapped repetitively using sidescan sonar and echo sounders. These data have been analyzed to determine the spatial and temporal distributions of new ice scour characteristics including morphology (depth below undisturbed seabed, width from berm crest to berm crest, incision width at undisturbed seabed, orientation etc.), density and impact rates (Myers et al, 1996) . A few individual ice scour events were also mapped to document variation in scour morphology along their axes. The results of the ice scour tracking of a particularly deep event, and the determination of seabed impact rates for new ice scours are discussed below.

Tracking an Ice Scour Event

The longest and deepest ice scour observed to date on the Beaufort Shelf was crossed 86 times by sidescan and echo sounder profiling systems and mapped along axis to determine variations in orientation, scour depth, width, infill and rise-up. This scour, N90-2 (Myers et al,1996) which starts as a double keeled event and ends as a single keeled event is located on the central shelf in water depths ranging from 53 to 41m. N90-2 occurs in marine clays, has a length of 50.5 km and a maximum depth of 8.5m. The pressure ridge keel which generated this extreme event had a depth of approximately 55m (water depth plus scour depth where the scour was first observed on profile data). Ice keel depths of 56 to 58m have recently been observed by submarine profiling of the Arctic sea-ice canopy by Wadhams (pers. comm., 1998).

The scour is first observed in 53m water depths as a 2m deep double keeled event which heads eastward between 80° and 100° over a distance of 28km. The ice keel then rotates, crosses over itself, and heads westward, as a single keeled event, in a direction which varies from 235° to 280°. From the cross-over (a loop 4km in length) the scour traverses an additional distance of 18.5km before disappearing as a 5.5m deep event, in 41.5m of water, in a maze of newer scours. In plan view the scour path resembles a large 'V' pointing east. In general, the scour path is straight, but becomes sinuous along some segments and is subject to abrupt but subtle changes in direction. On the easterly trending, northern leg, changes in the relative positions of the 2 keels suggest significant rotation of the ice floe along track. On the westerly trending southern leg the 2 keels have rotated into an in-line configuration to generate a single keel event.

Scour depth varies between 2 and 8.5m along axis, but most commonly varies between 6 and 8m. Along the first 12km of the northern leg, scour depth increases from 2 to 7m as the ice keel

incises deeper into the seabed. Along the balance of the northern leg and for most of the southern leg (38.5km) scour depth undulates between 6 and 8m. This 2m variation in scour depth along this long segment appears to parallel the variation in thickness of the surficial marine clays. At the maximum scour depth of 8.5m, the surficial clays also reach their maximum thickness of 10m. Over this 38.5km stretch, in which water depth decreases, the scour base elevation (scour depth plus water depth) closely follows the bathymetry, resulting in significant scour rise-up.

Over its full length, scour N90-2 experiences a vertical rise-up of 8m over a distance of 50.5 km. The base of the scour rises up from 55m to 47m relative to sea surface. Scour N90-2 is first observed in 53m water depths with a scour depth of 2m and disappears in 41.5m water depths with a scour depth of 5.5m, a difference of 8m. If the ice keel was to be subsequently exposed to deep water again, it is not clear whether or not the keel would drop down the 8m it was observed to rise up.

Scour width decreases from 80 to 20m along track and incision width decreases from 50 to 15m. Width appears to vary as a function of keel orientation (double or single event) as well as scour depth. Berm width varies from 5 to 75m along axis while berm height varies from less than 0.5m to 4m. In general berm size appears to vary with scour depth.

Scour N90-2 is infilled along its entire length. This infill varies both in thickness and character. Along the northern leg the infill varies from 1 to 2 m in thickness and appears unstratified. Along the southern leg sediment infill is stratified with 2 dominant layers. The lower layer varies from 1.5 to 2m in thickness and is acoustically similar to infill found in the northern leg. This lower layer is overlain by another layer 0.6 to 0.8 m thick. Why the infill differs between the northern and southern legs is not clear. Infill pinches out on the sidewalls of the scour, suggesting differential deposition resulting from current action. In addition, scour N90-2 is locally infilled with sediment piles deposited by newer scours as they intersect and cross-cut N90-2. The origin of the infill is not clearly understood and could result from a number of contributing processes: fall-back and settlement immediately following scouring, pelagic sediment rain, cross-cutting scour deposits, and seabed and berm erosion. Aging scours by estimating infill sedimentation rates may be of limited value unless infill processes are clearly understood.

Nevertheless, the age of scour N90-2 was estimated by applying regional sedimentation rates of 1mm per year to the pelagic infill thickness. By this process scour N90-2 would be approximately 2000 +/- 200 years old. Knowing predicted scour impact rates for these water depths (0.0075 impacts/km/yr, next section), the number of newer scours crosscutting N90-2 (approximately 10/km) and allowing for superimposition (next section) results in an estimated age of 2000 +/- 200 years. The deepest and longest scour observed on the shelf may be approximately 2000 years old. Confidence in the calculated age is reinforced by the convergence of two independent methods of estimation. Improved understanding of sedimentation rates within scours and predicted scour impact rates have resulted in a scour age estimate in this paper which is 10 times older than first estimated by Myers et al, 1996.

Ice-Keel Impact Rates

The analysis of 16 years of repetitive mapping acoustic profile data from the Beaufort Shelf has resulted in the identification of 5329 new scour events and the generation of a database useful for both spatial and temporal analyses (Shearer and Blasco, in prep). Scour impact rates were calculated by using the database to determine the number of new scours per kilometre of seabed which have occurred between resurvey intervals of 1, 2, 4, 6, or 8 years. New scours were further binned into 1m water depth intervals (from 6 to 38m) and subdivided by scour depth class (<1m, 1-2m, and >2m) for the following analyses.

Scour impact rates calculated on a yearly basis resulted in a wide variation from year to year. For example, in water depths of 8-30m, yearly data compilations yielded impact rates which varied from 0 to 12 impacts/km/yr. Averaging data over a 6 to 8 year time interval reduced this variability to 0 to 3 impacts/km/yr. The occurrence of multi-keeled scour events mixed with single keeled events and/or the yearly variation in the seaward extent of the land-fast ice zone may be the cause(s) of the wide variation in impact rates. The presence of the land-fast ice limits both pressure ridge build-up and keel movement, thereby reducing the opportunity for scouring of the seabed.

The distribution of scour impact rates versus water depth appears to fit two distinct exponential distributions (data plots are linear on semi-log paper). The table below summarizes the key points on the impact rate curve.

Shallow Water

Water Depth	Impacts/km/yr
8m	1.5
20m	1.2
25m	1.0

Deep Water

Water Depth	Impacts/km/yr
20m	4.5
25m	1.0
30m	0.24
32.5m	0.1
35m	0. 048
40m	0.01
45m	0.002

On semi-log paper impact rate data plot up as two linear segments which intersect at the 25m isobath. The two observed distributions may result from impacts controlled by two different ice regimes - land-fast and dynamic ice zones. Impact rates for the land-fast ice appear to range from 1.5 to 1 impacts/km/yr for water depths of 8 to 25m respectively. Impact rates for the dynamic ice zone (including the shear zone) range from 4.5 to 0.01 impacts/km/yr for water depths of 20 to 40m respectively. The high impact rate at the 20m water depth fits the dynamic zone segment

of the exponential distribution, and may result from the significantly higher number of ice keels found in the shear zone and ice movement in this zone. High impact rates associated with the shear zone peak at the 20m isobath. The exponential distributions for the two ice regimes intersect at the 25m water depth. There is a significant decrease in scour impact rates beyond the 25m isobath. This may be due to the decline in pressure ridges (hence available keels for scouring) beyond the shear zone. The exponential distribution would predict an impact rate of 1 impact/km/100 years for water depths of 40m. In terms of actual data the deepest water in which a new scour has been documented is 38m (a single event 0.4m deep). A more rigorous statistical treatment of these complex data is required to refine the relationship of scour impact rates with water depth. However, the foregoing relationship appears robust and is remarkably consistent for different regions across the shelf, even separated by 200 km.

New Scour Depth Distribution

As noted above the new scours were binned into 3 scour depth classes: <1m, 1-2m and >2m, and their frequencies plotted versus water depth. Three distinct water depth zones with significantly different new scour depth regimes were observed. The 3 water depth intervals identified were 8-17m, >17-20m, and >20-35m. A significant change in the scour depth regime occurs in the >17-20m water depth range. In addition, scour depths do not appear to increase with water depth beyond the 20m isobath. The following table illustrates this change in scour depth regime with water depth interval. Depth data were normalized by totalling all the new scours within the specified scour depth interval and calculating the percentage contribution based on the total number of new scours in all classes. New scours generated by both first-year and multi-year ice are included in the analysis.

Water Depth	**Scour Depth Class**		
	<1m	**1 - 2m**	**>2m**
8 - 17m	96	3.8	0.2%
>17 - 20m	73	23.5	3.5%
> 20-35m	71	24	5%

Within the >17-20m and >20-35m water depth intervals the scour depths for all classes are similar, but differ significantly from the 8-17m water depth interval. This might suggest that the shallowest water depth interval is dominated by first year pressure ridge keels within the land-fast ice zone while the other 2 depth intervals are dominated by first-year and multi-year pressure ridge keels in the shear and dynamic ice zones. It is not clear whether the 0.2 % deep scour (>2m) contribution to the shallow water interval is due to a rare first year pressure ridge keel with an extreme depth or due to an odd multi-year keel which has scoured its way into shallow water. Whether first year pressure ridge keels have sufficient inter-block strength to scour to depths greater than 2m is not known. However, on the United States Beaufort shelf a first year pressure ridge keel within a floeberg scoured the seabed to a depth of 3 to 4.5m in 32m water depths in 1992 (Eldred, pers. comm., 1993). This may indicate that first year pressure ridges may scour more deeply than assumed.

Although scour impact rates do not vary across the shelf, scour depth distributions do change.

Scour depths decrease across the shelf from west to east. To demonstrate this decrease, two data sets from the 20-23m water depth interval from the western and eastern areas of the main shelf (survey lines 200km apart) have been summarized in the following table.

For the same water depth interval a significantly higher percentage of deeper scours occurs in the west. Geographically there is an abrupt change in scour depth regime at 133.5° west longitude. This longitude also defines the seabed transition between soft clays to the west and dense sands to the east. Seabed conditions may have some control on scour depth.

Location 20-23m Water Depth	**Percentage of New Scours in Scour Depth Class**		
	<1m	**1-2m**	**>2m**
west	41	50	9%
east	68	30	2%

Seabed Disturbance

Knowledge of scour impact rates and the scour density on the seabed (spatial frequency), allows for the calculation of the percentage of seabed disturbed over time by ice scouring. The number of scours on the seabed varies from 15 to 20 per km depending on scour width. Using the scour impact rates described above for specified water depths and assuming 20 scours per km, the percent of seabed disturbed over a 100 year interval can be calculated. To be accurate allowance must be made for scour superimposition, the chance that any new scour may overlap another new scour.

The scour impact rate at 25m water depths is 1 impact/km/yr. At 20 scours/km 5% of the seabed would be rescoured every year. Without superimposition the seabed would be totally rescoured in 20 years. However, in the second year of rescouring, 5% of the original 5% could be rescoured because of superimposition. As a result, after 20 years only 64% of the seabed would be disturbed. In this manner seabed disturbance has been calculated for differing water depths and illustrated in the table below.

Water Depth	**% seabed disturbed in 100 years**
8 - 25m	99
30m	70
32.5m	40
35m	22
40m	5
45m	1

At 40m water depth 5% of the seabed would be rescoured in 100 years. These results suggest that over geologic time scales sea-ice scouring of the seabed of the Beaufort Shelf is a significant bottom disturbance process.

References

Eldred, J., personal communication, 1993, ARCO Alaska Inc., Anchorage, Alaska.

Myers, R., S. Blasco, G. Gilbert, J. Shearer, 1996, 1990 Beaufort Sea Ice Scour Repetitive Mapping Program, Environmental Studies Research Funds, Calgary, Alberta. Report 129, 147 p., appendices.

Shearer, J.M., and Blasco, S.M., (in prep), Observations of Sea-Ice Rescouring Rates for the Canadian Beaufort Shelf, Geological Survey of Canada report.

Wadhams, P., personal communication, 1998, Scott Polar Research Institute, University of Cambridge, Cambridge, England.

An Approach to the Optimisation of the Burial Depth of Underwater Pipelines on the Arctic Offshore

Igor V. Stepanov[1 2], Oleg Ya. Timofeyev[12], Alexander V. Klepikov[1], Valerey N. Malek[1]

[1]State Research Center of the Russian Federation - Arctic and Antarctic Research Institute, St. Petersburg, Russia
[2] St. Petersburg State Marine Technical University, St. Petersburg, Russia

INTRODUCTION

When laying underwater pipelines in shallow water regions of Arctic seas, the task of analysing the risk of damage to these objects by keels of drift hummocks or icebergs appears before a designer. The conventional way for avoiding damage to pipelines is to bury them into the soil. To supply reliable protection of objects on one hand and to avoid excessive costs of laying and operation on the other hand, it is necessary to have the answer to the following question: At what minimum depth should the pipeline be buried so that the possibility of its damage would not be higher than some required value?

To provide an answer to this question was the aim of an investigation, carried out by the authors with reference to the designing of underwater crossing of Baydaratskaya Bay for systems of the pipelines «Yamal-Europe». The engineering research studies were developed by joint research team of Arctic and Antarctic Research Institute and St.Petersburg State Marine Technical University under contracts with «Eco-System» company. More recently the authors received funding from the Russian State Foundation for Fundamental Research. This work is aimed at the investigation of sea ice gouging in the western part of the Russian Arctic (mainly at Barents and Kara Seas). In this paper a brief overview of the developed approach and the results obtained from 1990 to 1998 are presented.

BAYDARATSKAYA BAY PIPELINE CROSSING: ENVIRONMENTAL CONDITIONS

Baydaratskaya Bay is located in the south-east part of the Kara Sea. The Bay is restricted by Yamal Peninsula in the north-east and by the main continent, Polar Ural Mountains region in the south-west. The total length of the crossing is about 70 km.

Seabed topography in the area of the crossing in presented in Figure 1 as lines of equal depth. With the exception of near shore parts of the route, the sea depth along the route varies from 12 to 21 m. This information about bathimetry, with corrections of depths along the route based on field sonar measurements, was extracted by the authors from navigation charts . The small crosses in the figure are knots of a mesh in which sea depth was specified for further simulation. Soils properties were fixed in the same points. The problem was that the geotechnical survey provided complete and exact information about soils properties only along the pipeline route. These data would be sufficient if soil along the route is harder than ice. The seabed itself in this case provides perfect protection of the pipeline against drift ice features. But usually soil strength

is less than the strength of ice. In this case maximum gouging depth depends on soil properties along the whole track of drift hummock movement, beginning from the first contact with the seabed until the end of the hummock motion. As the gouge length can reached many kilometers, the authors asked geothechnics to provide information about soil properties in the wide corridor along the pipeline route: its width was more than 40 km. The region of the crossing was subdivided into areas with near homogeneous soil properties (Figure 1).

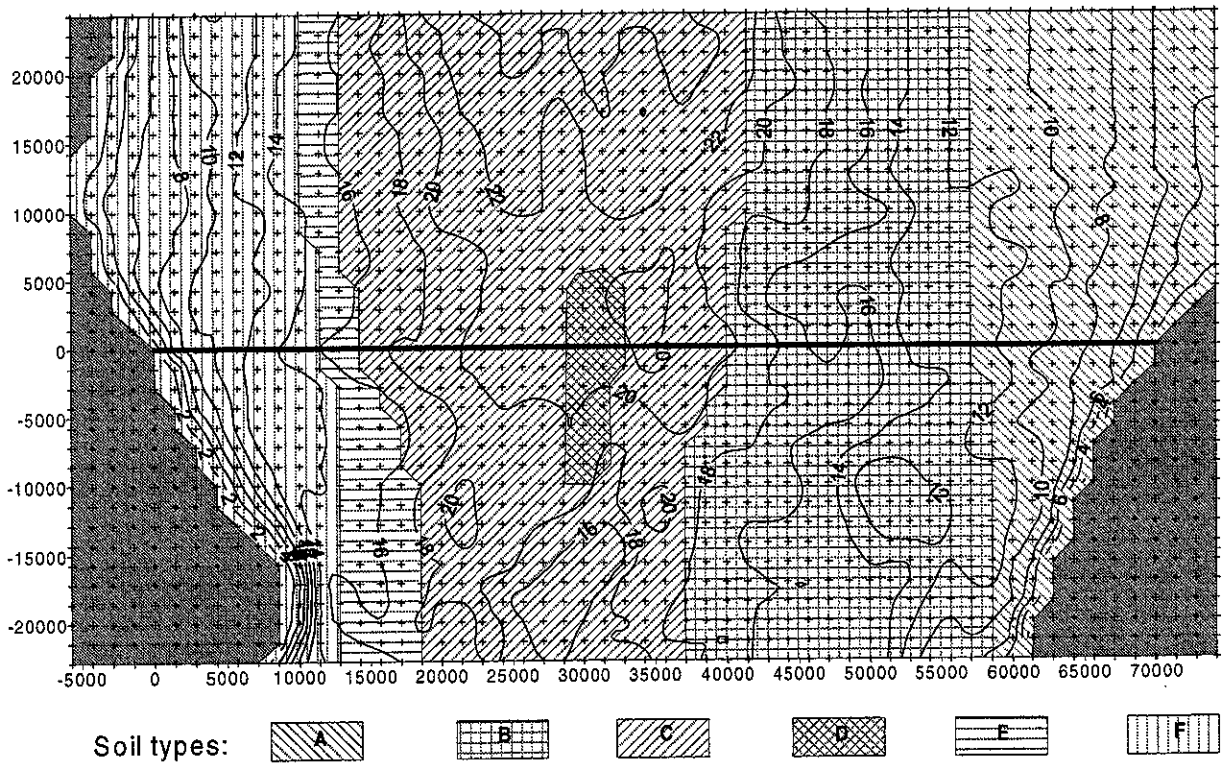

Figure 1. Bathymetry and seabed soils in the region of Baydaratskaya Bay pipeline crossing (the route of the crossing is shown in a solid thick horizontal line)

The information about currents was required for an estimation of hummock drift velocity. Current velocities were evaluated on simulation results and records of current moorings that had been installed along the pipeline route. The simulation was performed by the State Oceanography Institute. Tide and storm surge components of currents were taken into account. In such a way the authors received multi-dimensional probability distributions of current velocities dependent on the location of a considered point along the pipeline route and current direction. Hummock drift velocities were estimated on current velocities through drag coefficients.

Ice conditions in the region have the following peculiarities. The first ice in Baydaratskaya Bay usually appears in mid October. Ice thickness increases by 8-10 cm every 10 days on average during autumn and winter seasons. It reaches more than 1.2 m in February. Maximum ice thickness is about 1.7 m. Melting starts in May and the sea in Baydaratskaya Bay usually becomes ice free by July. The average duration of the ice free period is 65 days per year. Pressure ridge formation is very typical for Baydaratskaya Bay. Ice ridges usually cover 60% of the area. Both floating and grounded hummocks or stamukhas are observed in the Bay. Sometimes the

height of the stamukhas' sail reaches up to 10 m and even more. The most intensive seabed gouging begins when level ice melts and almost disappears. This point is important because it allowed the authors to assume that the gouging was caused by separate drift ice ridges and not ridged ice fields. Icebergs have never been observed in the Bay.

PREDICTION OF MAXIMUM GOUGING DEPTHS

The most natural and conventional way of predicting maximum gouging depths is by measuring these depths along the pipeline route with the use of a sonar. The problem is that measured depths are usually less than actual depths of penetration of hummocks' keels. This difference is more considerable in the case of weak soil (like sand). The furrow is partly infilled right behind the drift ice feature and further infilled due to wave and current action.

This is the reason why the authors developed a numerical procedure for predicting maximum gouging depths and then compared the theoretical predictions with the measurement data. The simulation is based on the Monte Carlo method, the application of which in this case may be presented in the following three stages:

- At the first stage, information about the investigated region is processed. Such data includes a topography of the sea bed, characteristics of soils, velocity and directions of currents and others. Additionally, as far as possible, a statistical evaluation of the laws of probability distribution and regression dependencies between fundamental parameters of ice features is carried out according to the results of the observations.
- The second stage involves formulating a deterministic model of the sea bed gouging by the ice feature which has known characteristics, moves with a definite velocity, and gouges the soil which has known properties. In this case the shape of that part of a hummock which interacts with the ground is assumed to be simplified.
- At the third stage, in the course of the computer numerical simulation, hummocks and other objects, processes and values of random character are simulated (or «generated»). The results of statistical analysis of the first stage are used for this purpose. Using these data plus deterministic values (topography of the seabed, properties of the soil) as input, and with the help of the dependencies obtained at the second stage, the process of gouging is simulated. Statistical processing of the simulation results allows us to evaluate the long-term probability distributions of the gouging depths and consequently, to specify the required profile of the burying depth of a pipeline.

Up to the present time the authors' investigations dealt with hummocks. This is the reason why the peculiarities of the shapes of these ice features were taken into consideration when simulating. However, if necessary, similar analyses may be carried out for simulating icebergs.

Aerial photographs were used as input data. Processing of aerial stereo photographs of ice ridges in the Bay provides an opportunity to simulate the shape and mass of hummocks in such a way that statistical characteristics of all basic shape parameters of the simulated ice features coincide with the same characteristics of observed natural ridges. (Description of the proposed approach and the obtained results are given in a paper by Igor Stepanov «Statistical Analysis of the Shape

Characteristics of Hummocks in Baydaratskaya Bay» in this volume).

Deterministic model of hummock/soil interaction developed by the authors based on similar ideas that were offered by Chari in his work on the gouging of the seabed by an iceberg. Some of Chari's assumptions (that if the bottom slope angle is small, the angle of internal friction of soil is small as well) were disputed. However the model remains quite simple, and this is important for the Monte Carlo procedure when we need to simulate many thousands of interaction events.

- In this model a hummock front which makes contact with the soil is assumed as an inclined rectangle. The angle of internal friction as well as the soil cohesion are taken into account. To calculate the resistance force of the soil against the movement of the hummock, an equation of the soil wedge equilibrium is used taking into consideration the following forces which act on the wedge (Figure 2):

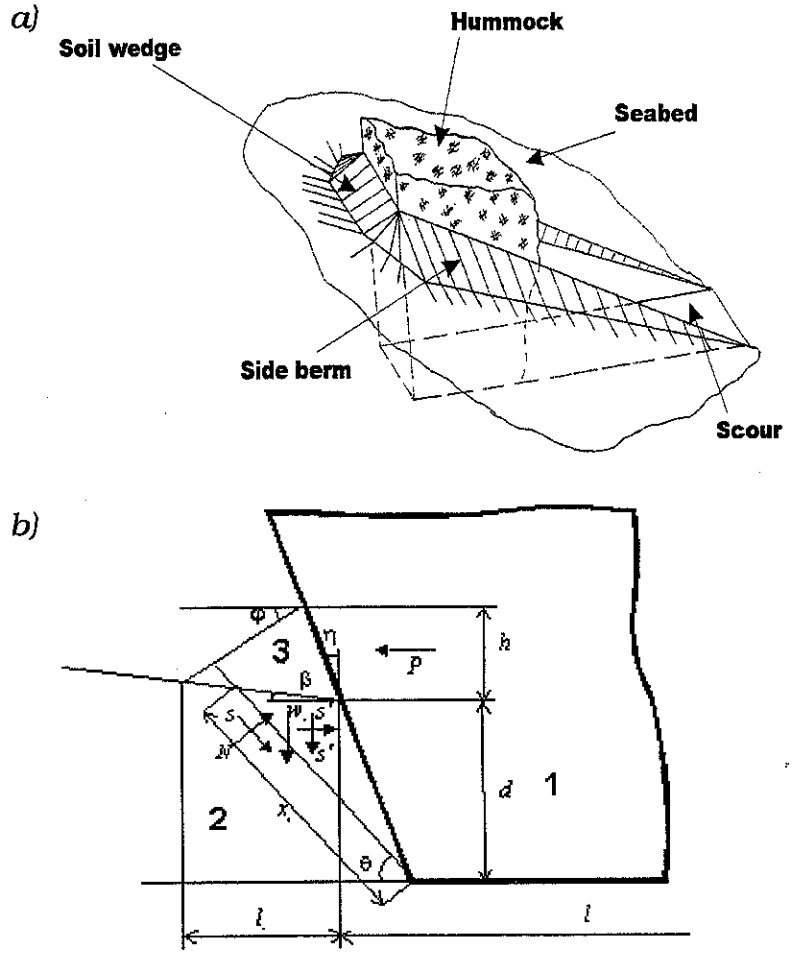

Figure 2. Interaction of a hummock with the seabed (a) and forces on the soil wedge that are taken into account (b).
***S, N** - tangential and normal components of the force of interaction of the wedge and stationary soil; **W** - weight of the soil wedge; **S'** - friction on the sides of the wedge.*
1 - hummock; 2 - seabed soil; 3 - soil wedge.

- tangential and normal components of the force of interaction of the wedge and stationary soil;
- weight of the soil wedge;
- friction on the sides of the wedge.

An expression for the soil resistance force is used; this force depends on the length of the furrow, the size of the berm ahead of the hummock, characteristics of the soil, the bottom slope, the width of the hummock keel and the angle of inclination of the hummock face. Besides, the equation between the volume of the furrow and the berm of ground ahead of the hummock, and on the side of the furrows involved, make it possible to represent the resistance force of the ground as a function of the furrow length.

With the understanding that the work of resistance force is equal to the initial kinetic energy of the ice feature, the total extent of the furrow is determined (initial kinetic energy is taken as a motional energy of the ice feature before its interaction with the ground). This allows the calculation of the maximum depth of the furrow which is relevant to the moment the hummock stops.

The described method of calculation is carried out for a uniformly sloping bottom. In the case of a more complicated topography of the sea bed, a model has been worked out in which the actual surface area of the bottom is presented as a number of plane sections. The slopes of some of these sections may be negative.

Probabilistic characteristics of the gouging depths are found from the results of the simulation of individual interactions between the hummocks and the soil at a given point. The interaction between the hummocks and the soil is simulated on a number of generated hummocks which interact with the ground at a random rate and in a random direction.

From the results of the simulation histograms of gouging depths being approximated by Waybull's distribution are obtained at examined points along the pipeline. Based on the estimates of the quantity of hummocks which pass above the point within a year and setting an excedance probability, a gouging depth within the rated period may be found. These calculations are to be performed for all chosen points along the pipeline, making it possible to obtain the results required.

By this means, it is possible to find profiles of expected maximum gouging depths of the soil within the life-time of the pipeline for a number of exceedance probabilities.

The authors understand quite clearly that any theory is only as good as can be proved by observation or measurement data. To obtain a quantitative comparison, a statistical analysis of side-scan sonar measurements which were performed by the company «Eco-System» in the region of Baydaratskaya Bay pipeline crossing was made. The results are presented on histograms in Figure 3.

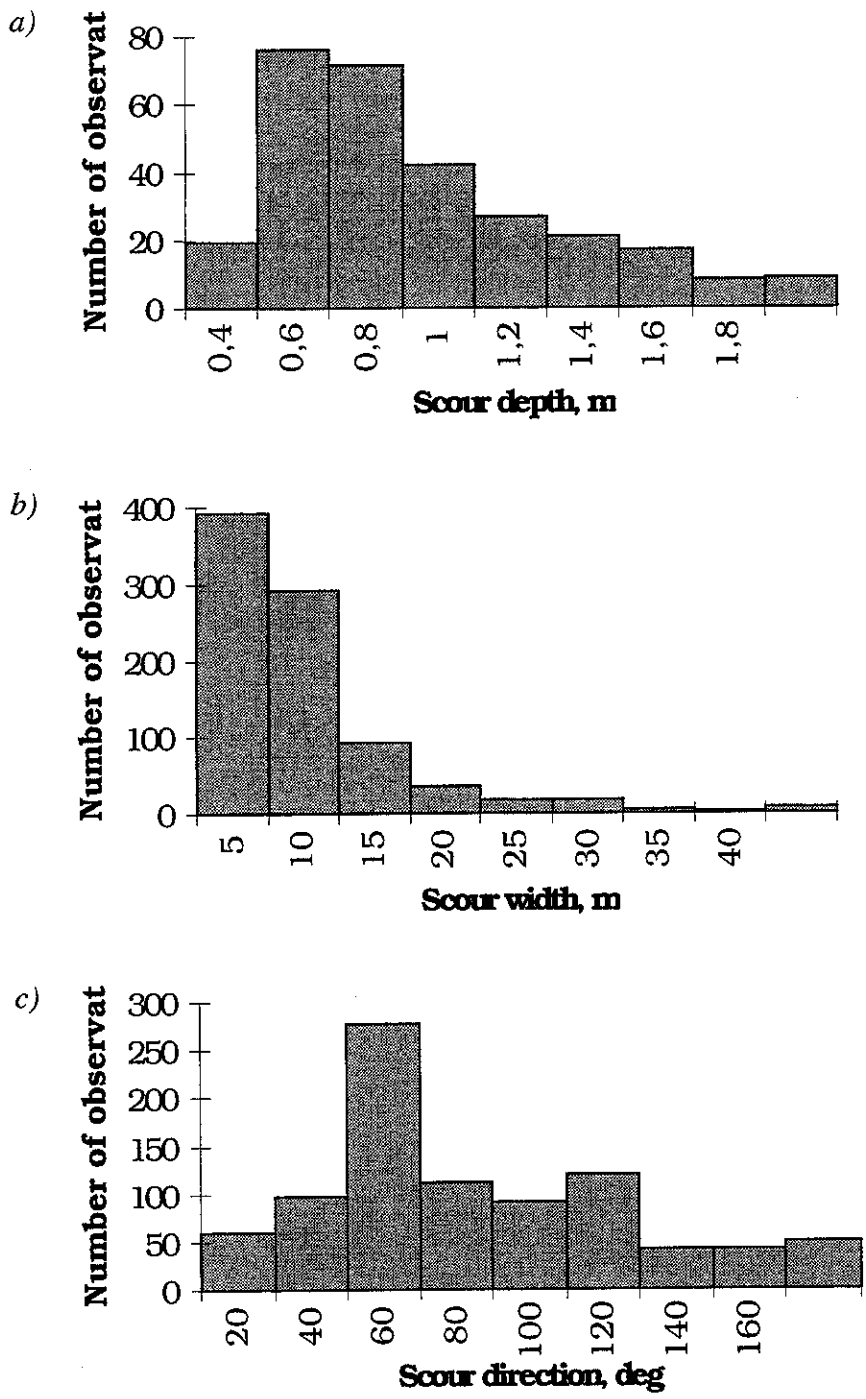

Figure 3. Distributions of gouge depth (a), width (b) and direction (c) (side-scan sonar observations)

Ice gouges were observed along the whole route of the pipeline crossing. The maximum fixed gouge depth was 2.2 m. Gouge widths were usually less than 20 m. The third diagram proves a

rather obvious fact that there are prevailing gouge directions. This prevalence will be more significant if we consider every particular point along the pipeline route. These three histograms were very similar to simulated probability distributions. But more importantly is the comparison of measured and predicted profiles of maximum gouge depth along the pipeline route. The comparison results are presented in Figure 4.

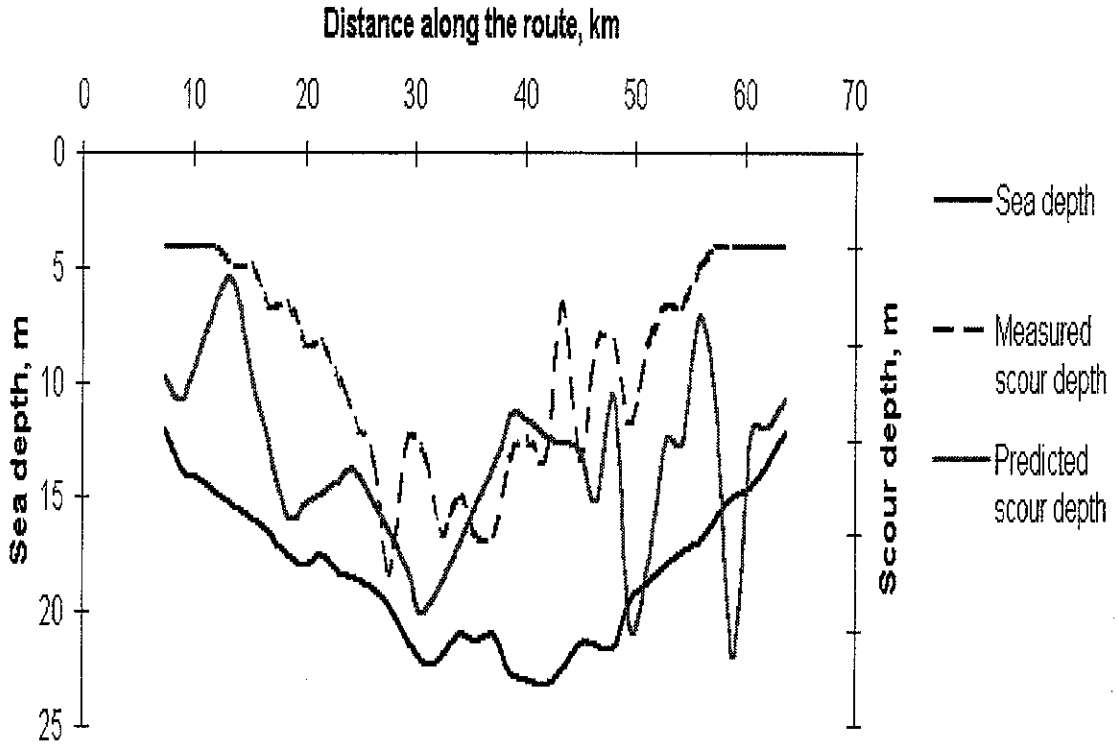

Figure 4. Comparison of theoretically predicted and measured gouge depth

Accuracy of the prediction is quite high for such a sophisticated problem. The discrepancy is considerable in parts of the route close to the shore. The authors assume that this is a result of more intensive infilling of the gouges in the area which has weaker soil.

ANALYSIS OF THE ICE/PIPELINE INTERACTION

The following three ice/pipeline interaction scenarios were considered (Figure 5):

- indirect interaction of a drift ice feature with the pipeline (through soil);
- direct impact of a drift ice feature against the pipeline;
- static action of the grounded hummock which is over the pipeline.

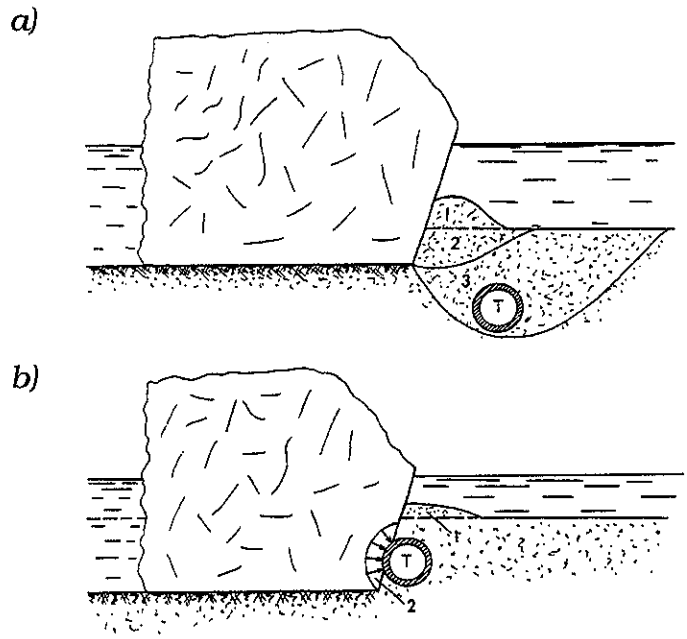

Figure 5. Scenarios of interaction of a drift ice feature with the pipeline. Indirect interaction of a drift ice feature with the pipeline (through soil) (a); direct impact of a drift ice feature against the pipeline (b)

It was taken into account that a hummock keel has voids filled by water and/or air. The relative volume of these voids, in accordance with data on the thermal drilling of hummocks in Baydaratskaya Bay, is 25 % in average. To overlap the average this parameter was varied in calculations from 0 % (solid ice without voids) up to 50 %.

The analyzed pipeline consisted of a steel tube 1.2 m in diameter and a concrete shell of 20 cm thickness. The steel and concrete were considered as linear materials; the relation between strain and stress in the soil was accepted as non-linear but time independent. Two variants of pipeline failure were distinguished:

- the cracking of the concrete shell, which is undesirable but not catastrophic;
- yield of tube still that was considered as a complete failure.

3D finite element modelling was used to estimate strains and stresses in the pipeline near the contact area. ANSYS and COSMOS software packages were employed for this purpose. For the analysis of the pipeline's response at a substantial distance from the contact area, a model that was similar to Winkler's foundation model, was introduced. It led to the necessity of solving Fredholm's integral equation and gave as output the bending moment and shear force distributions along the pipeline.

The results of this analysis were as follows:

- indirect interaction in any situation does not cause pipeline failure;
- stresses in the pipeline near the contact area never exceed acceptable levels (even if the

hummock's keel overlaps the pipeline diameter completely); this conclusion looks quite obvious taking into account the relation between the strength of ice and the strength of steel and concrete;

- direct impact of ice feature against the pipeline may cause pipeline failure at a distance of several tens of meters from the contact area and should be avoided.

It should be emphasised that although the proposed methodology of analysis of ice/pipeline interaction is quite general, the above written conclusions are applicable only for certain pipeline parameters and soil properties.

FINDING AN OPTIMAL BURIAL DEPTH

The main input information for obtaining an optimal burial depth is finding the probability distribution of maximum gouging depths and consequently, the pipeline failure for each section of the pipeline. It was assumed that the required reliability value is known as well. For this particular application, reliability was defined as the probability that during the life-time of the pipeline there would be no failure due to the action of an ice feature.

Strictly speaking, even with the same reliability there might be an infinite number of alternatives for the pipeline laying profile (i.e., having increased a laying depth of one part of the pipeline length and reduced that of another part, the same value of reliability may be obtained). Thus, it makes sense to formulate the problem of searching for an optimal profile of the pipeline burying depth, i.e. that profile whereby the cost of the pipeline laying, for example, is minimal, and the pipeline's reliability is not less than is required. It is also possible to use other optimisation criteria.

To solve this problem, methods of non-linear programming were applied. As a goal function, the cost of the pipeline laying was used; that cost was considered to be dependent on the technology of laying, sea depth, burial depth, soil type, etc. Any analytical or numerical procedure may be introduced as the goal function. Constraints taken into account were those arising from technological reasons and regulation requirements. In particular, a profile of minimal burying of the pipeline (the actual profile has to lie under that of the minimal burying profile of the pipeline) and minimal radius of the pipeline axis curvature were prescribed. Constraints are taken into account by introducing a penalty function that is minimised by modified Nelder-Meed method.

A computer software system based on this approach was developed. Figure 6 shows a computer screen-print as an example of carrying out the software system of searching for the optimal profile. The calculations resulted in recommended ordinates for the optimal profile of the pipeline burying.

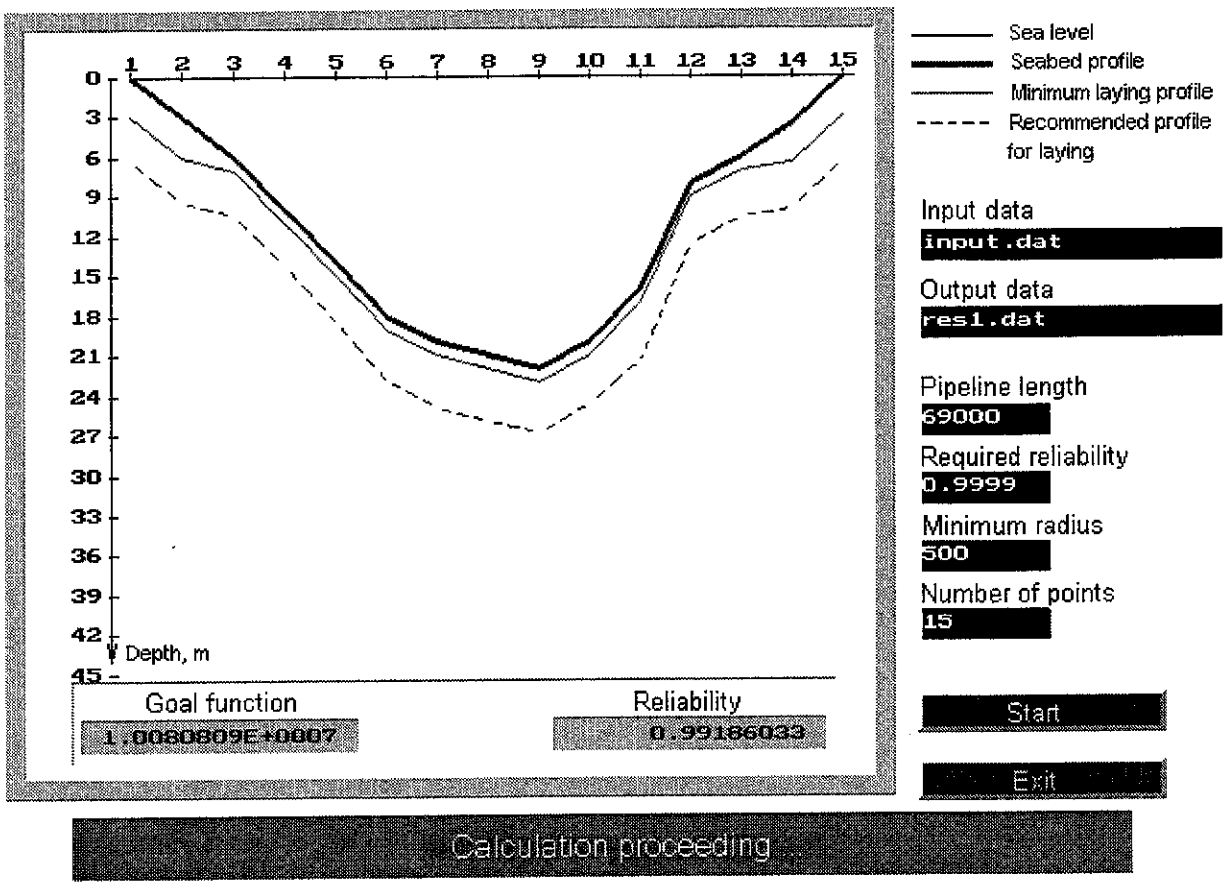

Figure 6. Computer screen-print: searching for an optimal burial depth profile

CONCLUSIONS

1.The described procedure provides an opportunity to solve the task: from the analysis of the environmental data to recommendations on an optimal profile of the pipeline burial depth.

2.The procedure is flexible enough to be adapted to a wide range of environmental conditions, pipeline peculiarities and technologies of the pipeline laying.

3.Theoretical predictions of gouge depth are proved with reasonable accuracy by measurement data.

4.A more adequate model of interaction of ice feature with soil (deterministic approach) and a wider range of ice features under consideration (not only separate ridges but also ice rubble fields like presented in Figure 7) are required to be included into the procedure.

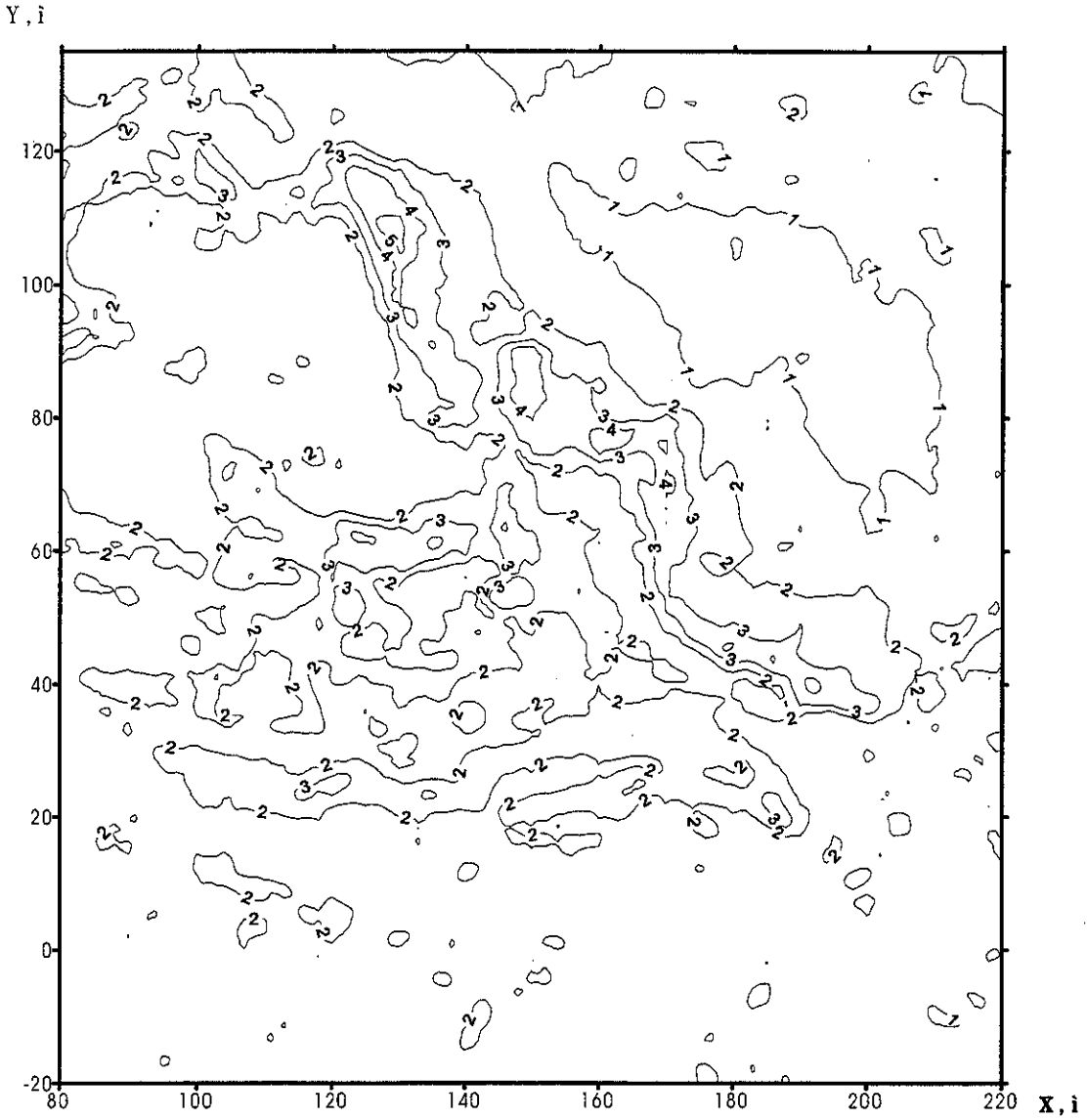

Figure 7. 3D plot of a rubble field (Kharasavey region, western cost of Yamal Peninsula)

W-12 Mechanical Model of Ice Gouging on Sloping Sandy Beach

Shinji Kioka, Hitachi Zosen Corp., Japan
Yuriko Terai, Nikken Consultants Inc., Japan
Natsuhiko Otsuka, North Japan Port Consultant Co., Ltd.
Hideki Honda, Department of Civil Engineering, Hokkaido University, Japan
Hiroshi Saeki, Professor, Department of Civil Engineering, Hokkaido University, Japan

Abstract

The coastal area facing the sea of Okhotsk in Hokkaido is annually covered with drifting ice. When these ice floes with a deep draft move toward the shore, they gouge sandy sea bottoms. Due to this ice gouging, marine resources along the shallow sandy coast are damaged, for example, seashells, buried structures and pipelines. In this study we describe the mechanism of ice gouging and obtain basic knowledge necessary to take preventive measures in future against damage by ice floes.

1. Introduction

When ice floes attached to the sea bottom of a shallow water area are moved to a shallower area by being pushed by an offshore ice field, they gouge the sandy bottom, a process called ice gouging. Reports exist of damage caused by this action of ice. For example, cases have been reported of some marine resources, such as sea urchins, being carried onto the shore while others were crushed to death by the weight of the sea ice itself; also buried structures have been damaged. To clarify the mechanism of ice gouging, we conducted a study of this ice action from experimental and theoretical bases, using a simple mechanical model. In our previous experiments, ice models of a rectangular parallelepiped were used, but the model ice used in this study was trapezoid in shape with a sloped front, similar to an actual ice floe, to use to study how ice forces acting on the sandy sea bottom change and how gouged surfaces change. This study was to not only understand the mechanism of ice gouging, but also to have a basic knowledge of how to take preventive measures against the kind of damage mentioned above.

2. Experimental Method

Fig-1 shows the devices used in the experiment. The bottom of a water tank was covered with sand and were inclined at 1/10 or 1/5. The bottoms were inclined steeply to make the model ice gouge more clearly, although in reality an ocean bed has a gentler slope. The sand used in the experiments is described later. An oil jack with a stroke moving up to 50cm horizontally was fixed to one end of the tank, then the model ice (described later) was installed in the front of the oil jack and was pushed in a horizontal direction at velocities of 0.4cm/s, 0.9cm/s and 1.7cm/s. The connector FREE, whose force of constraint acting on the vertical direction is rather weak, was set between the oil jack and the model ice, and a load cell was set between the FREE and the jack. Then the ice forces were measured by the load cell (the pushing force with the jack). At the same time, the horizontal distance from where the model ice began to move, i.e. gouging distance, and the gouging depth carved by the ice, were measured. Here, the ice made a small rotational motion; we regard this ice movement as approximately

horizontal because the angle of rotation was negligible.

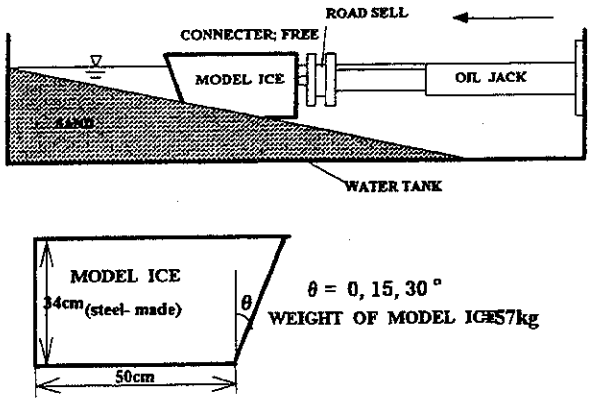

Sand used in the experiments
Grain diameter: 0.147 mm
Angle of internal friction: 37 °
Angle of repose: 34 °
Submerged unit weight: 0.0016 kgf/cm^3

Fig-1. Diagram of the experimental devices

3. Formulae of calculations for ice forces using a simple mechanical model

Various external forces act on the model ice (Fig-2). These include the earth pressure acting on the front and sides of the model ice, the subgrade reaction and dynamic friction acting on the bottom of the model ice, and the buoyancy of the whole model. We disregarded the consecutive changes in the internal friction angle, nonuniformity of relative density of sand and the problems of permeability, because they are complicated here.

We assumed that the model ice moves along a function, $Y = \zeta(x)$ (called the gouging curve in this study), and we made this ζ the curve of the sixth order by using the method of least squares, from the observed values. When this gouging curve is settled definitely, the ice force (F) of the model ice can be obtained from (1) the equation of motion in the horizontal direction, (2) the equation of motion in the vertical direction and (3) the stability conditions of the ice. At this time, the ice force (F) corresponds to the pushing force with the oil jack in this experiment.

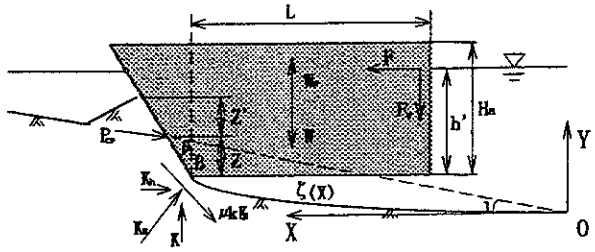

Legend
Z'; accumulation height of sand, Z; gouging depth, W; weight of the model ice, W_F; buoyancy, K; subgrade reaction in the vertical direction, F; ice force, F_V; frictional force in the vertical direction between the model ice and the connector, h'; draft of the model ice, H_a; height of the model ice, μ_k; coefficient of dynamic friction between the model ice and the sand, P_{cp}; passive earth pressure

Fig-2. Mechanical model for ice gouging

3-1. Earth pressure (P_{cp}) acting on the front of the model ice

The earth pressure acting on the front of the ice is passive earth pressure. When using the Coulomb model, it is expressed as the formula (1). The sand in front of the ice has a two-angled slope.

$$P_{CP} = \frac{1}{2}\gamma H^2 B K_P \qquad (1)$$

Here,

$$K_P = \frac{\cos^2(\alpha+\phi)}{\cos^2\alpha\cos(\alpha-\delta)\left\{1-\sqrt{\frac{\sin(\phi+\delta)\sin(\phi+i)}{\cos(\alpha-\delta)\cos(\alpha-i)}}\right\}^2}$$

$$\alpha = \cot^{-1}\left[\frac{\{\tan(\beta-\theta)+\tan(i+\theta)\}\cos i+(z'/z)^2\sin i}{(z'/z)^2\cos i+\sin\theta\{\tan(\beta-\theta)+\tan(i+\theta)\}}\right]$$

$$H = \frac{Z\cos(i+\theta)\cos i}{\cos(i+\alpha)\cos\theta}$$

where B is the width of the ice, and δ is the friction angle

between the ice and the sand.

3-2. Earth pressure (P_s) acting on the sides of the model ice

The earth pressure acting on the sides of the ice can be active, at rest or passive, depending on the situation. In the experiments, a little great passive earth pressure was adopted.

$$P_s = \gamma K_{ps}\left[\int_{\kappa}^{X}\int_{0}^{Z'(\xi)}\eta\,d\eta\,d\xi + \int_{X}^{X+(Z+Z')\tan\theta}\int_{\xi\cot\theta}^{Z'(\xi)}\eta\,d\eta\,d\xi\right] \quad (2)$$

here κ meets $Z'(\kappa) = 0$.

$K_{ps} = \tan^2(\pi/4 + \phi/2)$

The gouging depth (Z) is expressed as follows:

$$Z = X\tan i - \zeta(X) \quad (3)$$

Here, $\zeta(X)$ is the gouging-curve, which is the locus of point B in Fig-2.

3-3. Accumulation height of sand (Z') during the movement of the ice

On the assumption that with no compression of sand and no decrease in the spaces between the sand grains, the quantity of the sand pushed aside by the model ice is equal to the sum of the quantity accumulated at the front and the quantity that flows out to the sides of the ice, and that the underwater angle of repose is constant at any place, its relationship can be expressed as follows:

$$\frac{1}{2}\frac{\cos(\theta-\beta)\cos(i+\theta)}{\sin(\beta+i)\cos^2\theta}Z'^2(X)B = B\left[\frac{1}{2}Z'^2\tan\theta(1-\tan\theta\tan i) + \int_0^X\{\xi\tan i-\zeta(\xi)\}d\xi\right] - \cot\beta\int_0^X Z'^2(\xi)d\xi \quad (4)$$

Here, when we use the following formula,

$$N = \frac{B}{2}\left\{\frac{\cos(\theta-\beta)\cos(i+\theta)}{\sin(\beta+i)\cos^2\theta} - \tan\theta(1-\tan\theta\tan i)\right\}$$

the general solution of the formula (4) is

$$Z'(X) = \frac{1}{N}\left\langle\exp\left(-\frac{\cot\beta}{N}X\right)\left[\int\exp\left(\frac{\cot\beta}{N}X\right)\{X\tan i-\zeta(X)\}+C\right]dX\right\rangle^{\frac{1}{2}} \quad (5)$$

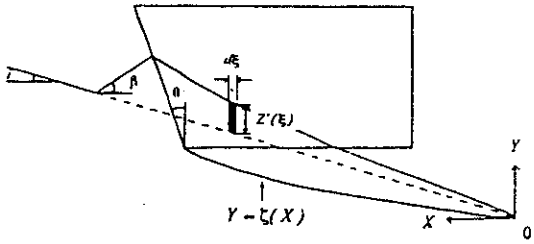

(a) side view

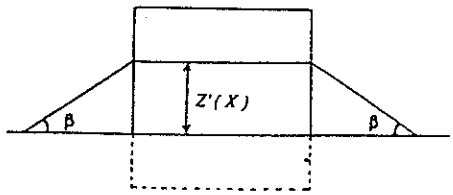

(b) front view

Fig-3. The model to calculate the accumulation height of sand

3-4. Equation of motion in the horizontal direction

The equation of motion of the ice is expressed as follows:

$$F - P_{CP}\cos(\alpha-\delta) - \mu_k(2P_s + K) - K\frac{d\zeta}{dX} = 0 \quad (6)$$

3-5. Equation of motion in the vertical direction

Since the velocity of the ice is constant in the horizontal direction, the acceleration is zero. However, the acceleration occurs in the vertical direction because we assumed that the ice moves along a function $\zeta(X)$. Consequently,

$$-MV_0^2\frac{d^2\zeta}{dX^2} + K\left(1\pm\mu_k\frac{d\zeta}{dX}\right) - W + \left(h'B + \frac{1}{2}h'^2\tan\theta\right)B\gamma_w \pm F_v - P_{cp}\sin(\alpha-\delta) = 0 \quad (7)$$

h' is the draft, and when h_o serves as the initial draft in X = 0, the following formula is obtained:

$$h' = h_o - \zeta(X) \quad (8)$$

3-6. Frictional force (F_v) acting on the back of the ice between the ice and the connector FREE

The ice has a subtle rotational motion. Assuming that the motion is horizontal, the following formula can be obtained from the equilibrium of moment at point B:

$$F_v = \frac{1}{L}\left[\begin{array}{l}\left(h'B + \frac{1}{2}h'^2\tan\theta\right)B\gamma_w L_G - WL_G - \frac{H}{3}P_{ep}\cos(\alpha-\delta) \\ -MV_0^2\frac{d^2\zeta}{dX^2}L_G - M_B + \{h-\zeta(X)\}F\end{array}\right] \quad (9)$$

where M_B is the moment with respect to point B on which the earth pressure on the sides of the ice acts, and L_G is the location of the center of gravity of the ice (from point B).

From the above description, the unknown quantities are F, K and F_v, all determined by the formulae (6), (7) and (9). As a result, the calculations for the ice forces can be made. Nevertheless, for $d\zeta/dX < 0$, the distribution of the subgrade reaction (K) or the location it acts on can be the unknown quantity, but it is considered to be approximately the same as for $d\zeta/dX > 0$.

4. Results and discussion

Figs-4(a), (b) and (c) show the cases with a slope gradient of 1/5, and (d), (e) and (f) a slope gradient of 1/10. Each graph compares the results with the angles of inclination, θ, of 0°, 15° and 30°, at the front of the ice. The plotted symbols are the observed values, while the curves are the calculated values. Below each graph are the gouging curves corresponding to the ice forces at each angle of inclination. At θ = 0°, 15° and 30°, there was a little dispersion when comparing the ice forces and clear correlations were not confirmed, that is, the systematic differences were small. On the other hand, it was confirmed that the gouging curves corresponding to the ice forces at each angle of inclination have almost systematic relationships. As θ increases, $\zeta(X)$ increases, hence a gouging extent tends to be small. The small systematic differences in the ice forces, although the $\zeta(X)$ differed, seems to be because $\zeta(X)$ was necessarily selected to make the quantity of work of the ice a minimum. We determined the formulae for the ice forces with the help of the observed value, $\zeta(X)$. If the above descriptions prove to be true, $\zeta(X)$ can be theoretically derived by introducing further parameters of the mechanical properties of sand. The ice forces increased while fluctuating, which shows a close relationship to the form of $\zeta(X)$. Actually, it was confirmed that when the inclination of $\zeta(X)$ (at the plotted point) is great, the ice force suddenly increases a little, and that when the inclination is gentle or negative, the ice force declines a little. This can be explained theoretically. However, we could not precisely reproduce this ice force by calculation because the observed values of $\zeta(X)$ and their least squared curves were not appropriate or themselves were not precisely reproduced.

Many of the calculated values agree relatively well with the observed values at i = 1/5. However, at i = 1/10, the observed values are a little greater, and they do not agree with the calculated values very well, probably because at $d\zeta/dX < 0$, the location on which the subgrade reaction (k) acted was not clear, and because the angle of rotation of the ice was neglected. In addition, the following causes are included: 1) During the movement of the ice, the consecutive changes in the mechanical properties of sand were neglected. 2) The coefficient of dynamic friction between the ice and sand was not constant. 3) The gouging curve, $\zeta(X)$, was not precisely reproduced. For these reasons, the formulae for calculations must be improved in future. At the same time, the behavior of the gouging curve must be clarified by theory or by systematic experiments, which remains to be solved in future because this study was made to obtain a basic knowledge.

5. Conclusions

The results of this study are:

1) The depth of gouging by ice varied according to the angle of inclination, θ, of the front of the model ice,

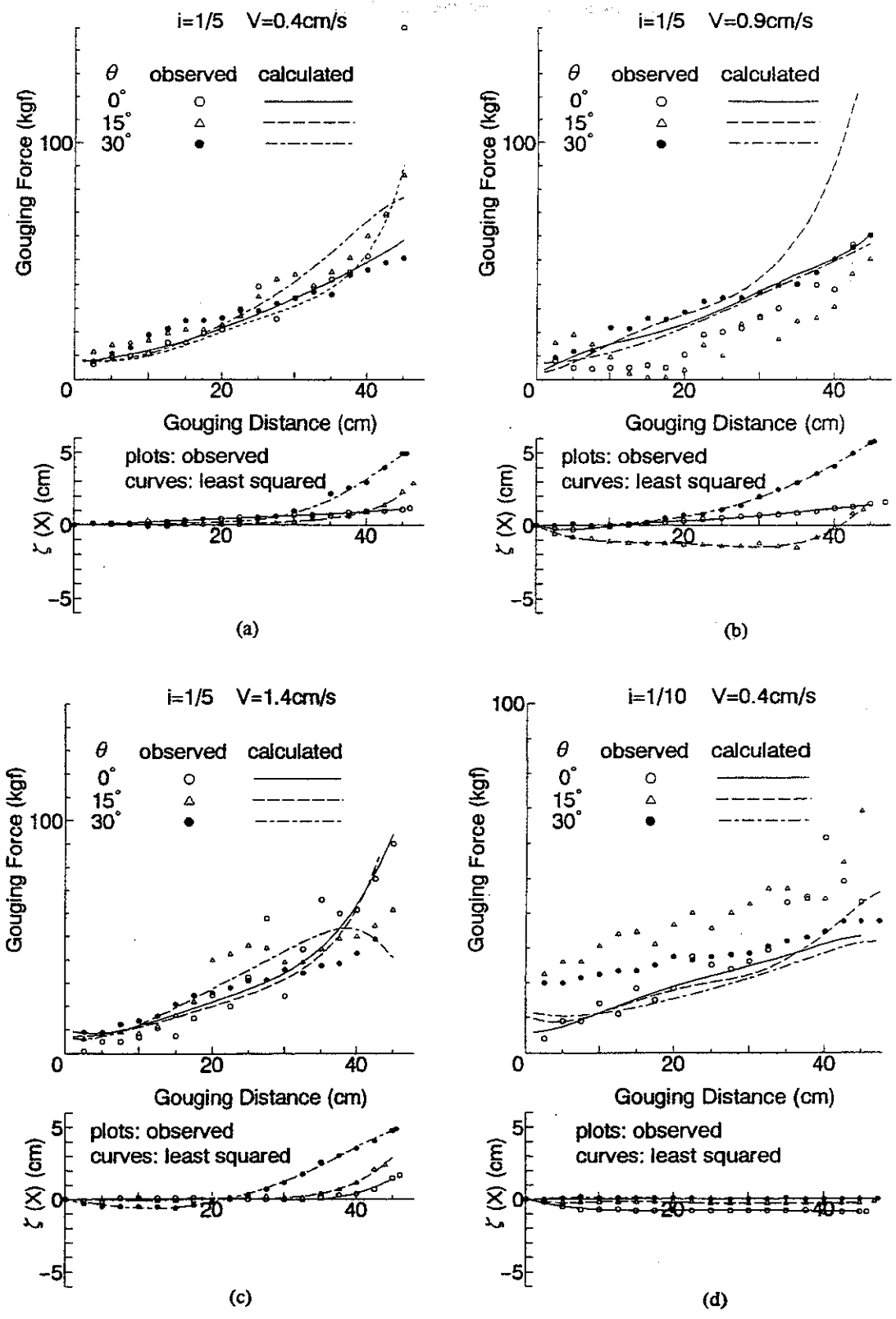

Fig-4. Comparisons of the ice force between the observed values and calculated values, and the relationships between the observed values and the form of gouged surface

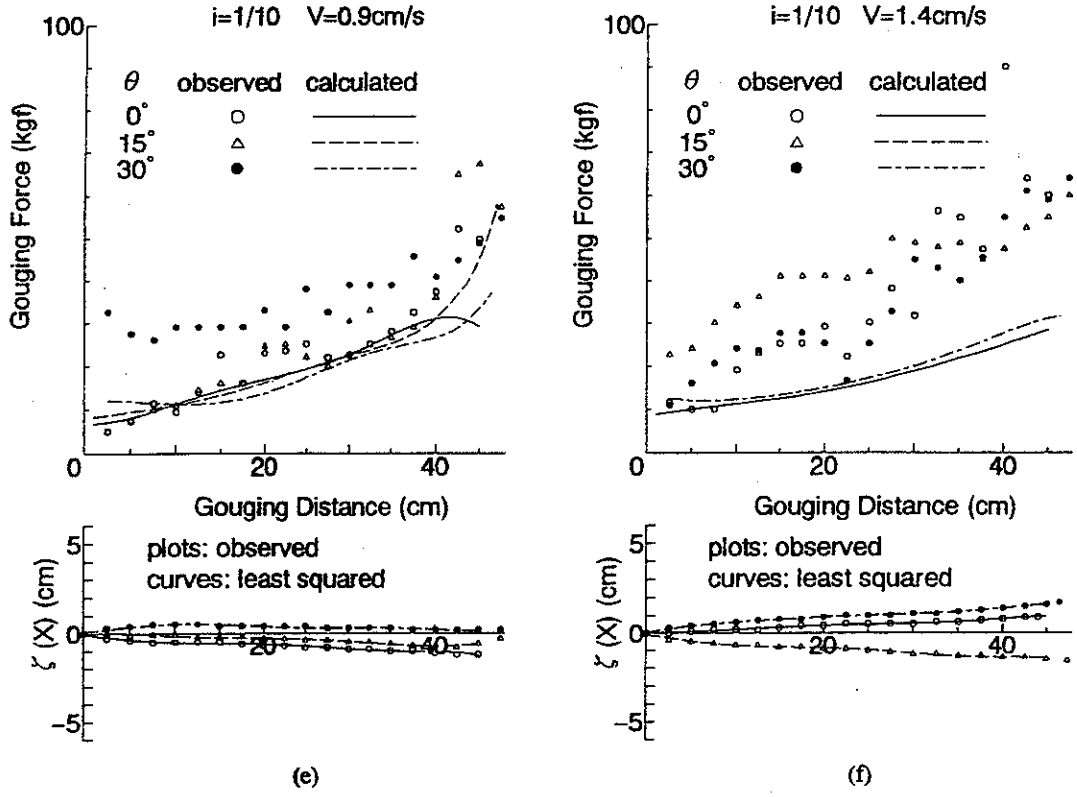

Fig-4. Comparisons of the ice force between the observed values and calculated values, and the relationships between the observed values and the form of gouged surface

and a tendency for the sand to be gouged less, as the θ increased, occurred.

2) No systematic differences occurred in the ice forces due to the difference in the θ.

3) For the changes in velocity of the movement of the model ice, the ice forces dispersed a little but they were not systematic differences.

4) When comparing the ice forces between the calculated values and the observed values, at an inclination of sand of 1/10, the observed values were a little greater, that is, they did not agree with the calculated values very well. However, at an inclination of 1/5, they almost agreed with each other.

5) The observed values of the ice forces depended greatly on the gouging curve or the inclination of the curve at the plotted point (the differential coefficient).

References

1) Kioka et al., (1995) Mechanism of Ice Gouging, Proceedings of Civil Engineering in the Ocean, Vol. 11, pp. 223-228.

2) Kioka, S. and Saeki, H., (1995) Mechanisms of Ice Gouging, Proceedings of Fifth International Offshore and Polar Engineering Conference (ISOPE), Vol. 2, pp. 398-402.

3) Kunimatsu et al., (1993) Damage of Fishery Resources due to Ice Gouging, Proceeding of Cold Region Technology Conference '93, pp. 381 - 386.

Statistical Analysis of the Shape Characteristics of Hummocks in Baydaratskaya Bay

Igor V. Stepanov[1 2]

[1] State Research Center of the Russian Federation - Arctic and Antarctic Research Institute, St.Petersburg, Russia
[2] St.Petersburg State Marine Technical University, St.Petersburg, Russia

SUMMARY

This paper contains a description of the approach to and the results of a statistical analysis as well as the application of these results to the simulation of ice gougings of the seabed. The main idea of the research was as follows. The author had all the information available concerning shapes of sails of several dozens of ridges. This was enough for the estimation of probability distributions of parameters of the ridges. But the problem was that thousands of simulated hummocks were required to perform the Monte Carlo simulation to obtain a reliable estimation of maximum gouging depths. Additionally, a procedure for the evaluation of the keel shape in dependence on the sail shape was required.

The input for the analysis was aerial stereo-photographs of ice ridge sails. The processing of these photos gave 3D plots of ridges like the one presented in Figure 1.

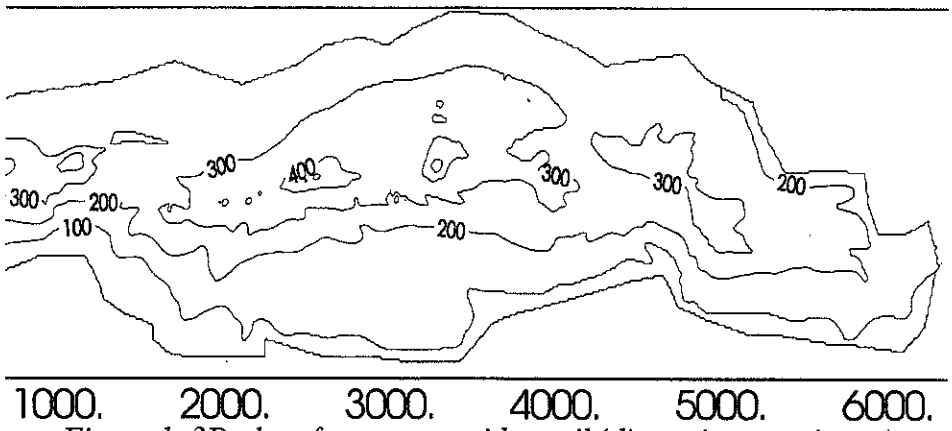

Figure 1. 3D plot of a pressure ridge sail (dimensions are in cm)

The data processing consists of the following steps:

- a rectilinear axis of a ridge was plotted for each feature;
- vertical sectional planes were passed through features perpendicularly to the axis at regular intervals;
- heights, widths of bases and areas of the resulting cross-sections were determined.

Further investigation was directed to the establishing of the probability distributions and regression dependencies for basic characteristics of above-water parts of ice features. As an

example a top-view of hummocks and its axis is shown in Figure 2 (crosses give crests of the ridges). Maximums in each cross-section were transferred to the vertical longitudinal plane passing through the axis of a hummock which gives a longitudinal profile of the hummock. Figure 3 presents plots of these resulting longitudinal profiles of the same ridges that are in Figure 2.

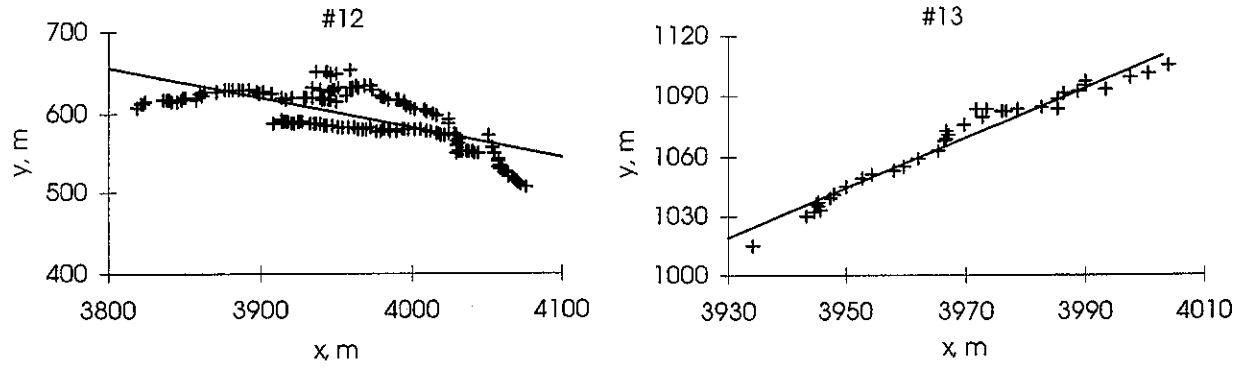

Figure 2. Pressure ridge crests

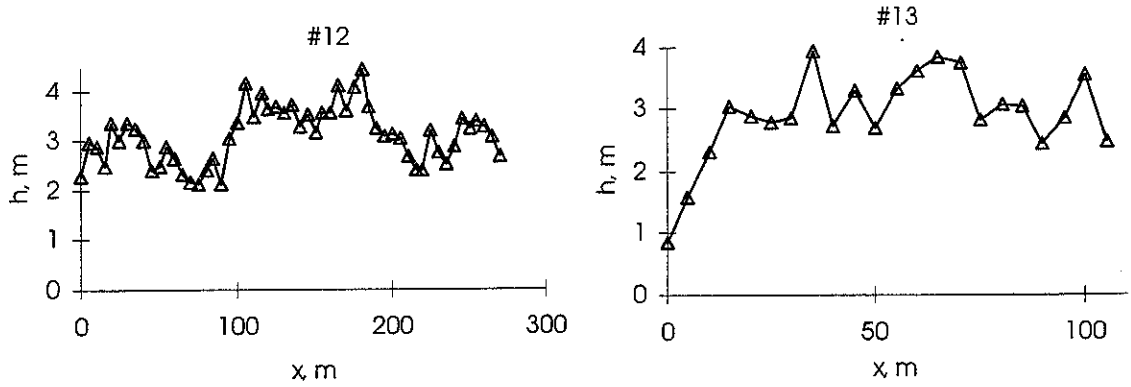

Figure 3. Longitudinal profiles of pressure ridge sails

Dependencies of the sail's cross-section area versus cross-section height and width of base were plotted and regressions were found (Figure 4). In accordance with Figure 4 sail heights of more than 10 m were observed. Floating hummocks with such heights of sails can not appear in the shallow region of Baydaratskaya Bay. Consequently, there were grounded hammocks (stamukhas). Meanwhile, as soon as no difference between the sail's shape of floating hummocks and stamukhas was detected, information about both categories of ice features was utilised. Another remarkable thing is that the angle of slope of both regression plots decreases with the increasing height h or width b. This means that cross-sections are not geometrically similar. Otherwise these plots should be linear. Consequently, the higher the sail the relatively narrower it is in a horizontal direction.

The following step was an estimation of probability distributions of ridge length and its average sail height (by definition, average sail height is mean value of coordinates of its longitudinal profile) and regression of standard deviation of longitudinal profile on average ridge height (Figure 5). The considered ice features were quite long: the average ridge length was equal 220 m with maximum value more than 400 m. Finally, the correlation function of longitudinal profiles was found (Figure 6).

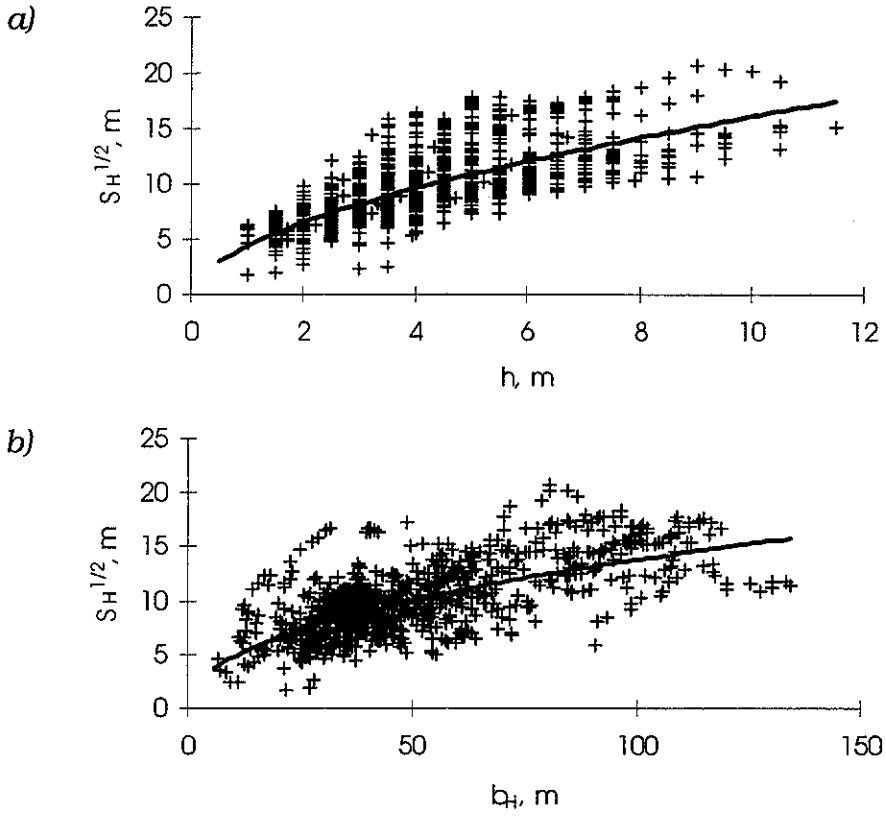

Figure 4. Regression of square root of sail's cross-section area S_H on height of the sail's cross-section h (a) and width of base of the sail's cross-section b_H (b)

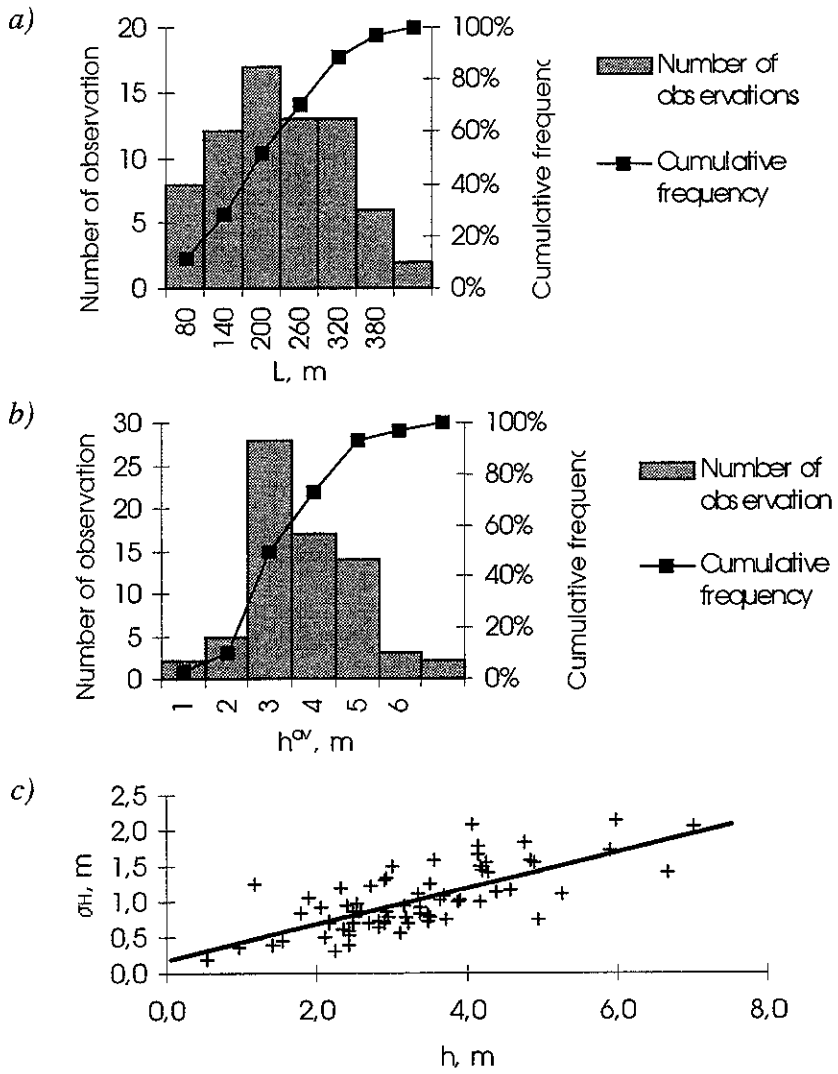

Figure 5. Distributions of ridge length L (a) and average sail height h^{av} (b); regression of standard deviation of longitudinal profile σ_H on average sail height h^{av} (c)

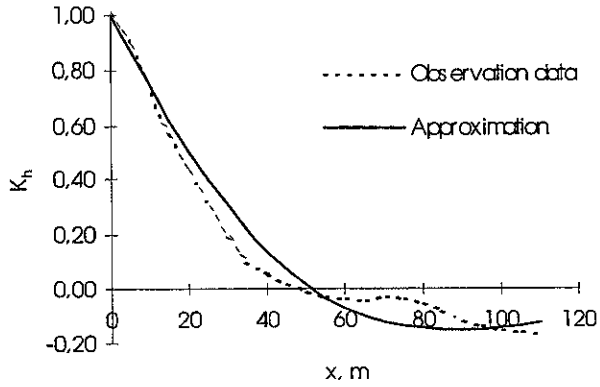

Figure 6. Correlation function of sail longitudinal profile: estimate and its approximation

The results of the above described statistical analysis was applied for ice ridges simulation (Figure 7) that was a component of the general procedure of the ice gouging in the Monte Carlo simulation.

The first step is simulation (we call it «generation») of the ridge length. This length is a definite number. The point is that the probability distribution, estimated on the simulated sample that consist of many «generated» lengths, should coincide with the probability distribution that was specified as input.

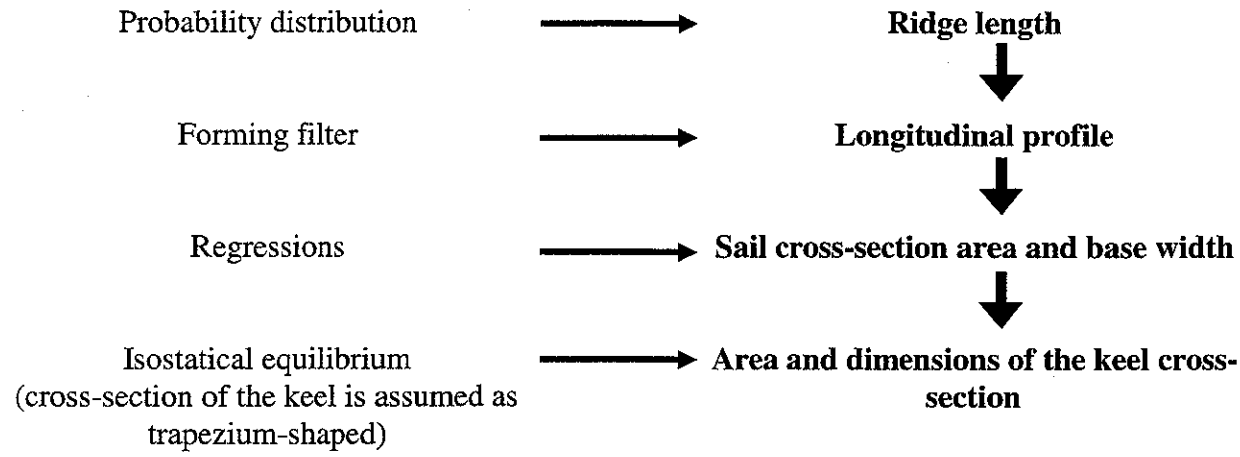

Figure 7. Flow-chart of ice ridge simulation algorithm

The following step is generating a longitudinal profile of the ridge. A forming filter method was applied for this purpose. The filter is a system of stochastic differential equations; for a particular case when the correlation function may be approximated by $K_h = e^{-\alpha|x|}\left(\cos\beta|x| + \frac{\alpha}{\beta}\sin\beta|x|\right)$ (see Figure 6) this equations are written as follows.

$$\frac{dH(x)}{dx} = f(x);$$

$$\frac{df(x)}{dx} = a_1 H(x) + a_2 f(x) + b_2 \varepsilon(x);$$

$$a_1 = -(\alpha^2 + \beta^2);\ a_2 = -2\alpha;$$

$$b_2 = 2\sigma_h \sqrt{\alpha(\alpha^2 + \beta^2)/\Delta x};$$

The system is stochastic because it includes a white-noise function ε, that is Gaussian distributed with zero average and standard deviation equal to one. The system is derived in such a way that its solution is a function with a correlation function that coincides with a prescribed correlation function. This solution is a «shape function» of a longitudinal profile: it has a zero average and a standard deviation equal to one. To get the profile, the shape function is multiplied by the generated value of standard deviation and a generated average sail height is added to the resultant function (plots presented in Figure 4 are used for the generating). Then using regression

dependencies, (see Figure 5) areas of the sail's sections and their width are calculated for a number of equi-distant cross-sections. In this way simulation of the ridge sail is completed.

To obtain the form of the ridge keel the following assumptions were employed:

- the hummock is to be in a position of isostatical equilibrium, i.e. the buoyancy force being proportional to the volume of the under-water part is equal to the gravitational force being proportional to the total mass of the hummock;
- the correlation function of the longitudinal profile of the sail coincides with that of the keel.

To supply an algorithm it was further assumed that the isostatical equilibrium is achieved in each cross-section. That assumption results in violating the relationship between the profiles of the sail and the keel that is observed under natural conditions. However, this violation is practically immaterial to calculate the process of gouging as the shape of the above-water part has no effect on it. Among the characteristics of the sail its mass is all that is necessary to simulate the gouging.

The next calculations are performed in the following order. The area of the under-water part of a cross-section is estimated on the condition that the gravitational force is equal to the buoyancy force. From the known empirical formulas under assumption that the under-water part of the cross- section is trapezium-shaped, values of the top (larger) and lower (keel width) bases are to be determined. This allows the calculation of the keel height. These steps are executed for a number of equi-distant cross-sections of the hummock which made assigning a total shape of the ice feature possible. Through the use of the numerical integration a volume of the hummock and consequently its mass are to be found. Thus the simulation of a hummock is completed.

CONCLUSIONS

1. Reliable statistical estimates of probability distributions and regression dependencies for all basic shape characteristics of ridge sails in Baydaratskaya Bay were obtained.
2. A numerical procedure for a simulation of hummocks' shapes was proposed; statistical characteristics of sails of simulated hummocks coincided with the characteristics of natural ice features.

THE 13TH INTERNATIONAL SYMPOSIUM ON OKHOTSK SEA AND ICE ICE AND THE ICE SCOUR & ARCTIC MARINE PIPELINE

STEADY-STATE ICE SCOURING OF THE SEABED

A.FORIERO

Associate Professor, Laval University, Civil Engineering Department
Pavillon Adrien Pouliot, Sainte-Foy (Quebec), Canada G1K 7P4
email: Adolfo.Foriero@gci.ulaval.ca

ABSTRACT

The seabed of coastal regions is frequently subjected to scouring or gouging by massive bodies of ice such as icebergs. This fact poses restrictions on the serviceability of marine pipelines and other related seabed structures. The extent of the scours depth and of the disturbed zone below is of utmost importance in their design. This paper describes an analytic approach based on the Strain Path Method that determines the stress and strain rate field in a creeping mode of deformation. The herein model is valid for a stationary state of stress, attained after a continuous redistribution from the initial elastic state. A conformal mapping scheme is utilized to transform the domain of interest to the complex plane thereby facilitating the determination of the velocity field. Finally a bounding technique based on the principle of virtual work is employed to determine a global force at the ice-soil interface.

INTRODUCTION

Ice scouring of the seabed is prevalent in the ice-overrun waters of the Northern shelves (Fig. 1). Generally the gouges produced as a result of scouring are several meters deep and induce deformations that extend deep into the ground. This fact is well documented in the abundant literature on the subject (Been et al. (1990), Palmer, A.C. (1993), Palmer et al. (1990a,b),Yang et al. (1996), Yang et al. (1994)) . Consequently trenched pipelines are susceptible to damage at depths below the maximum scour depth. The secure burial-depth of the pipeline must then be established as a preventive measure to failure, and is an integral part of the design process. An ice-scour model is therefore required in order to evaluate the extent of the disturbed zone via the strain field.

Herein the Strain Path Method is utilized to analyze the subscour soil deformations. This technique was developed by Baligh (1985) to describe the fundamental mechanisms of deep penetration in soil. By reason of the severe kinematic constraints during continuous or steady-state ice-scouring, strain rates are essentially independent of the shearing resistance of the soil. Therefore the ice-scouring problem is considered to be strain-rate controlled and deformation rates are determined based only on kinematic considerations

and boundary conditions. The deviatoric stress field is determined by specifying a constitutive model.

Marine soils, as other geologic materials undergo time-dependent deformations and stress relaxation under sustained loading. Time-dependent deformation results from both volumetric and shear stresses. The rate of volume change or volumetric creep results both from primary consolidation, governed by the expulsion of water from the soil voids, and by secondary compression, governed by the viscous resistance of the soil structure. In the present analytic model volumetric creep is discarded. The assumption is made that ice scouring under constant velocity is relatively rapid in saturated marine clays. Since the soil-deformation is too rapid for water to be expelled and the permeability of clays is low, an undrained condition is postulated. Instead the analytic model incorporates a constitutive equation based on deviatoric creep where time-dependent deformations are associated with distortions subjugated to no volume change.

IDEALIZATION OF ICE SCOUR

Figure 2 shows the region in the real and complex transformed plane. A two-dimensional plane strain analysis is carried out. The angle of attack of the ice keel θ is made variable with respect to the horizontal axis. From the point of view of an observer standing on an ice feature, the rigid ice keel acts as an obstruction to the moving sea-bed soil. To solve such typical problems one requires an expression for the complex potential given as

$$\Omega(z) = Vz + G(z) \tag{1}$$

where G(z) is such that

$$\lim_{|z|\to\infty} G'(z) = 0. \tag{2}$$

This physically means that at sufficiently great distances from the ice feature the absolute value of the velocity assumes a constant value (in this case V). A conformal mapping scheme is realized and a typical mesh for an angle of attack of 30° degrees (of the ice keel) is shown in Figure 3. This demonstrates the versatility of the conformal mapping generation scheme by observing that straight lines in the complex plane ζ (Fig.3a) transform into different curves emerging from the ice keel shape in the physical z plane (Fig. 3b), this with a simple change in the angle of attack of the ice keel.

The strain rates in the physical plane are expressed in terms of the velocities

$$\dot{\varepsilon}_{xx} = \frac{\partial V_x}{\partial x} \qquad \dot{\varepsilon}_{yy} = \frac{\partial V_y}{\partial y} \qquad \dot{\varepsilon}_{xy} = \frac{1}{2}\left(\frac{\partial V_x}{\partial y} + \frac{\partial V_y}{\partial x}\right) \tag{3}$$

in which $\dot{\varepsilon}_{xx}$, $\dot{\varepsilon}_{yy}$ and $\dot{\varepsilon}_{xy}$ are respectively the normal strain in the x-direction, the normal strain in the y-direction and the engineering shear strain. The velocities are solved for in the complex plane and transformed back to the real or physical plane. The effective strain rate

$$\dot{\varepsilon}_e = \left(\frac{2}{3}\dot{\varepsilon}_{ij}^c\,\dot{\varepsilon}_{ij}^c\right)^{\frac{1}{2}} \qquad (1 \le i, j \le 3) \qquad \textbf{(4)}$$

is obtained as

$$\dot{\varepsilon}_e = \frac{2}{\sqrt{3}}\left\{\frac{m^2\pi}{\sqrt{a^2+d^2}\,\sin(m\pi)}V\left(\xi^2+\eta^2\right)^{\frac{-2m-1}{2}}\left(\left(\xi-1\right)^2+\eta^2\right)^{\frac{2m-1}{2}}\right\} \qquad \textbf{(5)}$$

where V, m, d and a are respectively the ice feature velocity, the normalized angle of attack $m=\theta/\pi$, the scour depth , while $a = d/\tan(\theta)$ as depicted in Fig. 2.

CONSTITUTIVE CREEP MODEL

The constitutive equation adopted herein is chosen on the practical grounds that: 1) It has been applied extensively and is quite popular, 2) It is simple to understand, 3) It is easily incorporated in computer programs and 4) it requires a single step creep test at various stresses and temperatures.

A typical creep curve is shown in Fig. 4a. As observed application of a stress first leads to a period of transient creep, during which the strain rate decreases continuously with time, followed by creep at constant rate for some period of time, and if the shear stress is still increased an acceleration in the creep rate leads to failure.

In general the total strain ε is usually assumed to be composed of an instantaneous strain, ε_o , and a delayed or creep strain $\varepsilon^{(c)}$:

$$\dot{\varepsilon} = \varepsilon_o + \varepsilon^{(c)}. \qquad \textbf{(6)}$$

The instantaneous strain, may contain an elastic and a plastic portion while the creep strain is generally composed of both primary and secondary (steady-state) strains. For the present purpose stationary or secondary creep is considered, and accordingly

$$\varepsilon = \varepsilon^{(i)} + \dot{\varepsilon}_{\min}^{(c)} t \qquad \textbf{(7)}$$

where $\dot{\varepsilon}_{\min}^{(c)} = \frac{d\dot{\varepsilon}^{(c)}}{dt}$ is the minimum (or steady-state) creep rate and t is the time. Based on the available literature on creep (Hult(1966), (Ladanyi(1972a)), it is found that both $\varepsilon^{(i)}$ and $\dot{\varepsilon}_{\min}^{(c)}$ are expressed respectively as

$$\varepsilon^{(i)} = \varepsilon_k \left(\frac{\sigma}{\sigma_{k\theta}} \right)^k \tag{8}$$

and

$$\dot{\varepsilon}_{\min}^{(c)} = \dot{\varepsilon}_c \left(\frac{\sigma}{\sigma_{c\theta}} \right)^n \tag{9}$$

where $\sigma_{k\theta}$ is a temperature-dependent modulus corresponding to a reference strain rate ε_k, and $k \leq 1$ is an empirical exponent. Similarly in equation (8) $\sigma_{c\theta}$ is the temperature-dependent creep modulus, corresponding to the reference strain rate, $\dot{\varepsilon}_c$, while $n \geq 1$ is an experimental creep exponent. This dependency of the minimum creep rate on the stress in uniaxial tests is clearly indicated in Fig. 4b (Hult (1966).

The above mentioned parameters are determined by plotting the creep test results in the appropriate log-log plots (Ladanyi, 1972). However evidence suggests that a limited amount of data pertaining to creep tests on marine clays is available. Moreover those tests whose data is befitting are rarely amenable to equation (9).

Interestingly enough Vaid et al. (1979) published creep data of a clay block sampled from the site of the Saint-Jean-Vianney slide in Quebec in June 1971, by the Ministere des Ressources Narturelles du Quebec. The samples were provided by the courtesy of Laval University. The clay in these tests is better known as Leda clay and is believed to have been deposited in the marine environment during the postglacial period. This marine clay is defined as a very sensitive clay because it experienced leaching by percolating fresh water and also because of the cementation at the inter-particle contacts. Figure (5) shows the strain rate versus time under a constant deviatoric stress in undrained triaxial tests. One notice that strain rates decrease to a minimum and ultimately increase until rupture.

The minimum strain rate in these tests is plotted against the deviatoric stress in a log-log plot in order to determine the creep parameters of equation (9) for Leda clay (Fig(6)). Two sets of creep parameters are obtained by way of the curves determined by linear regression. For the clay originating in the upper and lower layer of the sampled-block the values of the creep-stress parameters are respectively:

Lower layer, n = 3.49, σ_c=525.0 kPa, $\dot{\varepsilon}_c$= 1.0x10^{-5} %/min. and

Upper layer, n = 6.31, σ_c=414.6 kPa, $\dot{\varepsilon}_c$= 1.0x10^{-6} %/min.

As expected and indicated by the n-values, the value of the clay sampled from the lower layer offers more resistance then that of the upper layer.

Here below a generalization of the state of stress and strain from the uniaxial to the triaxial state is achieved by assuming the validity of the von Mises flow rule and volume constancy for all plastic deformations including the creep strains. This generalization leads to the well-known Norton-Bailey power law creep equation

$$\dot{\varepsilon}^{(c)}_{e\,\min} = \dot{\varepsilon}_c \left(\frac{\sigma_e}{\sigma_{c\theta}} \right)^n \qquad \textbf{(10)}$$

where the equivalent stress, strain and strain rate are respectively

$$\sigma_e = \left(\frac{3}{2} S_{ij} S_{ij} \right)^{\frac{1}{2}} \qquad (1 \le i, j \le 3) \qquad \textbf{(11)}$$

$$\varepsilon_e = \left(\frac{2}{3} \varepsilon_{ij} \varepsilon_{ij} \right)^{\frac{1}{2}} \qquad (1 \le i, j \le 3) \qquad \textbf{(12)}$$

and

$$\dot{\varepsilon}_e = \left(\frac{2}{3} \dot{\varepsilon}_{ij} \dot{\varepsilon}_{ij} \right)^{\frac{1}{2}}. \qquad (1 \le i, j \le 3) \qquad \textbf{(13)}$$

In tensorial notation equation (10) is expressed as

$$\dot{\varepsilon}^{(c)}_{ij} = \frac{3\dot{\varepsilon}_c}{2\sigma_{c\theta}} \left(\frac{\sigma_e}{\sigma_{c\theta}} \right)^{n-1} S_{ij} \qquad (1 \le i, j \le 3). \qquad \textbf{(14)}$$

This allows us to solve for the deviatoric stress field S_{ij} in terms of the strain rate fields $\dot{\varepsilon}_{ij}$, specifically

$$S_{ij} = \frac{2}{3} \left(\frac{\sigma^n_{c\theta}}{\dot{\varepsilon}_c} \right) \sigma_e^{1-n} \dot{\varepsilon}_{ij} \qquad (1 \le i, j \le 3) \qquad \textbf{(15)}$$

which further reduces to

$$S_{ij} = \frac{2}{3}\left(\frac{\sigma_{c\theta}^{n}}{\dot{\varepsilon}_{c}}\right)^{\frac{1}{n}} \left(\dot{\varepsilon}_{e}\right)^{\frac{(1-n)}{n}} \dot{\varepsilon}_{ij} \qquad (1 \le i, j \le 3). \tag{16}$$

By substituting equations (3) and (4) into (16) and subsequently (16) into (11), the effective strain is obtained as

$$\sigma_{e} = \frac{2}{3}\left[\left(\frac{\sigma_{o}^{n}}{\dot{\varepsilon}_{o}}\right)\left(\frac{2}{\sqrt{3}}\right)\left[\frac{m^{2}\pi V}{\sqrt{a^{2}+d^{2}}\,\sin(m\pi)}\right]\left(\xi^{2}+\eta^{2}\right)^{\frac{-2m-1}{2}}\left(\left(\xi-1\right)^{2}+\eta^{2}\right)^{\frac{2m-1}{2}}\right]^{\frac{1}{n}}. \tag{17}$$

GENERAL ENERGY BOUND THEOREM

Generally the stresses σ_{ij} and strains ε_{ij} are obtained from W, the strain energy function and Ω, the complementary energy functions via

$$\sigma_{ij} = \frac{\partial W}{\partial \varepsilon_{ij}} \qquad \varepsilon_{ij} = \frac{\partial \Omega}{\partial \sigma_{ij}}. \tag{18}$$

Moreover the postulate for material stability formulated by Drucker (1951) imposes the restrictions

$$\int_{\dot{\varepsilon}_{ij}}^{\varepsilon_{ij}} \left(\sigma_{ij} - \sigma_{ij}^{*}\right) d\varepsilon_{ij} \ge 0 \qquad (1 \le i, j \le 3) \tag{19}$$

on the pair of strain states ε_{ij} and ε_{ij}^{*} with corresponding stress states σ_{ij} and σ_{ij}^{*}, where for each pair of indices, (i, j) the σ_{ij}^{*} is constant over the interval of integration from ε_{ij}^{*} to ε_{ij} $(1 \le i, j \le 3)$. The foregoing inequality has an alternate form namely that

$$\Omega\left(\sigma_{ij}^{*}\right) + W\left(\varepsilon_{ij}\right) \ge \sigma_{ij}^{*}\varepsilon_{ij} \qquad (1 \le i, j \le 3). \tag{20}$$

If the stress and strain fields σ_{ij}^{*} and ε_{ij} are given inside the continuum then the stress field and the body forces must be in a state of internal equilibrium as expressed by

$$\frac{\partial \sigma_{ij}^{*}}{\partial x_{j}} + F_{i}^{*} = 0 \qquad (1 \le i, j \le 3). \tag{21}$$

External equilibrium requires that the surface tractions T_{ij}^{*} be in equilibrium with the stresses, and consequently,

$$\sigma_{ij}^{*} \nu_j = T_i^{*} \qquad (1 \le i, j \le 3) \qquad \textbf{(22)}$$

where ν_j denotes the outward unit normal at the point being considered. Because of the existing equilibrium states between the quantities T_i^{*}, F_i^{*}, and σ_{ij}^{*} and compatibility relationships between u_i and ε_{ij},

$$\varepsilon_{ij} = \frac{1}{2}\left(\frac{\partial u_i}{\partial x_j} + \frac{\partial u_j}{\partial x_i}\right) \qquad (1 \le i, j \le 3) \qquad \textbf{(23)}$$

the principle of virtual work entails

$$\int_A T_i^{*} u_i \, dA + \int_V F_i^{*} u_i \, dV = \int_V \sigma_{ij}^{*} \varepsilon_{ij} \, dV \qquad (1 \le i, j \le 3) \qquad \textbf{(24)}$$

where A and V are the area and the volume of the continuum respectively. Integrating (20) with respect to volume retains the direction of the inequalities, which after substitution into the right-hand side of equations (24) (neglecting the body forces) gives

$$\int_V \Omega\left(\sigma_{ij}^{*}\right) dV + \int_V W\left(\varepsilon_{ij}\right) dV \ge \int_A T_i^{*} u_i \, dA \qquad (1 \le i, j \le 3). \qquad \textbf{(25)}$$

In these inequalities, equalities hold, whenever the tensors σ_{ij}^{*} and ε_{ij} are the exact solutions conformable to a particular boundary value problem.

APPLICATION TO ICE SCOURING UNDER CREEP CONDITIONS

For a multiaxial creep law, the energies can be written as

$$W\left(\dot{\varepsilon}_{ij}\right) = \int_0^{\varepsilon_{ij}} \sigma_{ij} \, d\dot{\varepsilon}_{ij} = \frac{n}{n+1} \sigma_{ij} \dot{\varepsilon}_{ij} \qquad (1 \le i, j \le 3)$$

and **(26)**

$$\Omega\left(\sigma_{ij}\right) = \int_0^{\sigma_{ij}} \varepsilon_{ij} \, d\sigma_{ij} = \frac{1}{n+1} \sigma_{ij} \dot{\varepsilon}_{ij} \qquad (1 \le i, j \le 3).$$

By substituting (26) into (25) yields

$$\frac{n}{n+1} \int_\vartheta \sigma_{ij} \dot{\varepsilon}_{ij} \, d\vartheta + \frac{1}{n+1} \int_\vartheta \sigma_{ij}^{*} \dot{\varepsilon}_{ij}^{*} \, d\vartheta \ge \int_A T_i^{*} \dot{u}_i \, dA \qquad (1 \le i, j \le 3). \qquad \textbf{(27)}$$

This inequality leads to an expression by superimposing a uniform flow velocity V to the actual one, with a global virtual load P acting at the centerline of the ice keel. For deviatoric creep one obtains

$$P \cdot V \leq \frac{n}{n+1} \int S_{ij} \varepsilon_{ij}^{*} \, d\vartheta \qquad (1 \leq \text{i, j} \leq 3). \tag{28}$$

This expression is possible since the ice feature is moving at a constant velocity and thus an undrained scouring of the sea bed is produced. Fundamentally this means no volume change but distortions (shear strains) are produced by the ensuing deviatoric stress field. A global value of resistance is thus obtained.

Utilizing (13) and (16) one obtains from the preceding inequality (28),

$$\frac{1}{V}\left(\frac{n}{n+1}\right)\left(\frac{\sigma_{c\theta}^{n}}{\dot{\varepsilon}_{c}}\right)^{\frac{1}{n}} \int_{\vartheta} \left(\dot{\varepsilon}_{e}\right)^{\frac{(n+1)}{n}} d\vartheta \geq P \tag{29}$$

which after substitution of the expression for $\dot{\varepsilon}_{e}$ (equation (4)) yields

$$V^{\frac{1}{n}}\left(\frac{n}{n+1}\right)\left(\frac{\sigma_{c\theta}^{n}}{\dot{\varepsilon}_{c}}\right)^{\frac{1}{n}}\left(\frac{2}{\sqrt{3}}\right)^{\frac{n-1}{n}}\left(\frac{m^{2}\pi}{\sqrt{a^{2}+d^{2}}\sin(m\pi)}\right)^{\frac{n+1}{n}} \Pi \geq P. \tag{30}$$

Π in equation (30) is an improper integral of the form

$$\Pi = \frac{\sqrt{a^{2}+d^{2}}\sin(m\pi)}{m\pi} \int_{\xi=-\infty}^{\xi=\infty} \int_{\eta=-\infty}^{\eta=0} \left(\xi^{2}+\eta^{2}\right)^{\frac{-(2m-1)(n+1)}{2n}+\frac{m}{2}} \left(\left(\xi-1\right)^{2}+\eta^{2}\right)^{\frac{(2m-1)(n+1)}{2n}-\frac{m}{2}} d\eta d\xi \tag{31}$$

Expression (30) is evaluated numerically for different geometric and creep-parameter values. Alternatively one can also calculate the global pressure by integrating the deviatoric stress field at the ice-soil interface. The two approaches lead to different values of global pressure (Foriero and Ladanyi (1989).

A typical simulation using the Saint-Jean-Vianney aforementioned creep stress parameter is depicted in Figure 7. For a depth of embedement d = 5m of the ice feature, the global load as a function of the ice-feature velocity at different angles of attack confirms the strain rate dependency of ice-scouring. For a constant value of the angle of attack, the global load increases with the velocity of the ice feature. Moreover one notice that the global load is quite sensitive to the value of this angle. This is explained by the change in the projected area of the ice feature as the angle of attack is increased.

Finally large as well as small scale model tests are required in order to ascertain the use of the Strain Path Method in the analysis of ice scouring. Moreover one cannot overemphasize a lack of laboratory tests in the determination of the creep parameters for marine clays.

CONCLUSION

A promising approach to ice-scouring of marine clays that accounts for large deformations is the Strain Path Method. In this method the velocity fields are estimated and differentiated with respect to the spatial coordinates in order to obtain the strain rates. The strain rates are introduced in a constitutive creep model in order to obtain the deviatoric stress field. The deviatoric stress field is then utilized in the determination of the global load.

Reiterating the present findings, for a statically indeterminate problem such as that of ice scouring of the seabed there is a redistribution of stress from the initial state to a final stationary state. The final stationary state of stress is compliant to a constitutive secondary creep law. Consequently the aforementioned analysis is only valid for steady state scouring of the seabed.

REFERENCES

Been, K., Kosar, K., Hachey, J., Rogers, B.T. and Palmer, A.C. (1990)."Ice scour models." 9th International Conference on Offshore Mechanics and Arctic Engineering, Houston, Texas, Vol. 5, pp. 179-188.

Baligh, M.M. (1985). "The strain path method." Journal of Geotechnical Engineering, ASCE, V. 111, No. 9, pp. 1108-1136.

Foriero, A. and Ladanyi, B. (1989). "A streamline solution for rigid laterally loaded piles in permafrost." Canadian Geotechnical Journal, 26, pp. 568-574.

Hult, J. A. H. (1966). "Creep in engineering structures." Blaisdell Publishing Co., Waltham, Mass.

Ladanyi, B. (1972). "An engineering theory of creep of frozen soil." Canadian Geotechnical Journal, 9, pp. 63-80.

Palmer, A.C. (1993). "The speed effect in seabed ploughing." Proceedings, Fourth Canadian Conference on Marine Geotechnical Engineering, St. John's, 3, 897-908.

Palmer, A.C., Konuk, I., Comfort, G. and Been, K. (1990). "Ice gouging and safety of marine pipelines." Proc. 22nd Annual OTC, Houston, Texas, May 7-10, OTC 6371, pp. 235-244.

Palmer, A., Konuk, I., Love, J., Been, K. and Comfort, G. (1989)."Ice scour mechanisms." Proceeedings, Tenth International Conference on Port and Ocean Engineering under Arctic Conditions, Lulea, 1, 123-132, Sweden, eds. K.B.E. Axelsson and L.A. Fransson.

Vaid, P.Y., Robertson, P.K., and Campanella, R.G. (1979). "Strain rate behaviour of Saint-Jean-Vianney clay." Journal of Geotechnical Engineering, 16, 34-42.

Yang, Q.S., Poorooshasb, H.B. and Lach P.R. (1996). "Centrifuge modeling and numerical simulation of ice scour." Soils and Foundations, Vol. 36, No. 1, pp. 85-96.

Yang, Q.S., Poorooshasb, H.B., Lach, P.R. and Clark, J.I. (1994). "Comparison of physical and numerical models of ice scour." Computer Methods and Advances in Geomechanics, Proceedings of The Eighth International Conference on Computer Methods and Advances in Geomechanics, Volume 2, pp.1795-1801.

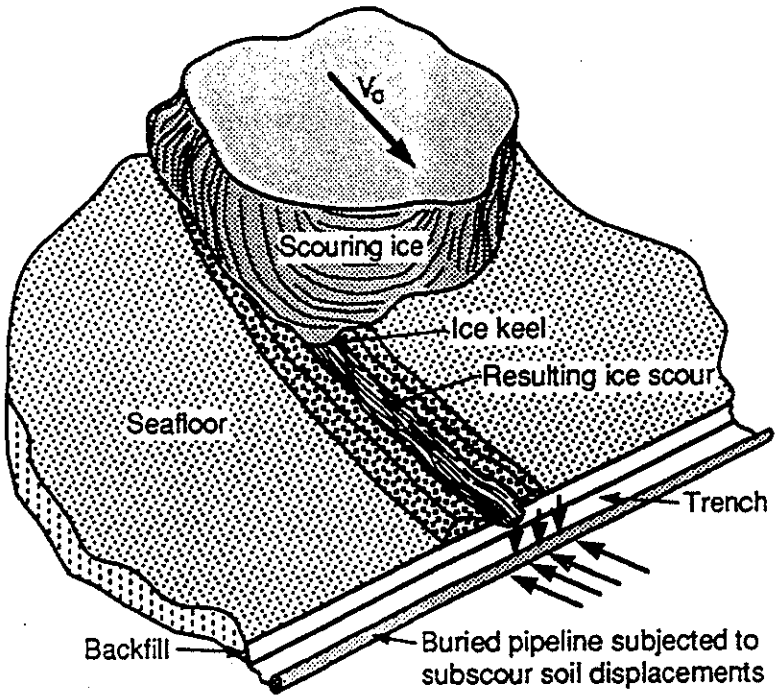

Fig. 1 - Subscour soil deformations beneath the keel of scouring ice

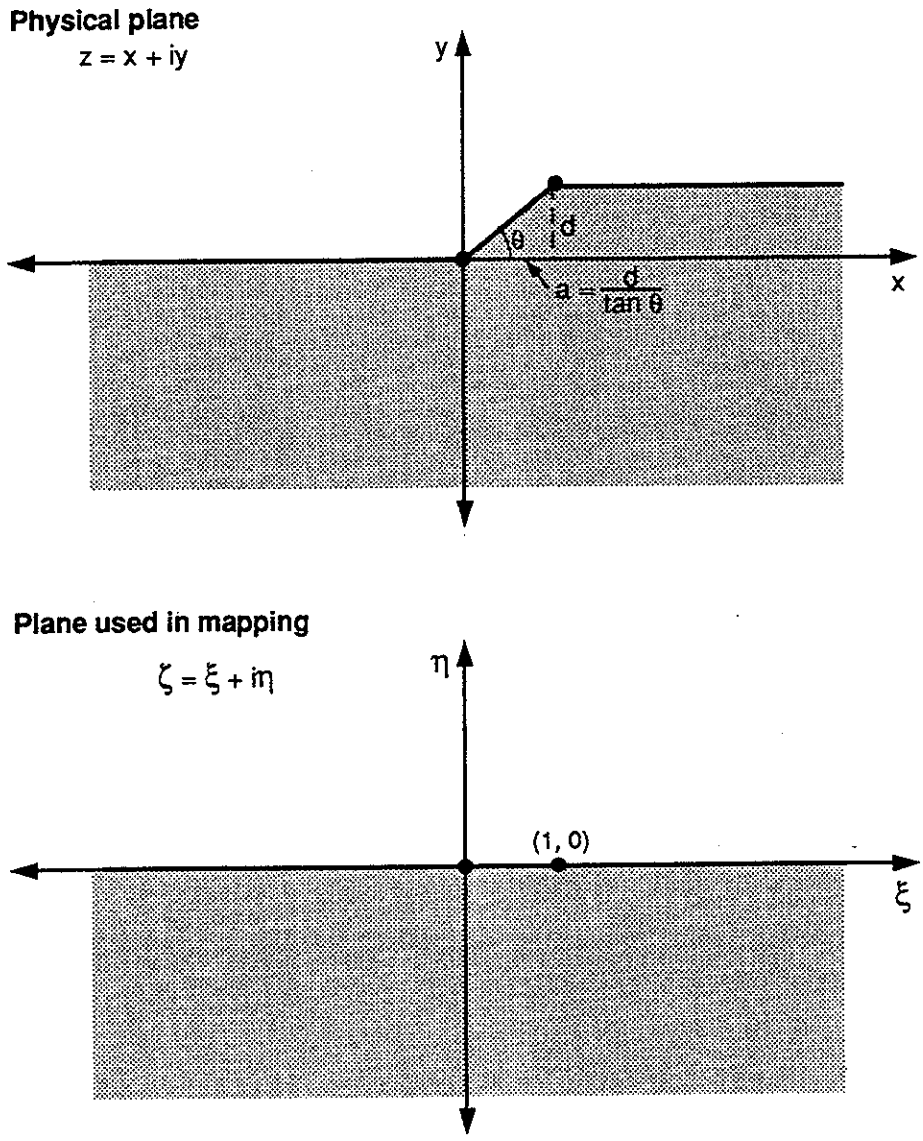

Fig. 2. Conformal mapping scheme

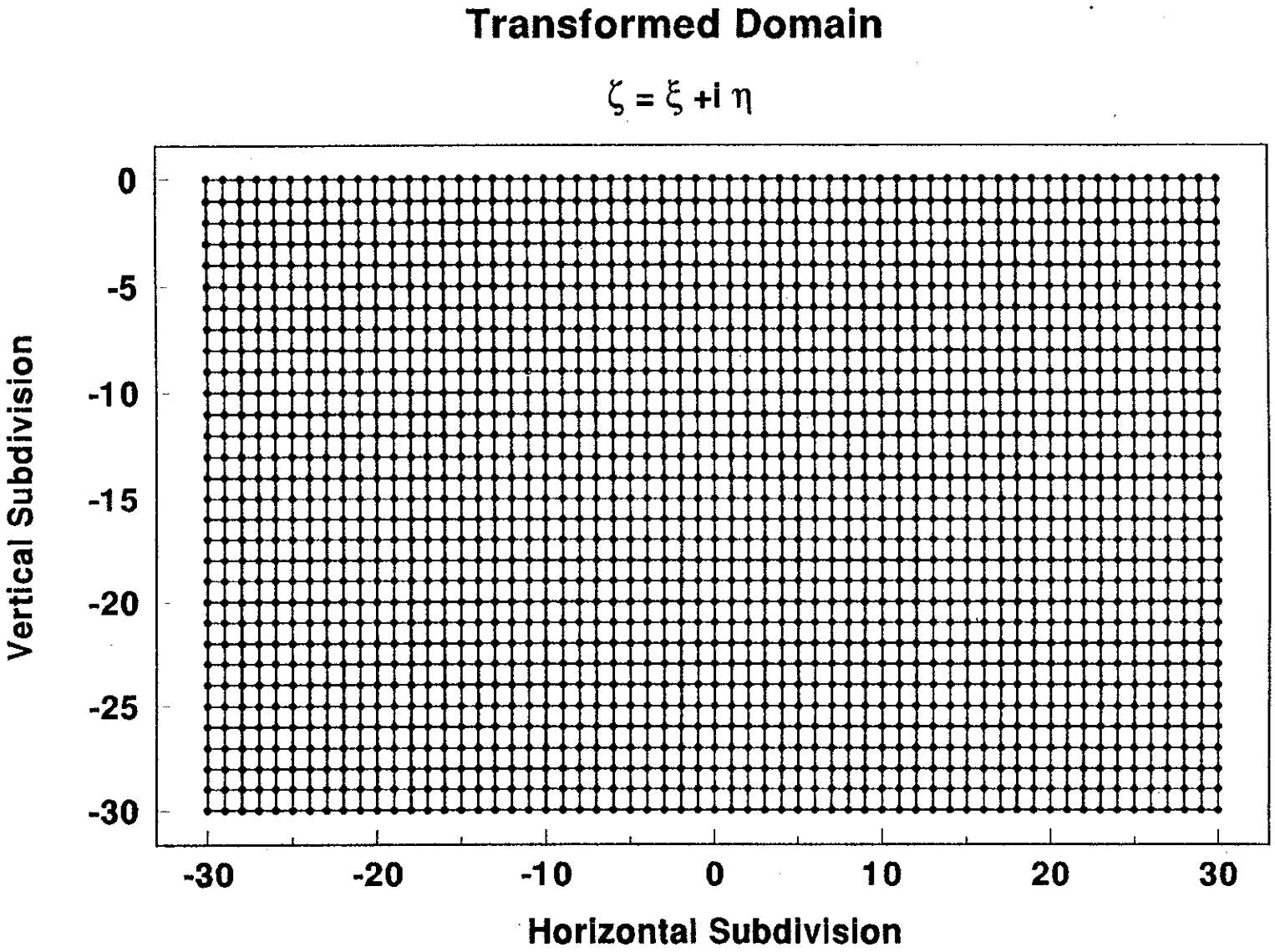

Fig. 3a. Rectangular Grid Used In The Mapping Scheme

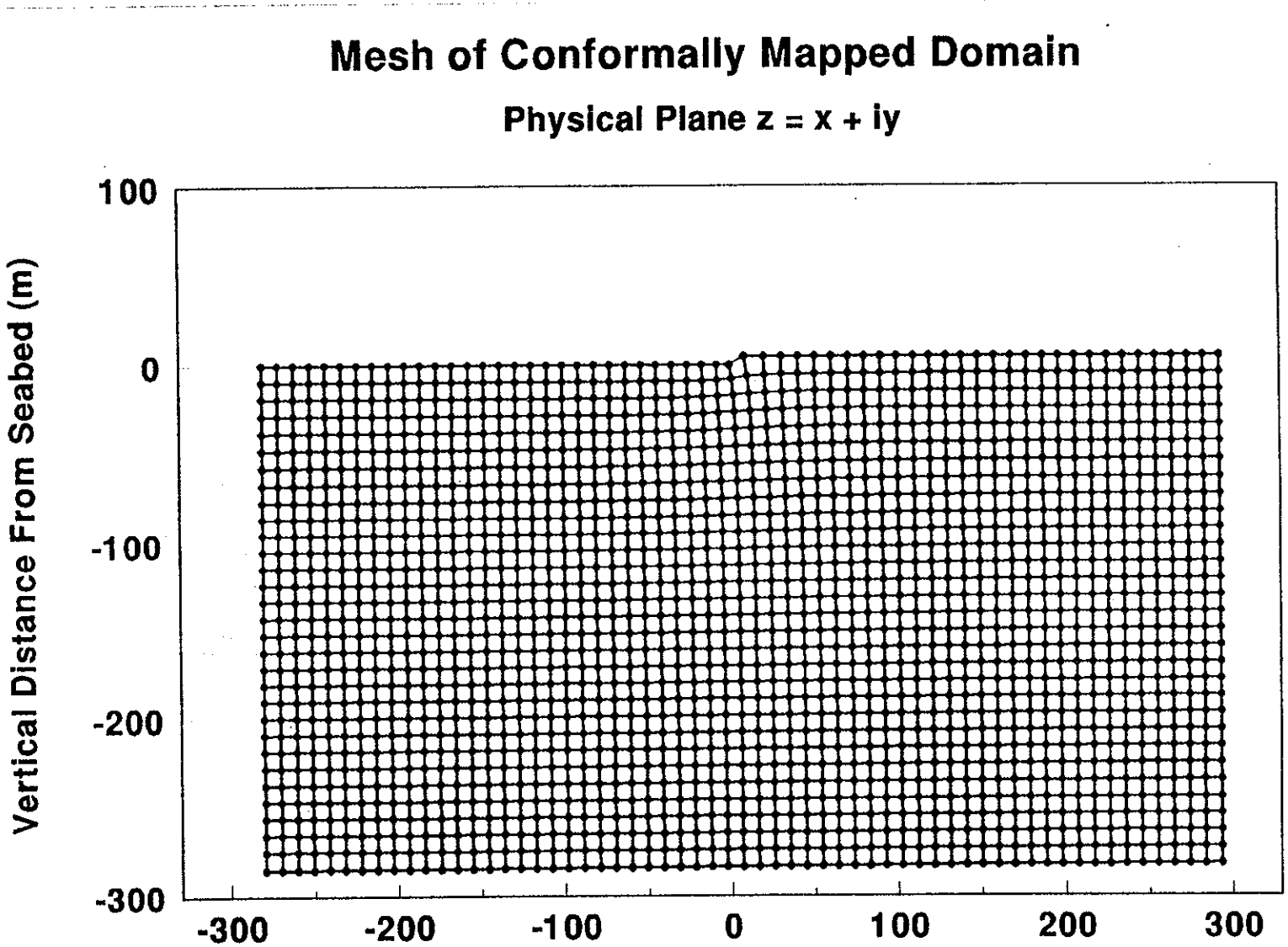

Fig. 3b. Conformally Mapped Physical Domain.

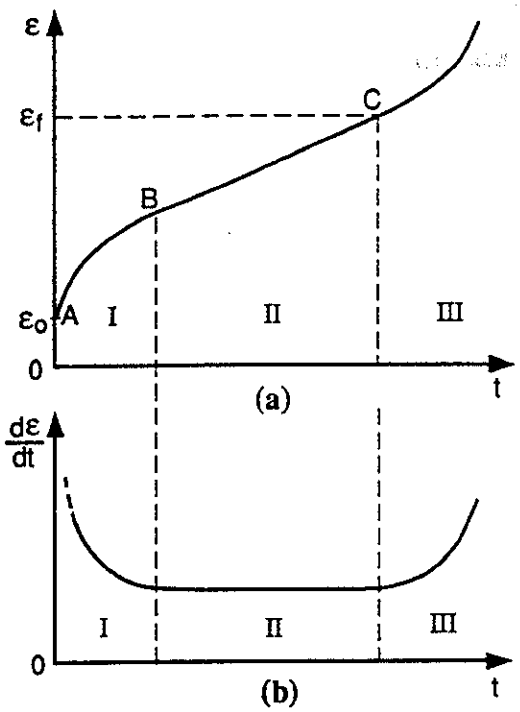

Fig. 4a. Stress and strain rate in constant stress creep test

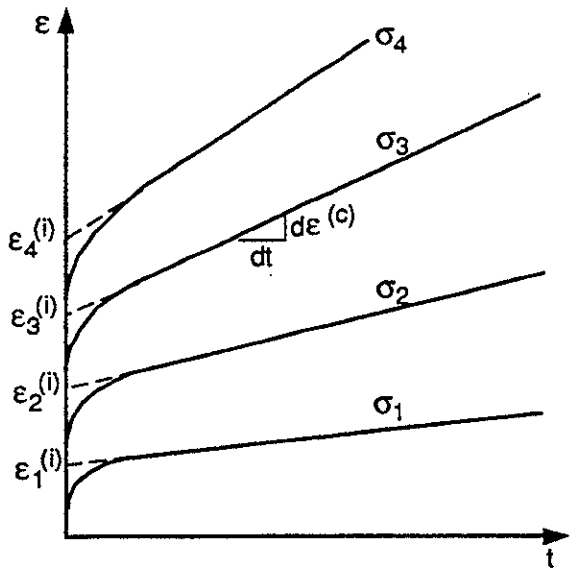

Fig. 4b. Linearized creep curves according to Hult (1966)

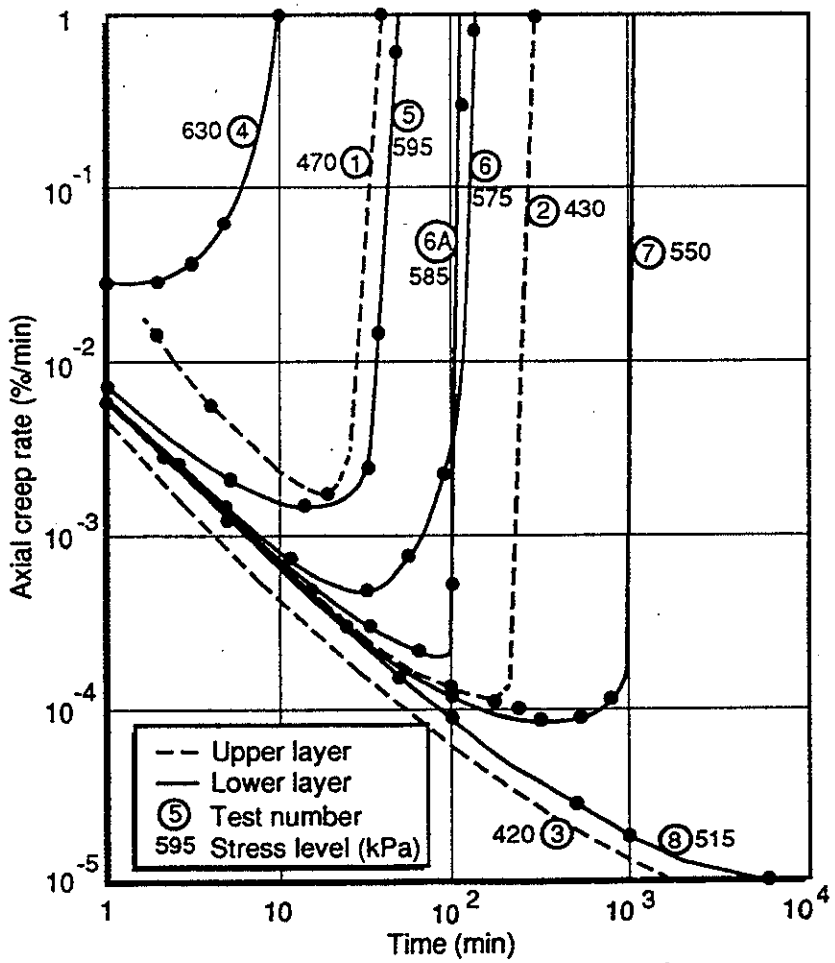

Fig. 5. Variation of creep rate with time in constant stress creep tests on SJV clay.

(after Vaid et al., 1979)

Undrained Creep Tests Under Sustained Deviatoric Stress

Saint-Jean-Vianney Clay, (Leda Clay) (Vaid et al. (1979))

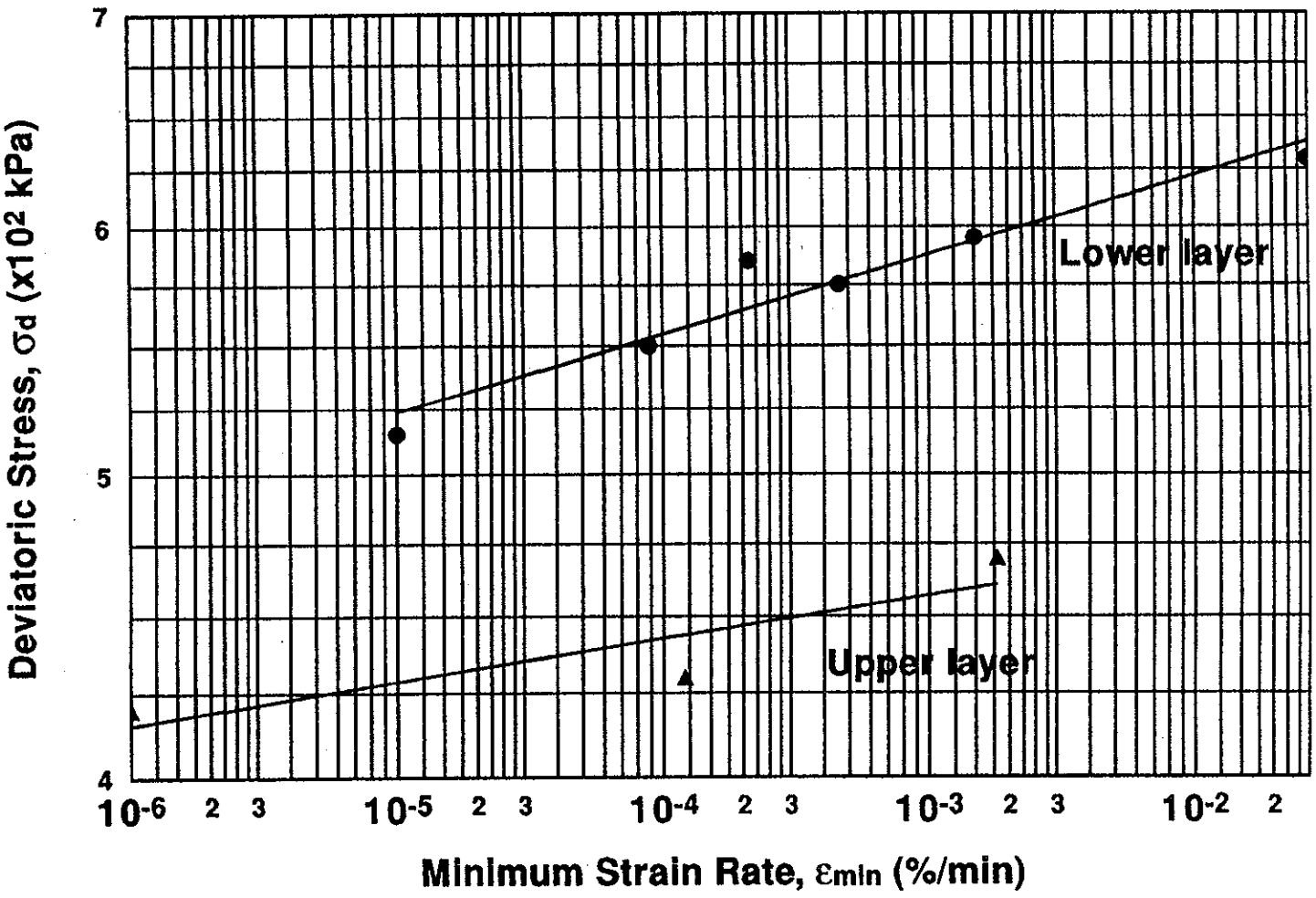

Fig. 6. Determination of Parameters in Equation (9).

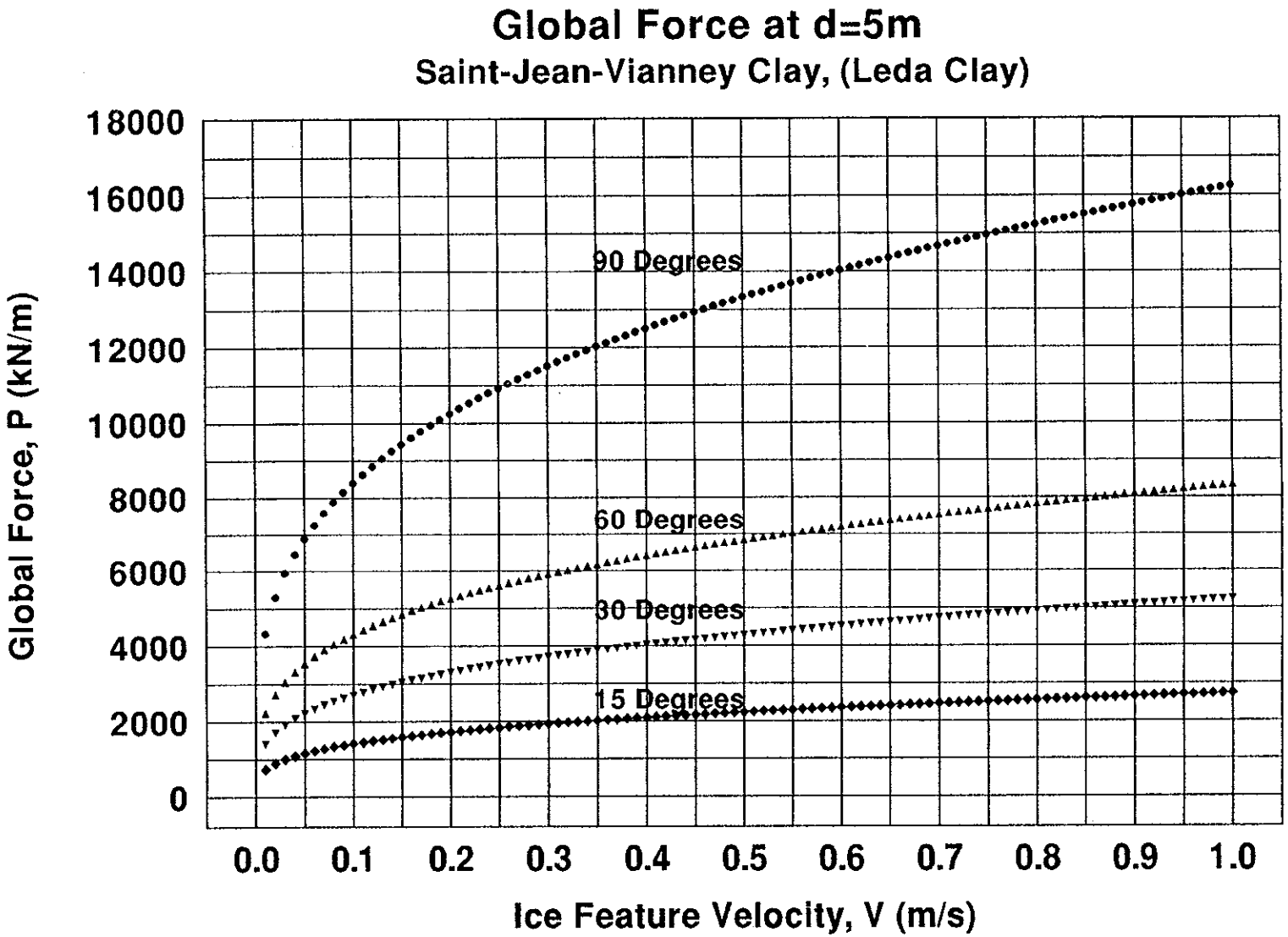

Fig. 7. Global Force As A Function of Velocity For Different Angles of Attack.

Seabed Exaration by Ice Formations

A. Beloshapkov[1], A. Marchenko[2] and A. Dlugach[3]

1. *Engineering-Production Society "Eco-System", Russia, 103051 Moscow, Trubnaya st. 23*
2. *Institute of General Physics, Russian Academy of Sciences, Russia, 117942 Moscow, Vavilova st. 38*
3. *AMIGE State Enterprise, Russia, 183031 Murmansk, Sverdlova st. 3*

Introduction

An exaration is a scouring of the sea floor by a drifting ice formation (IF) penetrating into the seabed. Ice formations include icebergs, pressure ridges and hummocks, and stamukhas. Icebergs are monolithic ice masses broken off glaciers reaching the ocean. In the Northern Hemisphere icebergs are produced by ice sheets of Greenland, Spitsbergen, Novaya Zemlya and other islands. In the Eurasian sector of Arctic icebergs are most common in the Barents Sea (mostly, in its northwestern portion), Kara and Laptev seas [1]. Ice hummocks and ridges form everywhere in the floating ice and consist of ice fragments. It is generally assumed that dimensions of underwater and above-water parts of ice ridges (keel depth and sail height) satisfy conditions of hydrostatic equilibrium. The term "stamukha' is conventionally applied to grounded ice hummocks or floes with keel embedded into sea floor due to moving ice pressure.

When a drifting iceberg ploughs seabed, deep and long furrows and craters are formed in the sea floor surface. To study the phenomenon is of great practical importance for the eastern coasts of Canada where icebergs are brought from Greenland by the East Greenland current. The icebergs damage cables and pipes laid upon the sea floor. Because of great size of the icebergs, scoured grooves may be seen at a depth of 100 m and more. Many investigators studied this phenomenon, both theoretically and by experiments (see [2-4], for example). Icebergs in the Rusian Arctic are considerably smaller, than those off Canadian coasts. Besides, they usually drift far from the Arctic transport routes and a majority of oil and gas deposits on the shelf.

Stamukhas' effect on the bottom ground is due to considerable static load resulting from their weight. In case the stamukha is put in motion by some outer forces, such as pressure of enclosing ice, wind, and currents, the effect increases noticeably and may change the sea floor micro-relief. Resulting grooves on the sea floor may extend for many kilometers. Grooves and scours are formed also in case of an ice ridge or hummock being grounded.

Contrary to icebergs, neither stamukhas, nor ice hummocks are monolithic; they are composed of numerous ice fragments with coefficient of packing not more than 0.7-0.8. Characteristic height and width of the base of ice hummock sail are respectively not more than 2 m and 10 m; its keel may be 20 m wide in its upper part. Side angles of an ice hummock both in its above-water and underwater parts usually do not exceed 40°. Stamukha's height above water is typically less than 10-15 m, its horizontal dimensions are 20 to 50 m, though stamukhas up to 400 m long occur occasionally. Most often stamukhas are grounded at depths less than 20 m.

Mass of individual stamukha or hummock drifting apart from ice field is considerably less than that of an iceberg, therefore they produce far smaller impact on the seabed. However the impact may noticeably increase in case of an IF moves together with the whole ice field. Deep and narrow furrows may also result from seabed scouring by separate protrusions from IF base.

In studies of exaration processes in a given geographical region our primary concern is to assess of grooves' dimensions and spatial distribution, as well as probability characteristics of their occurrence. Consequently, the studies were based on experimental data on soil properties, seabed topography, probability of ice formations of certain parameters appearing in the region under study, typical marine currents velocities, as well as on numerical models of a single act of scouring.
The present paper contains some results obtained by investigations of the seabed scouring by floating ice formations in the Baydaratskaya Bay, at the underwater crossing of the "Yamal-Europe" main gas pipeline (fig. 1); the engineering survey and researches have been performed by EPS "Eco-System" and the AMIGE State Enterprise. For data earlier obtained for the region see [5-8].

Experimental studies

The Baydaratskaya Bay is a narrow inlet of the Kara Sea which separates the Yamal Peninsula from the Uralian coast. The sea depth is up to 22 m in the region under investigation, and bottom sediments are sandy and clayey in composition (fig. 2) [8]. The floor of the bay is crossed by numerous exaration grooves; the latter are clearly seen in the records of echo-sounding, seismo-acoustic profiling, and hydrolocation by side scanner (HLSS). An example of exaration grooves recorded by echo-sounder is shown in fig. 3. A fragment of HLSS record (after SE AMIGE materials) is shown in fig. 4.

In the field works carried out by EPS "Eco-System" a high resolution echo-sounder was used which permitted to analyze bottom landforms along a profile near the designed crossing route. In the course of data processing, the profile was arbitrarily divided into three sections: the western offshore sector at depths of 13 to 20 m; the central portion of the bay delimited by the 20 m isobath; and eastern offshore sector at depths of 11 to 20 m.

The western offshore section shows increase in seabed landform number with depth. Within 13 to 14 m and 14 to 15 m depth intervals, only one or two grooves per 1 km of the profiles have been recorded, their depth being less than 0.2 m relative to the sea floor surface. The grooves are bordered with low ridges (less than 0.2 m). The sea floor dissection index (grooves number per 1 km of the profile) within the indicated intervals averages to 1.2 - 1.3. The width of grooves measured between the bordering ridges may be up to 40 m here, while total width of the grooves does not exceed 3 to 5% of the profile length within the given depth interval.

In the next depth interval (15 to 16 m) the sea floor dissection increases to 8.2%. Both individual grooves and series of two or three closely spaced grooves occur, their depth does not exceed 0.2 m. The total width of the seabed deformations is somewhat higher - up to 15%. At depths of 14 to 16 m a number of rampart-like landforms have been found; they rise about 0.3 to 1 m above

the sea floor, and their width measured at the base may be 100 m and more. Their origin is not quite understood as yet [8]. Nothing of the kind has been found in other sections of the profile.

At a depth 16 to 17 m the western offshore zone shows an increase in the dissection index to 11.6 grooves per I km. Besides distinct grooves, gently sloping linear hollows occur everywhere on the floor. It may be suggested that they are bottom landforms smoothed by ice. Individual grooves within this depth interval are up to 0.3 m deep, and total width of seabed deformations is almost twice as large as that within the previous interval (28%).

From 16 to 18 m the grooves increase abruptly in number and occupy almost all the floor surface along the profile. The sea floor dissection index increases three-fold, the grooves total width rising accordingly - up to 72.4%. Grooves deeper than 0.5 m with respect to average position of the surrounding sea floor occur only occasionally.

In the western sector the sea floor dissection reaches its maximum values at 18 to 20 m below sea level. The grooves number per 1 km of the profile exceeds 50. Typical depth increases to 0.5 m, and 3 grooves 0.5 tp 1 m deep were found within the last depth interval (19 to 20 m).

When considering the western section of the profile on the whole, it should be noted that exaration features are distributed irregularly along the profile. The sea floor is the least dissected at depths of 13 to 15 m and slightly more so - at 15 to 17 m. The maximum dissection has been found at depths of 17 to 20 m, its value being 1.5 to 2 times above the average one (29.2). Single grooves prevail in the nearshore zone to a depth of 17 m, while in the deeper part grooves and ridges are very close to each other. No relationship has been found between seabed sediments and the irregularities of the surface. The deepest grooves (0.5 - 1.0 m) are found at depths of 19 to 20 m.

In the central part of the Baydaratskaya Bay practically entire surface of the sea floor bears distinct landforms. In the west, between 20 and 21 m isobaths, a relatively small number of grooves (75) was recorded. As the isobaths are comparatively close to each other, the dissection index is also high - 67 per 1 km, and about 83.6% of the floor is disturbed by grooves.

The deepest part of the bay (lying below the 21 m isobath) features the greatest amount of the grooves which cover practically the whole surface of the sea floor. Some grooves within this section are distinguished for their width (up to 76 m) and depth with reference to adjacent floor surface (up to 1 m). The sea floor within 21 to 20 m depth interval adjoining the eastern section is relatively smooth, with minimum disturbances.

On the whole, the central portion of the bay is characterized by the highest and relatively uniform width of the seabed deformations (65.9%, on the average), with prevalence of small grooves (80% of total number). Here some of the largest landforms were recorded, box-shaped in the cross-section. Their depth may reach 1 m, and the width between the bordering ridges - 76 m. They usually occur in groups within rather limited areas of the floor. Total number of the largest grooves amounts to 19, 12 of them are box-shaped, and the rest 7 are V-shaped (with narrow bottom). This - central - part of the profile is the only one where such large landforms were found.

The eastern site of the offshore crossing route features essentially gentler angles of the seabed surface as compared with the western sector, yet it produces practically no effect on the degree of the floor dissection. The grooves number is relatively small (63) within the depth range of 20-19 m, though they are usually wider here (up to 66 m); as the length of the profile section within this depth range is rather small, the index of total width of seabed deformations appears relatively high (82.4%). Shallow grooves, less than 0.5 m deep, are prevalent. This part of the bay floor is similar in characteristics to the western side at depths of 20 to 21 m.

Maximum number of grooves has been recorded at depths of 17 to 19 m. Because of smaller seabed gradients, the distance between isobaths is greater in the east than in the west and therefore the proportion of seabed deformations is almost 1.5 times less. The grooves depth is also smaller.

In the ranges of 17 to 16 and 16 to 15 m a sharp decrease is recorded both in grooves amount and their dimensions. An insignificant increase in grooves number, as well as in their depth and width is noticed in the eastern sector at a depth of 15 to 14 m, where the dissection density is 63.1 per 1 km of the profile, and the proportion of the seabed deformations amounts to 91.6%. Such an increase of the grooves number may be ascribed to the fact that here has been the mean long-term position of the fast ice edge during the winter, with ice ridges, ice hummocking, rafted ice and stamukhas being formed here and probably crushed ice reaching the seabed.

Closer to the coast, at depths of 14 to 11 m, the seabed grooves number is slightly reduced along with a decrease in their depth and width. In common with the western sector, only single grooves not more than 0.2 m deep are found here; no system of grooves has been recorded.

The eastern offshore section shows an uneven dissection, grooves are smaller than in the west. Maximum dissection is found at depths of 17 to 19 m and 14 to 15 m.

On the whole, the analysis of experimental data oo the seabed profile along the crossing route in the Baydaratskaya Bay permits the following conclusion:
- the maximum dissection of the sea floor is recorded in the central part of the bay;
- an average value of the sea floor dissection index (grooves number per 1 km of the profile) amounts to 36.5;
- total width of the sea floor deformations makes up more than a half of the profile length (52.5%).

Exaration grooves in the Baydaratskaya Bay are prone to erosion and infilling by sediments. However, special features of hydrodynamic regime, bottom sediments composition and properties are responsible for prolonged conservation of exaration landforms in the bay. Both field experiments and laboratory modeling of the seabed erosion show that neither wind-induced waves, nor currents recorded in the deep-eater portion of the bay can produce significant erosion of cohesive ground at a depth greater than 15 m. At shallower depths (less than 15 m) cohesive grounds may be eroded during storms. Loose soils (sands) are subject to erosion by waves and currents along the whole length of the crossing route [5].

Basic equations

Consider one dimensional state of the problem, when the trajectory of center of gravity of ice formation (IF) is horizontal straight line. Any rotations of the IF are not considered. The equations, describing a motion of the IF follow from the low of impulse conservation

$$M_i \frac{dv}{dt} = -R + F, \quad \frac{dx}{dt} = v, \tag{3.1}$$

where M_i is the mass of the IF, v is the velocity of the IF, R is the force, acting on the sea bed by the IF in the direction of the horizontal axis x, F is resultant external force, acting on the IF from sea ice cover, sea streams, wind and so on, t is a time.

The force, acting on the IF from sea streams is defined by square low [9]

$$\boldsymbol{F}_{wi} = \rho_w C_w S \, | \boldsymbol{v}_w - \boldsymbol{v} | (\boldsymbol{v}_w - \boldsymbol{v}) \tag{3.2}$$

where C_w is the drag coefficient, v_w and v are the velocities of the sea stream and the IF respectively. The parameter $S=W_1W_2$ defines the effective area of a submerged part of the IF related to the x direction. W_1 is the width and W_2 is the height of the submerged part of the IF. The mass of the IF can be estimated by the formula $M_i = \rho_w W_1 W_2 W_3$, where W_3 is the length of the IF.

The force, acting on the IF, is equal to $\boldsymbol{F} = \boldsymbol{F}_{\text{wi}} + \boldsymbol{F}_{ii}$, when the IF is connected to an ice field. $\boldsymbol{F}_{ii}$ is additional force, acting on the IF from the ice field. The force $\boldsymbol{F}_{ii}$ doesn't exceed the value, related to the ice ridging near the IF. The pressure, needed for the ridging of an ice cover is estimated by the $\pi_r = 1/2 k \rho_i \Delta_\rho g h_i^2$ [10], where h_i is the ice thickness, ρ_i is ice density, $\Delta_\rho = (\rho_w - \rho_i)/\rho_i$ and $k \in (1,15)$. Therefore the minimal value of the modulus of F_{ii} is estimated by the formula

$$\boldsymbol{F}_{ii} = \pi_r W_1 \tag{3.3}$$

It is assumed that the force R depends on the value h of the penetration of the IF into the sea bed, on the parameters, characterizing a rheology of the sea bed: the angle of internal friction and soil cohesion, on the geometry of a part of the IF, interacting with the sea bed. It is assumed that the deviation of sea bottom from horizontal plane is small. In the first approximation we suppose that this deviation equals zero.

Thus it is assumed, that $R=R(h,...)$ and $F=F(v_w\text{-}v,...)$, where the dots relates to the external parameters, the variations of which don't depend on the motion of the. The function $h(t,x)=H_0(t)-H(t,x)$, where $H(t,x)$ is sea depth and $H_0= H(t,0)$, is known. The equations (3.1) forms a closed system in this case.

Note, that the soil reaction $-R$ on the frontal part of the IF, interacting with sea bed, depends on the parameters, characterizing physical and geometric properties of the embankment, formed

from the loose sea bed soil, in the frontal part of the IF. This dependence isn't taken into account in this paper. The consideration of this dependence can increase R only, and decrease the depth of the scour finally.

On the other hand the calculation of the embankment near the scour is necessary for the definition of the evolution of micro relief of the sea bottom near the scour. The typical process of scour formation by the penetration into sea bed of trapezoidal part of the IF is performed on the fig. 5. The width of frontal surface of this part equals w_1, and the angle between the frontal surface and vertical axes is equal to θ. A part of sea bed soil, forced on the sea bed by the ice in front of the IF, forms the embankment with the height h_{ls}. It is assumed that slope angle of loose soil in the embankment equals φ. This loose soil replaces to the edges of the scour and forms soil ridges behind the IF.

Geometric sizes of these ridges are defined by the balance of bottom soil, forced on the surface of sea bed by the ice, and loose soil, replaced from the embankment into the soil ridges. It is assumed, that the embankment consists from three parts: the triangular prism and the two quarters of the cone (see fig. 5). Therefore the shape of the embankment is defined by only one parameter h_{ls} for given values of φ and θ.

The equation of mass balance of loose soil in the embankment has following form

$$\begin{aligned} &\rho_{ls}\frac{dV_{ls}}{dt} = v(\rho_s h w_1 - \rho_{ls} h_{ls}^2 \cot\varphi), \\ &V_{ls} = \frac{1}{2}(\tan\theta + \cot\varphi) w_1 h_{ls}^2 + \frac{\pi}{6} h_{ls}^3 \cot^2\varphi + h h_{ls}^2 \tan\theta \cot\varphi, \end{aligned} \tag{3.4}$$

where V_{ls} is embankment volume, ρ_s and ρ_{sl} are the densities of unperturbed sea bed soil and loose soil respectively. The equation (3.4) defines the change of embankment height h_{ls} in time under the motion of the IF.

A model of sea bed soil

Lets assume, that the internal stresses into the sea bed soil satisfy to the system of the equations for the static equilibrium

$$\sum_{j=x,y,z} \frac{\partial \sigma_{ij}}{\partial x_j} = \delta_i^3 \rho_s g. \tag{4.1}$$

The full deformation of the soil consists on the elastic and plastic parts, the bulk deformation of the soil is small. The condition for the realization of plastic deformation has following

$$\Phi(\sigma_1 - \sigma_2, \sigma_2 - \sigma_3, \sigma_1 - \sigma_3) = 0, \tag{4.2}$$

where Φ is a convex function of its arguments and σ_i are principal values of the stress tensor.

If $\Phi = 0$, then the strain rate is defined by associated flow rule for the plastic motions

$$e_{ij}^{p} = \lambda \frac{\partial \Phi}{\partial \sigma_{ij}}, \quad \lambda \geq 0. \tag{4.3}$$

In the case, when $\Phi < 0$, the Hooke law is used for the definition of deformations

$$\sigma_{ij} = \Lambda_1 \varepsilon_k^k \delta_{ij} + \Lambda_2 \varepsilon_{ij}, \tag{4.4}$$

where Λ_1 and Λ_2 are elastic modules.

Strain and atrain rate tensors are defined by following formulas

$$e_{ij} = \frac{1}{2}\left(\frac{\partial v_i^s}{\partial x_j} + \frac{\partial v_i^s}{\partial x_i} \right) = \frac{d\varepsilon_{ij}}{dt} \tag{4.5}$$

where v_i^s are components of three dimensional vector of the velocity of a soil particle.

The equations (4.1) – (4.5) are considered in the region V_0, performed on the fig. 6. The boundary of this region consists from unperturbed surface of sea bed and from scour surface. Unperturbed surface of sea bed is performed by the sum of the half-plane Γ_2, laying in front of the IF, and the half-plane Γ_3 with cut out strip $A_5A_4A_3A_6$, laying behind of the IF. The surface of the scour consists of the sum of the surface $A_1A_2A_3A_4$, marking as Γ_1, the lateral faces $A_8A_1A_4A_5$ and $A_7A_2A_3A_6$ and scour bottom $A_8A_1A_2A_7$. The total surface of the lateral faces and the bottom is marked by Γ_5. The inclined plane, containing Γ_1, is marked by Γ_4.

It is considered the next boundary conditions for (4.1) – (4.5)

$$\Gamma_1: \quad \sigma_{ij}\tau_i n_j = 0, \; v_i^s n_i = v\cos\theta \tag{4.6}$$

$$\Gamma_2: \quad \sigma_{ij} n_j = 0 \tag{4.7}$$

$$\Gamma_3: \quad v^s = 0; \quad \Gamma_5: \quad v^s = 0 \tag{4.8}$$

Physical sense of (4.6) is reduced to the equality to zero of shear stresses and to the kinematic condition of the equality of normal velocities of soil particles and the IF on the frontal surface Γ_1. The condition (4.7) means the absence of normal and shear stresses on the surface Γ_2. It would be naturally to consider on the surfaces Γ_3 and Γ_5 the conditions like to (4.7). The displacement of sea bad soil can be not zero on the surfaces Γ_3 and Γ_5. It is assumed, that this displacement is small. The kinematic conditions (4.8) are approximate. The using of (4.8) is more convenient for the finding of the estimations for the force R.

Theorems on the bounds of the force, acting on the IF from sea bottom soil

The solution of (4.1) - (4.5) relates to the carrying out of complicated numerical calculations. Let demonstrate, that the force R can be estimated without these calculations. We shall use the theorems on the estimations of upper and lower carrying capacity [11].

Consider the principle of Mises

$$(\sigma_{ij} - \sigma_{ij}^*)e_{ij}^p \geq 0 \tag{5.1}$$

where σ_{ij} and e_{ij}^p are some tensors of stresses and strain rate, bounding by associated flow rule (4.3), which are the solution of some problem on the soil motion, and σ_{ij}^* is tensor of admissible stresses, satisfying the condition $\Phi \leq 0$. For the finding of upper bound of R consider as σ_{ij} and e_{ij}^p the tensors, related to the solution of the problem on the soil motion, satisfying to the kinematic conditions, and in the capacity of σ_{ij}^* real stress tensor. For the finding of the lower bound of R assume, that σ_{ij} and e_{ij}^p are related to the real solution and σ_{ij}^* is the solution of the problem on the limiting equilibrium state of a soil wedge.

Let find the upper bound. Let e_{ij}^p is strain rate tensor satisfying to the kinematic conditions, v_i^p are the components of soil velocity and σ_{ij}^* is real stress tensor. Multiplying (4.1) on v_i^p, we have

$$\int_{V_0} \sigma_{ij}^* e_{ij}^p dV = \int_{\partial V_0} \sigma_{ij}^* v_i^p n_j dS - \rho_s g \int_{V_0} v_z^p dV \tag{5.2}$$

where V_0 is the volume, occupied by sea bed soil, ∂V_0 is the boundary of this region, n_j are the components of the external normal to ∂V_0. Tensor e_{ij}^p is defined by following formula $e_{ij}^p = 1/2(\partial v_i^p / \partial x_j + \partial v_j^p / \partial x_i)$.

Consider kinematically admissible scheme of soil motion in front of the IF, performed on the fig. 7. With accordance with this scheme the forcing out of soil prism $A_1 \ldots A_6$ has place under the motion of the IF. The soil volume equaling to $w_1 hvdt$ is forced out sea bed, while the IF replaces on the distance $dx=vdt$. It is assumed, that soil prism $A_1 \ldots A_6$ is in the state of limiting equilibrium, and the condition (4.2) occurs inside it. From the boundary conditions (4.6)-(4.8) follow, that surface integral on ∂V_0 in the formula (5.2) is reduced to the intergal on Γ_1.

Therefore the formula (5.2) can be written in the following form

$$\int_{V_0} \sigma_{ij}^* e_{ij}^p dV = R_n v^p \cos(\eta+\theta) - \frac{1}{2}\rho_s g w_1 h^2 \frac{\cos(\theta+\psi)}{\cos\theta} v^p, \quad R_n = R\cos\theta \tag{5.3}$$

Strain rate tensor e_{ij}^p, relating to the considerable kinematically admissible scheme of soil motion, has in the frame of reference (x_1, x_2, x_3) (see fig. 8) following form

$$\begin{aligned} &e_{13}^p = -\frac{v^p}{2}\delta(x_1), \quad e_{23}^p = \frac{v^p}{2}(\delta(x_2) - \delta(x_2 - w_1)), \\ &e_{12}^p = e_{11}^p = e_{22}^p = e_{33}^p = 0. \end{aligned} \tag{5.4}$$

Let construct the field of internal stresses σ_{ij} inside the soil, satisfying plastic condition (4.2) inside the prism $A_1 \ldots A_6$ and related to the strain rate e_{ij}^p by associated flow rule (4.3). Let mark

$$\begin{aligned} &\sigma_{11} = \sigma_{22} = \sigma_{33} = \sigma, \quad \sigma_{12} = 0, \\ &\sigma_{13} = -\tau, \quad \sigma_{23} = \pm\tau. \end{aligned} \tag{5.5}$$

Tensor σ_{ij} has a jump inside the prism $A_1 \ldots A_6$. The value $\sigma_{23} = \tau > 0$ on the face $A_1A_4A_5$, and $\sigma_{23} = -\tau < 0$ on the face $A_2A_3A_6$. The principal values of σ_{ij} don't depend from the sign of σ_{23}, and maximal shear stress is equal to $2\sqrt{2}\tau$. The quantity τ characterizes soil resistance under shear deformations and further is named as soil cohesion. One can see, that $\lambda \geq 0$ inside the prism $A_1 \ldots A_6$.

From (5.4) and (5.5) follow

$$\int_{V_0} \sigma_{ij} e_{ij}^p dV = \frac{\tau v^p h}{\sin\psi}\left(w_1 + \frac{h\cos(\theta+\psi)}{\cos\theta}\right) \tag{5.6}$$

Integrating (5.1) on the volume V_0 and taking into account the inequality (5.1), find following bound

$$\begin{aligned} &\frac{\tau}{\sin\psi}\left(\frac{\cos\theta}{\cos(\theta+\psi)} + \frac{h}{w_1}\right) + \frac{1}{2}\rho_s g h \geq \langle R_n \rangle, \\ &\langle R_n \rangle = \frac{R_n \cos\theta}{h w_1}, \quad R_n = \int_{\Gamma_1} \sigma_{ij}^* n_i n_j dS \end{aligned} \tag{5.7}$$

where $\langle R_n \rangle$ is averaging stress on the face Γ_1.

The bound (5.7) can be improved by the minimization of the left side of the inequality on the angle ψ. Minimal value of the left side of (6.5) is reached by $\psi = \psi_0 = 1/2(\pi/2 - \theta)$, when $w_1 \to \infty$. The calculations show, that the difference of minimal value the left side of (6.5) from its value by $\psi = \psi_0$ is not more one percent by $h/w_1 < 3$. Thus, the following bound has place

$$R_n^+ \geq \langle R_n \rangle, \quad R_n^+ = 2\tau f(\theta, h/w_1) + \frac{1}{2}\rho_s g h$$
$$f(\theta, h/w_1) = \frac{\cos\theta}{1-\sin\theta} + \frac{h}{\sqrt{2}\, w_1} \frac{1}{\cos(\theta/2) - \sin(\theta/2)} \tag{5.8}$$

Find lower bound of $\langle R_n \rangle$. Let σ_{ij} and e_{ij}^p are related to the real solution of the problem. Stress tensor σ_{ij}^* is the solution of the problem on limiting equilibrium of soil wedge [11], laying between the plates Γ_2 and Γ_4, and forced by external normal load on the face Γ_4. The limiting value of the external stress is equal to $R_n^- = 2\tau(1+\theta)$. Assumed, that the soil stresses are constant outside of the wedge.

After the integration of (5.1) on the volume V_0 we find

$$\langle R_n \rangle \geq R_n^- + \rho_s g \int_{V_0} v_z dV (v h w_1)^{-1} \tag{5.9}$$

From the law of mass conservation and incompressibility of the soil follow $\int_{V_0} v_z dV \geq 0$.

Therefore the following bound has place

$$R_n^- \leq \langle R_n \rangle \leq R_n^+ \tag{5.10}$$

From this follow, that $R \in (h w_1 R_n^-, h w_1 R_n^+)$.

The difference of lower bound from the real value of $\langle R_n \rangle$ can be large, so the stresses σ_{ij}^* are not taken into account weight of the soil and three dimensional phenomena. The approximation the integral in (5.9) with using of the kinematically admissible scheme of soil motion gives following bound, taking into account soil weight

$$\langle R_n \rangle \geq R_{n,1}^-, \quad R_{n,1}^- = R_n^- + \frac{1}{2}\rho_s g h \tag{5.11}$$

The dependencies of $\gamma_1 = R_n^+ / R_n^-$ and $\gamma_2 = R_n^+ / R_{n,1}^-$ from θ are performed on the fig. 8 for various values of soil cohesion τ and the ratio h/w_1 by $h = 2$ m. One can see, that taking account of soil weight considerably constricts bounding interval for the averaging stress $\langle R_n \rangle$.

The size of this interval for soils with cohesion $\tau > 30$ KPa considerably less, then for the soils with cohesion $\tau < 10$ KPa. The bounding interval decreases by the decreasing of the ratio h / w_1. Physically it is clear, so the main resistance of the soil is formed due to soil pressure on the face Γ_1, where soil motion is near to plane. Therefore the influence of forces, not taken into account in the expression for R_n^-, decreases.

Results of numerical calculations

The longest scours are formed by stationary or quasi stationary motions of the IF. It is interesting to study the conditions, needing for stationary scouring, when $dv/dt = 0$ and $dV_{ls}/dt = 0$. The external forces, acting on the IF, are defined from the static equation $R = F$. From this formula by $R = hw_1 R_n^-$ follow upper bound for scour depth. In dimensionless notation the upper bound is defined by the formula

$$\delta = \frac{\tau_0}{2\mu\tau(1+\theta)}\left(\frac{W_2}{W_1}\frac{\rho_w C_w v_0^2}{\tau_0}\frac{\Delta v^2}{v_0^2} + \frac{\pi_r}{\tau_0 W_1}\right) \tag{6.1}$$

$$\delta = \frac{h}{W_1}, \quad \mu = \frac{w_1}{W_1}, \quad \Delta v = v_w - v$$

The formula (6.1) defines upper bound of scour depth, when the IF moves under the influence of sea current and ice cover, ridging near the IF.

C_w	W_1	W_2	W_3	τ_0	v_0	ρ_w	ρ_i	k	θ	h_i
0.6	20 m	20 m	80 m	50 KPa	1 m/s	10^3kg/m^3	930 kg/m^3	15	$\pi/6$	1 m

Table 1. The typical values of physical constants.

The typical values of physical constants, used for the numerical modeling, are performed in the Tab. 1. The values τ_0 and v_0 are related to extremally possible values of soil cohesion and sea currant velocities in the considerable region. The value C_w is similar to the value of the drag coefficient in the problems relating to the calculation iceberg drift [9].

The dependencies of δ on the ratio τ/τ_0 are performed on the fig. 9 for various values of dimensionless parameter μ, defining the width of a part of the IF, penetrating into the sea bed, by $\Delta v = 0.5$ m/s. It is shown, that scour depth is less than 1 m, if $w_1 > 5$ m and $\tau > 10$ KPa. If the width $w_1 \approx 1$ m, then scour depth can reach several meters. The scour depth is not more than 2 m, when soil cohesion $\tau \approx \tau_0$, even if $w_1 \approx 1$ m.

In the stationary case from (3.4) follow $\rho_s h w_1 = \rho_{ls} h_{ls}^2 \cot\varphi$. The dependence of embankment height h_{ls} from w_1 and h is performed on the fig. 10 for ρ_{ls}/ρ_s=0.8 and φ=π/6. One can see, that

embankment height can reach several meters, if scour depth more than 1 m and scour width more than 3 m. These results are not observed in the natural conditions. It means, that soil ridges near the scour are eroded under the influence of sea currents sufficiently fast.

The results of numerical modeling in nonstationary cases are performed on the fig. 11. It is assumed, that some part of the IF penetrates into inclined sea bed. The first contact has place by t=0. Scouring has place, while the IF moves. The scour depth has extremal value in the stop moment of the IF. The dependence of scour depth h from soil cohesion τ later 3 hours after the beginning of the scouring is performed on the fig. 12 for various values w_1 and external forces. The upper curves relate to the calculations for $R = hw_1R_n^-$, and the lower curves relate to the case $R = hw_1R_n^+$. The real scour depth lays between these curves. It is assumed, that fluid depth $H = H_0 - h(x)$, where $h(x)$=0.001 x. The velocity of sea current v_w=0.8 m/s.

The results, performed on the fig. 11 *a* and *b* are associated with the cases, when initial velocity of the IF v=0 by t=0. In the next time moment the penetration of a part of the IF into sea bed has place under the influence of external forces F_{wi} and F_{ii}. The results, performed on the fig. 11 *c* and *d* are associated with the cases, when free IF drifts with the velocity of sea current under the influence of drag force F_{wi} only, and v=v_w by t=0. The first contact with sea bed occurs by t=0. The width of the parts of the IF is equal to w_1=5 m (*a,c*) and w_1=15 m (*b,d*).

The calculations show, that drift velocity of the IF is equal zero by t=3 h. Scour depth is more than 1 m only in the cases, when $w_1 < 5$ m and $\tau < 10$ KPa. In the other cases scour depth is not more than 1 m.

Conclusion

On the whole, analysis of the experimental data obtained for the sea floor profile in the vicinity of the pipeline crossing route over the Baydaratskaya Bay reveals the seabed dissection to reach its maximum at the central part of the bay; mean index of the sea floor dissection, that is number of grooves per 1 km of the profile length, is 36.5, while total width of the floor deformation makes up more than a half of the profile length (52.5%).

At a depth greater than 15 m grooves stay intact for a long time, not being prone to erosion or filling with sediments; the grooves depth and configuration depend primarily on initial scouring by ice and subsequent processes of the material crumbling down or flowing down the groove's sides. Gradients of groove's sides and those of bordering ramparts depend on the angle of repose characteristic of the material in question. At shallow depths, storms of a typical for the region strength produce the ramparts abrasion and grooves filling. Grooves on a sandy seabed are subject to erosion and filling along the whole length of the underwater crossing.

Numerical calculations based on the developed model of IF forcing into the seabed at given ground cohesion and outer forces permit to estimate maximum value of the IF penetration into the bed in a single act of scouring. In case further factors related to possible ice crushing and IF vertical displacement are taken into account, the calculated depth of grooves can only be only reduced.

As follows from the calculations performed for ground cohesion in excess of 10 kPa, the maximum scour depth does not exceed 1 m in case the IF is more than 5 m wide at the contact with the seabed. In case of the IF width is of order of 1 m, the scour depth may be far greater.

To make the model more sophisticated by introducing vertical and lateral displacements of IF in the processes of scouring may be worthwhile in investigating of the grooves concentration and orientation as related to the sea floor depth and topography. Of some interest is exploration into changes of the sea floor micro-relief resulting from periodical reciprocate movements of IF with individual protrusions scratching seabed.

References

1. Zaharov, V.F. 1996. Sea ice in climatic system. S-Pb.:Hydrometeoizdat. (in Russian)
2. Chari, T.R.& J.N. Allen. 1974. An analytical model and laboratory tests on iceberg sediment interaction.. *Proc. IEEE Int. Conf. on Eng. in the Ocean Environment.* New York: Inst. of Electrical and Electronic Engineers, Inc. 1:133-136.
3. Clark, J.J., Paulin, M.J. & F.Poorooshasb. 1990. Pipeline stability in an ice-scoured seabed. *Proc. First (1990) European Offshore Mech. Symp.* Trondheim, Norway: 533-549.
4. Woodworth-Lynas, C.M.T. & J.V. Barrie. 1985. Iceberg scouring frequencies scour degradation on Canada's eastern shelf areas using sidescan mosaic remapping techniques. *Proc. POAC 85.* Narssarssuaq,Greenland:419-442.
5. Beloshapkova, S., Beloshapkov, A., Sovershaev, V., Antsyferov, S., Goncharov, A. 1995. Features of sediment dynamics in the region of the underwater pipeline crossing construction across Baydaratskaya Bay in Kara sea. *Proc. "Fourth Int. Conf. on Coastal & Port Engineering in Developing Countries (COPEDEC IV)",* Rio de Janeiro, Brazil: 97-111.
6. Ryabinin, V.E., Danilov, A.I., Elisov, V.V., Klepikov, A.V., Kurdumov, V.A., Malek, V.N., Smirnov, V.N., Stepanov, I.V., Timofeev, O.Ya. 1995. Marine ice bottom gouging: Some mechanisms and an approach to depth evaluation. *Proc. Sea Ice Mech. and Arctic Modeling Workshop.* Anchorage. Alaska. 2:276-285.
7. Klepikov, A.V., Malek, V.N., Stepanov, I.V., Timofeev, O.Ya., Spichkin, V.A. 1997. Sea ice and its impact on the bottom at the region of the Baydaratskaya Bay pipeline underwater crossing. *Book of abstracts of the III Int. Conf. "Development of Russian Arctic Offshore",* St.-Petersburg,192-193. (in Russian)
8. Odisharia, G.E., Tsvetsinsky, A.S., Remizov, V.V., et al. 1997. *Baydaratskaya Bay Environmental Conditions. The Basic Results for the Pipeline "Yamal-Center" Underwater Crossing Designe.* Moscow:GEOS. (in Russian)
9. Robe, R.Q. 1980. Drift and destruction of icebergs. In the book *"Dynamics of snow and ice masses".* Ed. by S.C.Colbeck. Academic Press: New York.
10. Goldstein, R.V., Marchenko A.V. 1997. On a choice of rheological relations for equations of the ice cover dynamics. *Proc. OMAE 1997,* Vol. IV, Arctic/Polar Technology, ASME, pp. 451-460.
11. Rabotnov, Yu.N. 1988. *Mechanics of solids.* M.: Nauka. (in Russian)

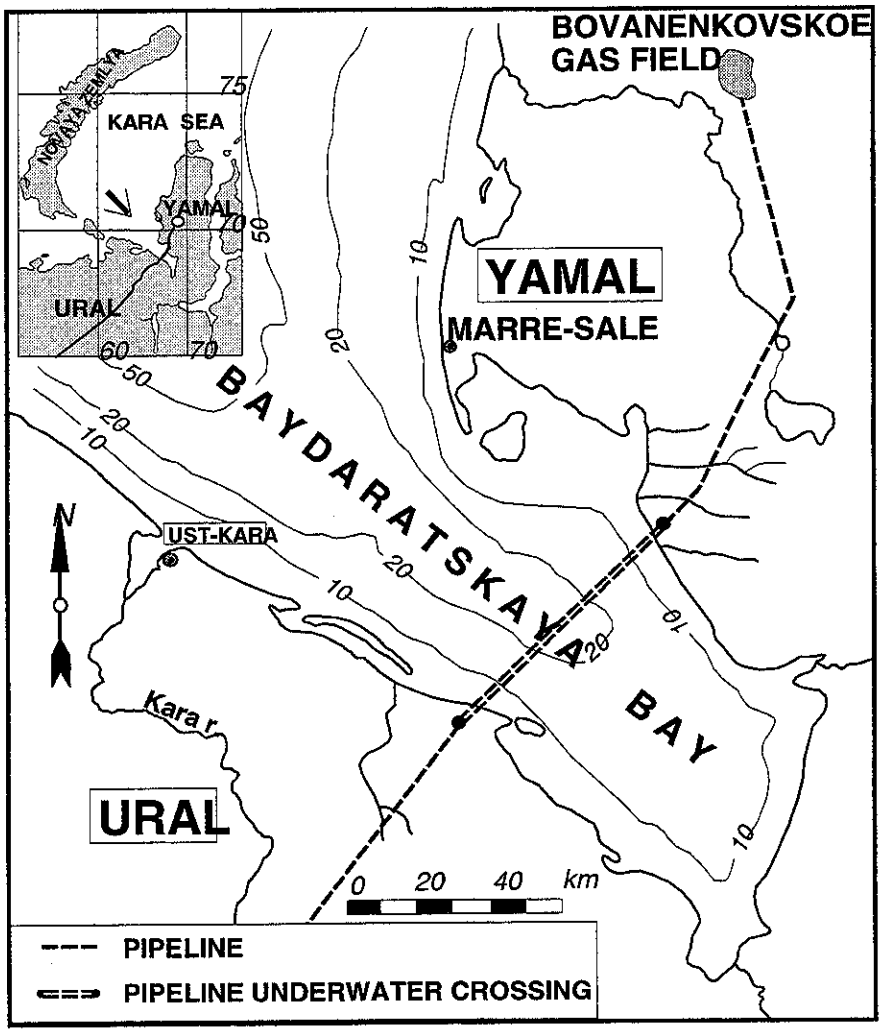

Figure 1. The region of pipeline underwater crossing Yamal-Europe

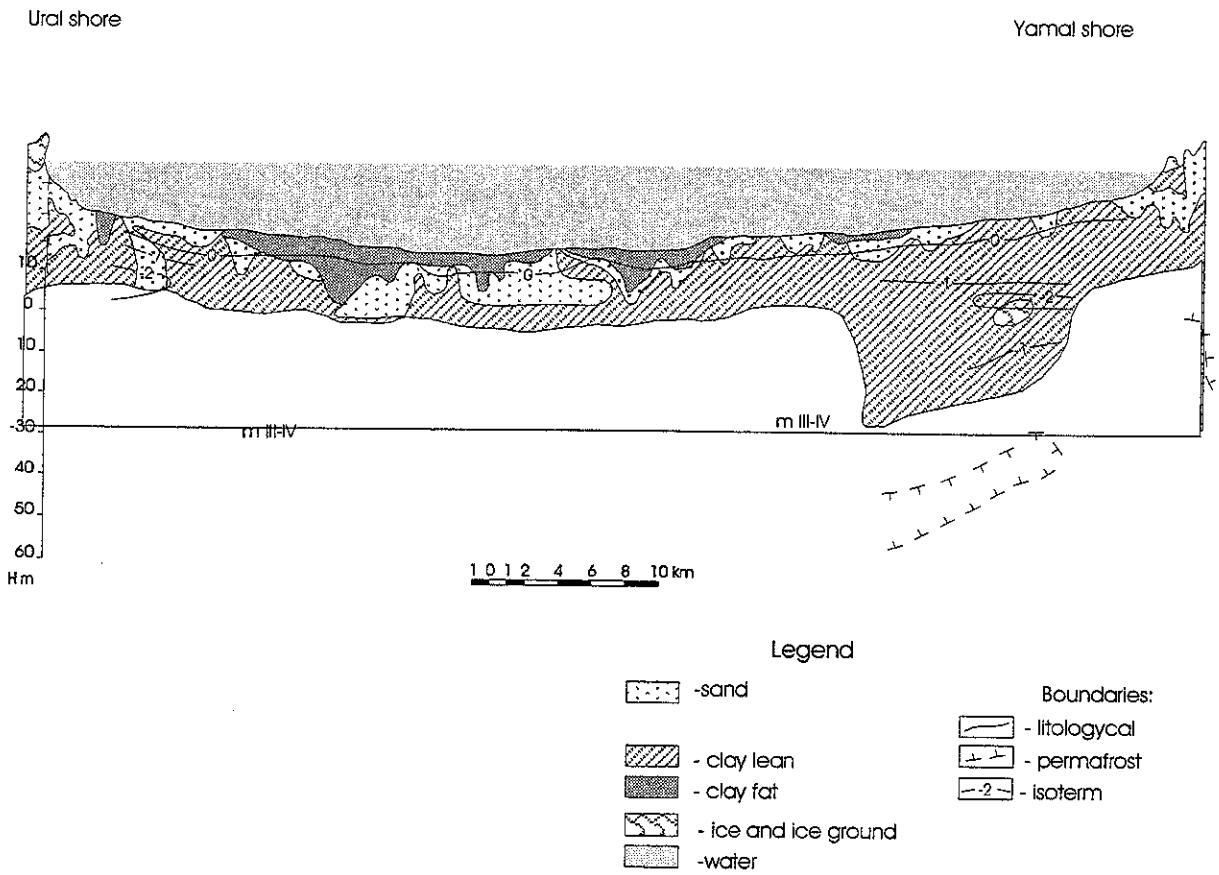

Figure 2. Schematic geological cross- section of the Baydaratskaya Bay

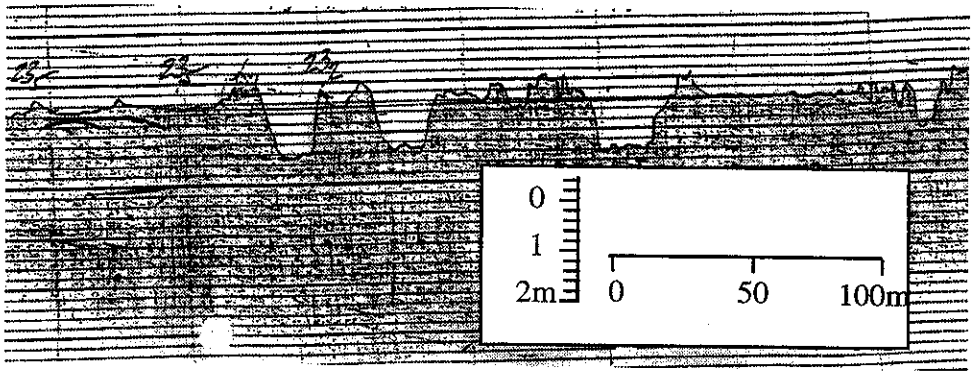

Figure 3. Example of exaration grooves recorded by echo-sounder

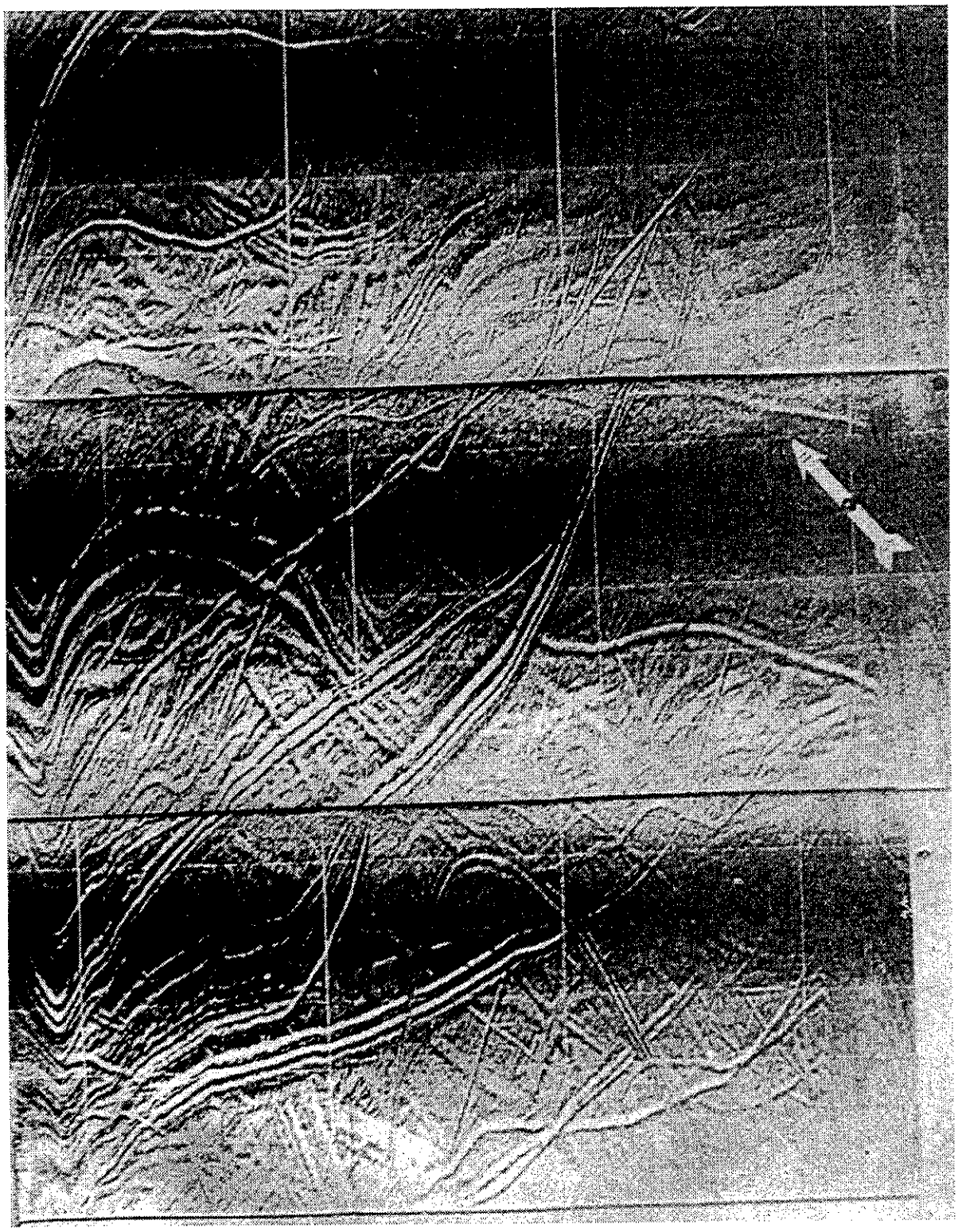

Figure 4. Partial HLSS record, after SE AMIGE materials.

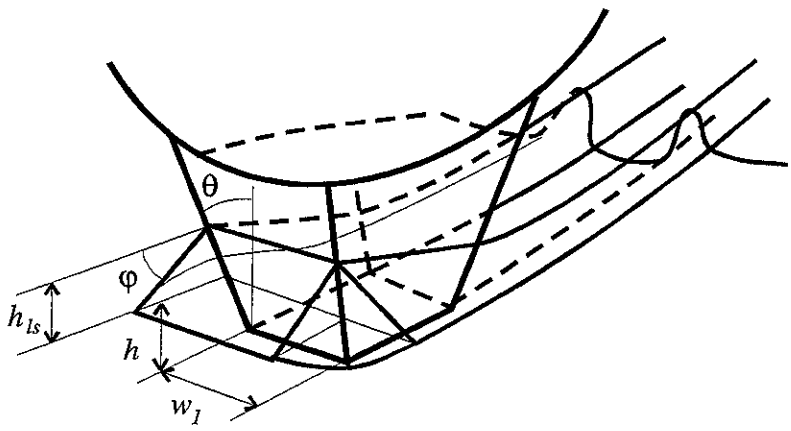

Figure 5. The penetration into sead bed a part of the IF.

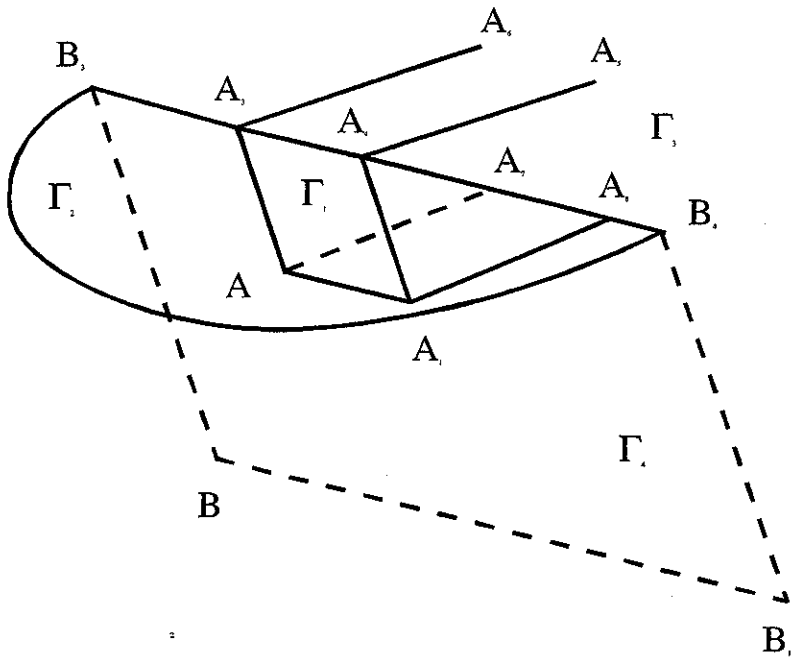

Figure 6. Boundaries of the volume , occupied by sea bed soil.

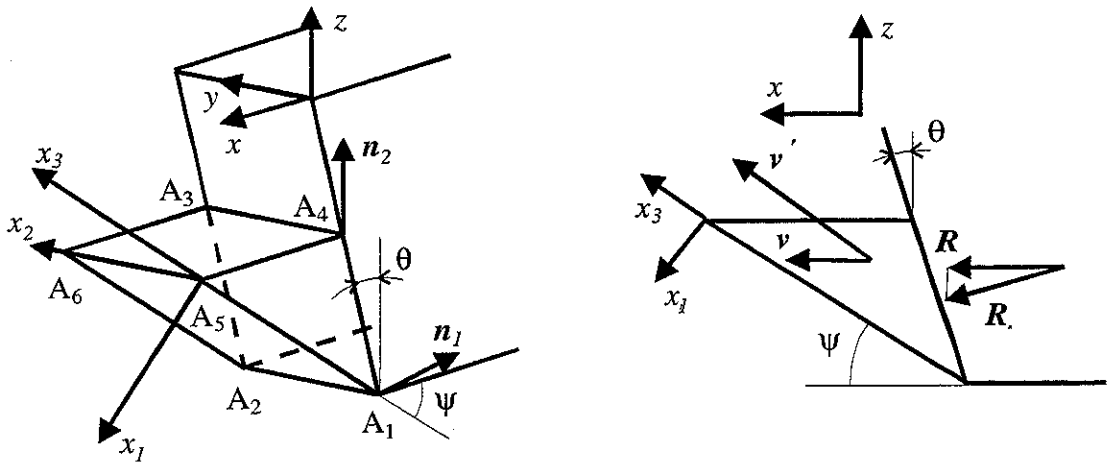

Figure 7. Kinematically admissible scheme of soil motion in the front of the IF.

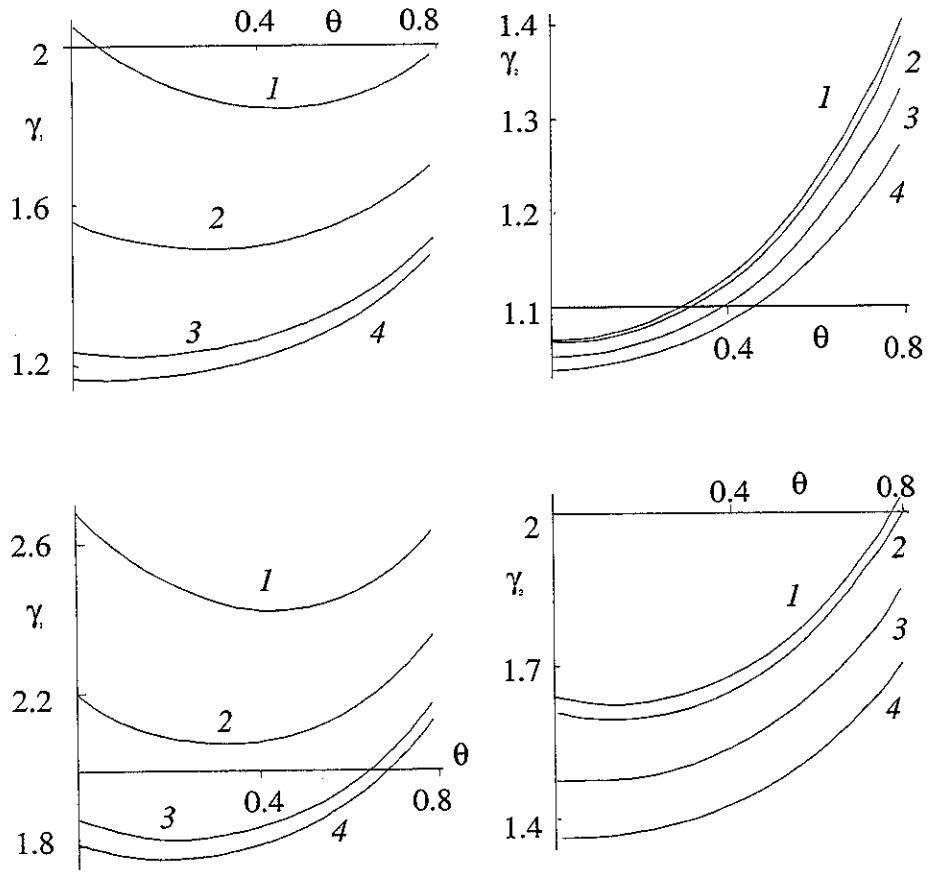

Figure 8. The dependencies of $\gamma_1(\theta)$ and $\gamma_2(\theta)$, by h =2 m; the ratio h/w_1 is equal to 0.1 (*a*,b) and 1 *(c,d);* soil cohesion is equal to 5 kPa *(1),* 10 kPa *(2),* 30 kPa (*3*) and 50 kPa *(4)*

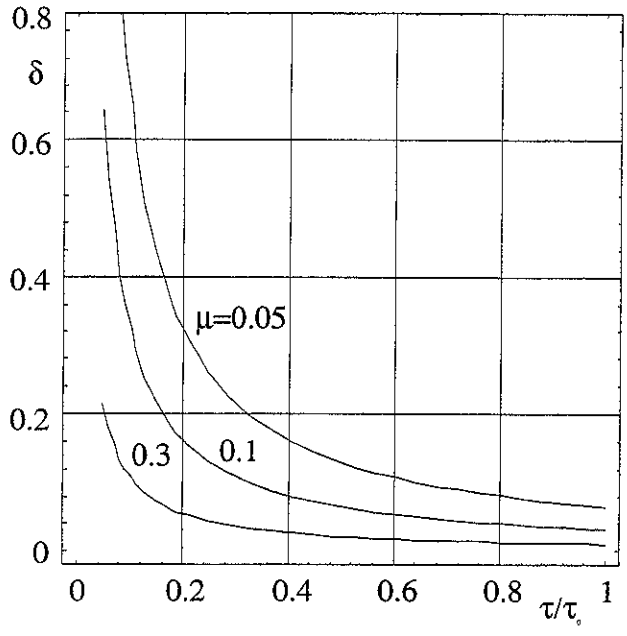

Figure 9. The dependence of scour depth from soil cohesion in dimensionless variables for stationary motion of the IF.

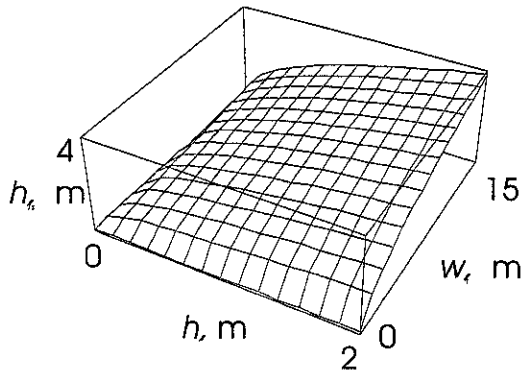

Figure 10. The dependence of the height h_{ls} of soil embankment in front of the IF from the width w_l of a part of the IF, penetrating into sea bed, and scour depth h for stationary motion.

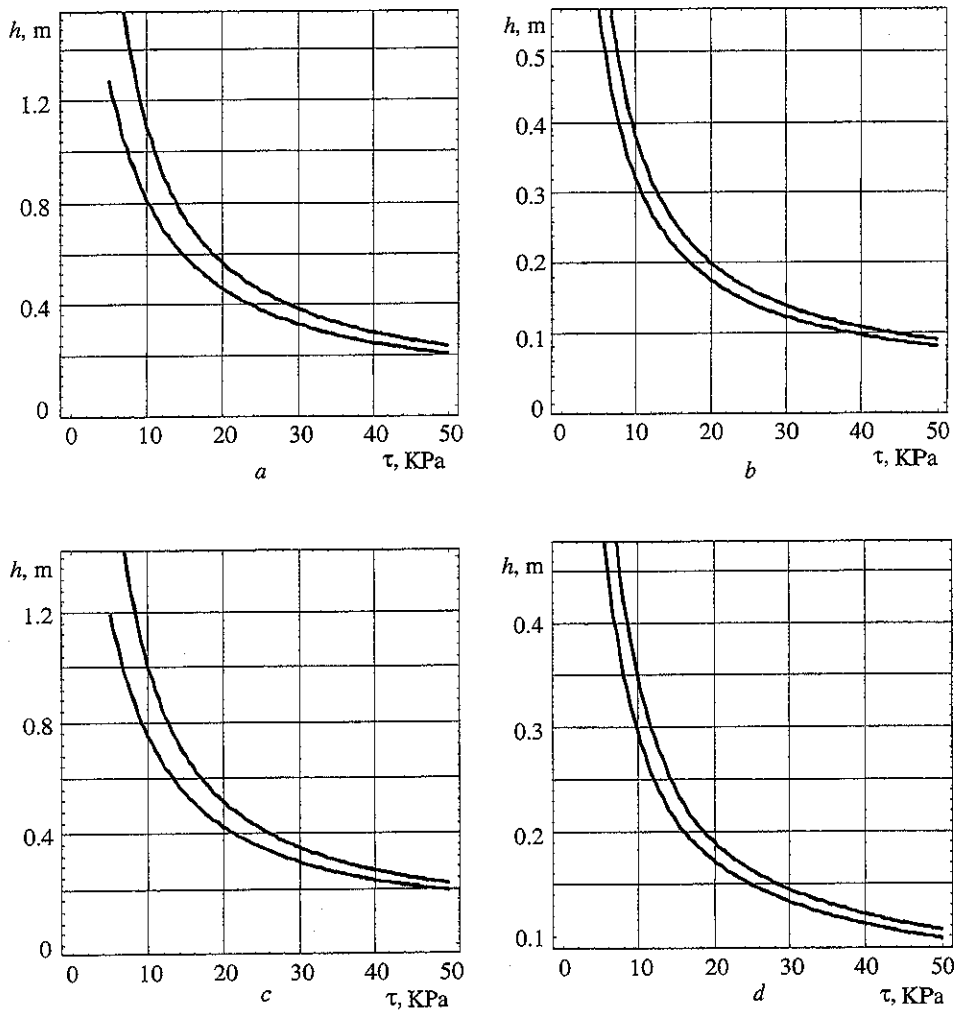

Figure 11. The dependence of scour depth from soil cohesion later 3 h after the beginning of the penetration of the IF into sea bed

Ice Scours and Ice Ridges of Lake Erie, Ontario, Canada

Jim Grass
Geotechnical Engineer, Ontario Hydro, Toronto, Ontario, Canada

In 1980, Ontario Hydro proposed the construction of a high voltage transmission cable system across the eastern basin of Lake Erie along a corridor105km long and 4.5km wide to connect the Nantichoke Generating Station in Ontario, Canada to the presently underdeveloped Coho site near Erie, Pennsylvania, USA to export electricity.

Investigations involving sediment sampling, diamond drilling from barges and detailed geophysical surveys (side-scan sonar and echo sounder) were carried out to determine lake bottom conditions for engineering design and construction. During the geophysical surveys, ice scours were discovered in soft, clayey soils on the Canadian side and in loose, silty sandy sediments on the American side. The ice scours were approximately 4.5 to 6 km long, 60 to 100m wide and up to 2m deep in the lake bed. Scours were found in water depths ranging from 13 to 25m. Near shore areas appear to be protected by extensive shore fast ice. The pattern of scours appears to be associated with fast ice mass distribution with the fast ice protecting some areas from scours by diverting the lake ice around or along the edges of the fixed ice. Scour depths are likely related to the type of lake bottom material encountered by the ice keels. Various depths of ice penetration along individual scours may be related to different strengths of materials encountered as the ice keel scours the lake bottom. In addition there appears to be tremendous internal movement of ice pieces as the ice keels are deformed during the dynamic scouring process which may also affect the scour characteristics.

Correlation of repeated geophysical survey data and ice scour related gas pipeline damage confirmed by divers on the Canadian side verified the recent age of the scours. Fresh scours found on the American side were formed during the winters of 1981 and 1982 as confirmed by repetitive geophysical surveys from year to year immediately after spring thaw. Scours on the Canadian side were preserved from year to year due to the clayey nature of the soils whereas scours on the American side were obliterated from year to year as water currents mainly during storm events redistributed the sandy sediment.

A helicopter supported ice observation program was carried out during the winter periods of 1981 and 1982 to map ice ridges and measure ice thickness. The actual rapid deformation of ice at the edge of a huge grounded ice island in the middle of Lake Erie was observed and filmed in February/March 1982. Very strong winds at the time were responsible for the lake ice sheet movement. Geophysical surveys in the spring of 1982 discovered an extensive ice scour at this location. The scour was 2.5km long, 30m wide and up to 1.5m deep in 16 to 19m water depth.

It was recommended that the proposed power cables be buried in shallow trenches, excavated into the lake bottom to a depth of up to 3m to protect the cables against damage from ice keels. This project was cancelled in 1982.

References

Grass, J.D. 1985. Lake Erie cable crossing - ice scour study. In, Workshop on Ice Scouring, 15 - 19 February, 1982, National Research Council of Canada Associate committee on geotechnical research, Technical memorandum No. 136: 1-10.

Grass, J.D. 1984. Ice scour and ice ridging studies in Lake Erie. IAHR Ice Symposium, Hamburg: 33-43.

VERIFICATION OF CENTRIFUGE MODEL RESULTS AGAINST FIELD DATA: RESULTS FROM THE PRESSURE RIDGE ICE SCOUR EXPERIMENT (PRISE)

C.M.T. Woodworth-Lynas, R. Phillips, J.I. Clark, F. Hynes, X. Xiao

C-CORE - Centre for Cold Ocean Resources Engineering
Memorial University of Newfoundland
St. John's, NF, Canada A1B 3X5

Abstract

This paper presents the preliminary findings of the investigation of soil structures that form as the result of ice keel scour-induced soil deformation produced by centrifuge models of ice keel scour. From the models four classes of structures are identified (lateral berm piles; sand boils; sub-scour bearing capacity-type failures; low angle thrusts) and compared with similar structures of large-scale, naturally-occurring scour marks. The remarkable correlations between modelled and observed structures indicates that the models replicate accurately the scouring process, and strengthens confidence in the interpretation of soil behaviour phenomena, such as vertical and horizontal loads and pore pressure changes, that cannot be observed in the field.

Introduction

Centrifuge model data must be shown to replicate the general morphology and structure of naturally-occurring scour marks at equivalent prototype scale. Such verification is vitally important because it indicates that the centrifuge models reproduce soil deformations observed in the field, and thus that there is confidence that the models are accurate predictors of the scouring phenomenon. Centrifuge models are capable of producing far more data than can be possibly retrieved from equivalent naturally-occurring scour marks (Table 1). This is because field data have only ever been collected from existing scour marks about which nothing is known of the ice features or of the scour-induced forces that created them. Field data collected from scour marks comprise surface morphology (width, depth and surface structures), of which the largest amount of information comes from marine geophysical surveys (high resolution sub-bottom profile and sidescan data) in the Canadian Beaufort Sea and on the eastern Canadian continental shelves [1,2,3]. These data are not discussed here. Sub-scour information comes from trench investigations of old (several thousand years) scour marks in consolidated soils that are now exposed on land, and include two-dimensional mapping of slip surfaces, distorted layering, relief of the incision surface, and measurement of slip surface attitude (dip and strike) and soil shear strength values. Validation of centrifuge scour models can be achieved by comparison of post-scour field and post-scour model soil structures. If there is good correlation between soil deformation structures documented in the field and in the models, there is confidence that the other model data (load and pore pressure changes) are valid for prototype-scale events.

Existing Field Data of Sub-scour Deformation

Model verification of sub-scour deformation is based on field data from three reported studies of scour marks in Manitoba, Ontario and Norway [4,5,6,7]. For each study the scour mark characteristics are given in Table 2. Cross-sections of the reported scour marks are shown in Figure 1. Longva and Bakkejord [7] studied two relict scour marks that formed in glacimarine clays by scouring icebergs in southern Norway. They show that beneath one 30 m-wide feature (scour mark II) laterally continuous laminae are deflected in low amplitude (0.7 m), open folds that mimic the scour mark trough surface (Figure 1a). Faulting is restricted to very small movements (<100 mm) along a suite of near-vertical fractures in a narrow zone beneath the central part of the scour mark and which extend to at least 2 m below the

scour mark trough. Minor reverse faults in scour mark II and detached slabs of clay up to 2 m long in scour mark I (70 m wide), at or immediately below (<0.5 m) the scour mark surface, indicate thrusting of material ahead and to the side of the scouring keel. For one cross section (scour mark II) the authors attempted a palinspastic reconstruction of the sediments before the scour event, and concluded that 67% of the cross sectional area of clay was physically removed by the (bulldozing?) keel, and that 33% was displaced downwards beneath the keel (to a maximum of 0.75 m vertical displacement as measured from Figure 11c of Longva and Bakkejord [7]).

From sandy delta-front sandy glacilacustrine storm deposits exposed along Scarborough Bluffs, Ontario, Eyles and Clark [6] described a 9 m-wide, 2 m-deep V-shaped scour mark interpreted to have been made by a lake ice pressure ridge keel (Figure 1b). Normal and reverse high angle faults occur beneath the rising flanks of this feature with maximum dip slip offset of 0.5 m (measured from Figure 10A of Eyles and Clark, [6]). However, the deepest penetrating faults (max 2 m long) occur on the highest part of the scour mark flanks so that below about 0.25 m beneath the deepest part of the trough, sediments appear to be unaffected. Lateral compression seems to have been dominant where the trough is widest, as shown by the presence of asymmetric and recumbent folds in a prominent layer on either side of the trough, whereas downward displacement appears dominant beneath the deepest part of the scour mark.

Scour marks are preserved in lacustrine clay sediments of former glacial Lake Agassiz in southern Manitoba. Scour marks here generally have similar dimensions to their modern marine counterparts, and formed in similar water depths. Work carried out by C-CORE researchers on four of these scour marks [4,5] showed that prominent conjugate faults are developed below one scour mark trough extending to at least 5.5 m beneath the deepest part of the scour mark incision surface. Stereo plots of structural data reveal that smaller, unconnected fault segments below all of the scour marks may also be conjugate sets. Conjugate faults are interpreted to have formed in response to bearing capacity failure of soil beneath the scouring keel. A sub-horizontal thrust fault beneath one scour mark is interpreted to have developed immediately ahead of a scouring iceberg keel and indicates that horizontal shear forces propagated to depths as great as 6 m below the lakebed.

Comparison of Field Data with PRISE Centrifuge Model Data

Four classes of soil deformation structures have been observed in the PRISE centrifuge models that correlate well with similar structures observed in the field. These structures include: lateral berm piles; sand boils; sub-scour bearing capacity-type failures; low angle thrusts. These structures are discussed below.

Lateral Berm Piles - On both sides of scour mark troughs are two co-linear piles of material that represent soil that has been displaced to each side by the scouring keel. Displacement can be caused by both bulldozing and by vertical heave, within the near field of the passive Rankine zones, of the seabed in response to downloading of soils in the scour mark trough. In the field, the best examples of berms are associated with modern marine scour marks where surface structures are exposed to observation by both sidescan sonar and from submersibles. Small-scale variability of berm structure is observed in examples of both modern marine and PRISE model scour marks (Figure 2). Field and model examples show development of both structureless piles and regions where apparent tension fractures create block-like topography (Figure 3), probably indicative of remoulding caused by bulldozing and of local seabed upheaval respectively.

Sand Boils - Sand boils are conical mounds of sediment that form by extrusion and deposition of material mobilized from below the sediment surface. They are indicators of sub-surface liquefaction. Sand boils were observed in one of the PRISE models (PRISE 07, Drive 2) where the scour cut depth was 2 m and attack angle was 15 degrees. This test was a model of clay (approximately 2.7 m thick) over dense sand. The scour event removed all but approximately 0.3 m of clay in the scour mark trough, and it was in the trough that the sand boils developed (Figure 4). The boils consisted entirely of sand that had been mobilized from below the clay layer. The sand boils formed some time after the keel had passed because they are developed on top of the cut surface and are perfectly formed showing no evidence of scour-induced deformation.

During the Dynamics of Iceberg Grounding and Scouring (DIGS) Experiment [2] in 1985, conical mounds, approximately 50 cm high and 80-100 cm diameter, were observed in the trough of a new scour mark on Makkovik Bank, Labrador Sea (Figures 5 & 6). Mounds were not observed outside the trough. No description or interpretation of these features was given. However, following observation of the PRISE 07 test, seabed video from a submersible dive on the scour mark was reviewed. The conical mounds consisted of loose soil of different colour and texture than the consolidated soil of the scour mark trough. Pieces of broken shell and

small pebbles were seen on the flanks of the mounds, but were not seen elsewhere in the scour mark trough. The relative differences in texture, colour and consolidation suggest that the mound material originated from a different soil unit. The perfect form of the mounds indicates that they formed after the scouring keel had passed, and their conical shapes are characteristic of the class of sediment extrusion features collectively known as mud or sand volcanoes. Combined evidence from the video suggests that the mounds are extrusive in origin, and are the result of sub-scour liquefaction that mobilized, and carried to the surface, soil of slightly different composition than soil comprising the scour mark trough.

In Norway, Longva and Bakkejord [7] mapped near-vertical sub-scour fractures beneath a scour mark. These fractures caused small displacements (<10 cm) of bedding planes and may have been related to scour-induced liquefaction and dewatering. However, no sand boils were described by these workers.

Sub-scour Bearing Capacity-type Failures - Pervasive bearing capacity failure surfaces were identified and mapped beneath one of the Manitoba scour marks [4,5]. Some of these failure surfaces extended more than 5.5 m below the scour mark cut depth and one showed relative offset movement of 3.5 m. Similar failure surfaces were mapped beneath the flanks of a V-shaped scour mark developed in sand in Ontario [6], although none of these extended below the maximum keel cut depth. The two scour marks from Norway [7] showed no evidence of bearing capacity failure surfaces, but did exhibit laterally continuous laminae that were deflected in low amplitude (0.7 m), open folds that mimicked the scour mark trough surface.

Bearing capacity failures were evident in some of the PRISE clay tests, although discrete failure surfaces could not be discerned (Figure 7). This failure mechanism correlates with that hypothesized for the Manitoba scour marks. With one exception bearing capacity failures did not develop beneath any of the sand tests

Low-Angle Thrust Faults - Thrust faults were observed only beneath two of the Manitoba scour marks (B and D). Here slabs of brown clay, their lower surfaces defined by low-angle thrust faults, rest on top of younger, deformed silty clays. Such structural stacking of older sediments above younger implies upward vertical, and horizontal components of movement of the brown clay slabs, and downward vertical displacement of tan-coloured silts to a position below the stratigraphic base of the silt and below the base of the scouring ice keel.

Below scour mark B a downfaulted clay block (Figure 8) rests on deformed silt below the outer berm. Below the inner northeast berm of scour mark B a clay slab has been overridden by the scouring ice keel because its upper surface is continuous with the scour mark incision surface on either side (Figure 8). Below the trough of scour mark D the presence of two sub-horizontal lenses of tan-coloured silt at 1.5 m depth suggests that the silt has been similarly structurally incorporated in the matrix of the brown clay.

It is interpreted that the clay slabs originated from a structurally lower region near the centre of the scour mark. Horizontal loads in the sediment ahead of the encroaching iceberg keel caused decoupling of the slabs along décollements within the brown clay. Forward, upward and outward translation of the "rigid" slabs occurred as the keel approached. The thrust surfaces penetrated through an overlying thin deposit of tan-coloured silt. Movement of the clay slabs over the silt possibly accounted, in part, for reworking of the younger material through the action of shear-dragging. The scouring keel overrode thrust slabs trapped in the central part of the scour mark trough, as at scour mark D and below the inner northeast berm of scour mark B, possibly causing additional reworking of the silt. Thrust slabs closer to the berms were pushed aside as the keel passed and may have collapsed, under self-weight, on the outer berm margins, as at scour mark B (trench 1) [4,5].

Three sub-horizontal faults, arranged one above the other, occur on the southwest margin of scour mark B. Although there are no tan-coloured silts beneath them the development of these faults beneath the scour mark margin suggests the sequential structural stacking of horizontal blocks of brown clay displaced, as in the other margin, from the central part of the scour mark by the scouring keel. Such stacking is envisaged as being responsible, at least in part, for generating positive relief of the scour mark berms in clay soils [4,7].

Similar, well-developed low-angle thrust faults were observed in sub-scour sediments of only one PRISE test (number 08). This test modelled a simple stratigraphy of sand (3.15 m thick) over clay. Model keel width was 15 m and the attack angle was 15 degrees. The cut depth was approximately 1.5 m so that there was no penetration of the keel through the sand to the clay. After the test within the scour mark trough there was no surface evidence of sub-scour movement. However, excavation of the sand layer within the scour mark trough revealed that the buried, originally flat clay surface had been deformed into a series of imbricately-stacked thrust slabs (Figure 9), approximately 0.75 m thick. Vertical dissection of the clay along the scour mark centreline showed clearly the stacked slabs (Figure

10). It is interpreted that movement of the scouring keel caused shear dragging [8] of the sand forward beneath it. Horizontal shear dragging in the sand caused dragging and detachment of thin slabs of clay in the zone immediately below the sand/clay contact. The leading edges of slabs 1 and 2 penetrated upwards into the sand so that profiles A and B, when seen in cross-section, would show a layer of detached clay sandwiched between zones of sand, as observed beneath the Manitoba scour marks.

Stratigraphic conditions for the model test (sand over clay) were broadly similar to those for the Manitoba scour marks (silt over clay) in that coarse soils overlay fine soils. The model test replicated the development of low-angle thrust faults and thin clay slabs that overrode younger, coarser sediment observed beneath the two Manitoba scour marks. The centrifuge model reveals the context in which the faults developed, namely a simple stratigraphy of coarse (sand) overlying fine sediment (clay), and indicates that in both cases the overlying coarse layer is responsible for creating thrust faults in the underlying fine sediment through horizontal shear-dragging induced by forward translation of the scouring keel.

Conclusions

Post-scour examination of the centrifuge models shows that surface and sub-surface, scour-induced deformation structures replicate well the prototype structures observed from full-sized scour marks in the field. These findings increase the confidence in interpretation of other data, particularly soil force data, that are provided by the centrifuge models.

We gratefully acknowledge the funding participants of PRISE:

- **ARCO Alaska Inc.**
- **Chevron Petroleum Technology Co.**
- **Exxon Production Research Co.**
- **Gulf Canada Resources**
- **Minerals Management Service**
- **Mobil Research and Development Corporation**
- **Mobil Oil Canada Properties**
- **National Energy Board (Canada)**
- **Natural Sciences and Engineering Research Council (Canada)**
- **Norwegian Research Council**
- **Petro-Canada Resources**

References

1. Lewis, C.F.M. and S.M. Blasco. 1990. Character and Distribution of Sea-ice and Iceberg Scours. In: Workshop on Ice Scouring and the Design of Offshore Pipelines, Calgary, April 18-19: 57-101.

2. Hodgson, G.J., Lever, J.H., Woodworth-Lynas, C.M.T. and Lewis, C.F.M. (editors). 1988. The dynamics of iceberg grounding and scouring (DIGS) experiment and repetitive mapping of the eastern Canadian continental shelf. Environmental Studies Research Funds Report No. 094, Ottawa, 316p.

3. Woodworth-Lynas, C.M.T., H.W. Josenhans, J.V. Barrie, C.F.M. Lewis and D.R. Parrott. 1991. The physical processes of seabed disturbance during iceberg grounding and scouring. Continental Shelf Research, 11 (8-10): 939-961.

4. Woodworth-Lynas, C.M.T. 1992. The Geology of Ice Scour. Ph.D. thesis, University of Wales, School of Ocean Sciences: 269p.

5. Woodworth-Lynas, C.M.T. and J.Y. Guigné. 1990. Iceberg scours in the geological record: examples from glacial Lake Agassiz. In: Glacimarine Environments: processes and sediments (J.A. Dowdeswell and J.D. Scourse, eds.). Geological Society Special Publication No. 53: 217-233.

6. Eyles, N. and B. Clark. 1988. Geological Society of America Bulletin, 100: 793-809.

7. Longva, O. and K. Bakkejord. 1990. Marine Geology, 92: 87-104.

8. Been, K. 1990. Mechanisms of failure and soil deformation during scouring. Workshop on Ice Scouring and Design of Offshore Pipelines, Calgary, April 18-19, 1990: 179-191.

Table 1. Comparison of Data Retrievable from Naturally-Occurring and Modelled Scour Marks.

Type of Data	Naturally-Occurring Scour Marks	Modelled Scour Marks
Sub-scour Deformation Structures	YES	YES
Orientation of Slip Surfaces in 2 Dimensions	YES	YES
Orientation of Slip Surfaces in 3 Dimensions	YES	NO
Soil Grain Size	YES	YES
Pre-Scour Soil Consolidation	NO	YES
Pre-, Syn- and Post-Scour Pore Water Pressure	NO	YES
Vertical and Horizontal Loads	NO	YES
Scour Mark Cut Depth	YES	YES
Ice Keel Width	YES (Inferred)	YES
Ice Keel Length	NO	YES
Ice Keel Attack Angle	NO	YES
Ice Keel Velocity	NO	YES
Contact Pressure on Keel Face	NO	YES
Total Stress in Seabed	NO	YES

Table 2. Characteristics of scour marks from which sub-scour deformation structures have been documented.

Location (and ref. No.)	Number of scour marks	Environment	Water Depth at time of scouring	Scour Mark Width	Scour Mark Depth	Soil Type	Age of Features (years)
Manitoba [4,6]	4	Glacial Lake	110 m	50 - 65 m	2-2.5 m	Clay	~9,900
Ontario [5]	1	Glacial Lake	20 m	9 m	2.5 m	Medium Sand	~60,000
Norway [6]	2	Glacial Flood	185 - 200 m	30 m 70 m	~1 m ~1 m	Clay	~9,200

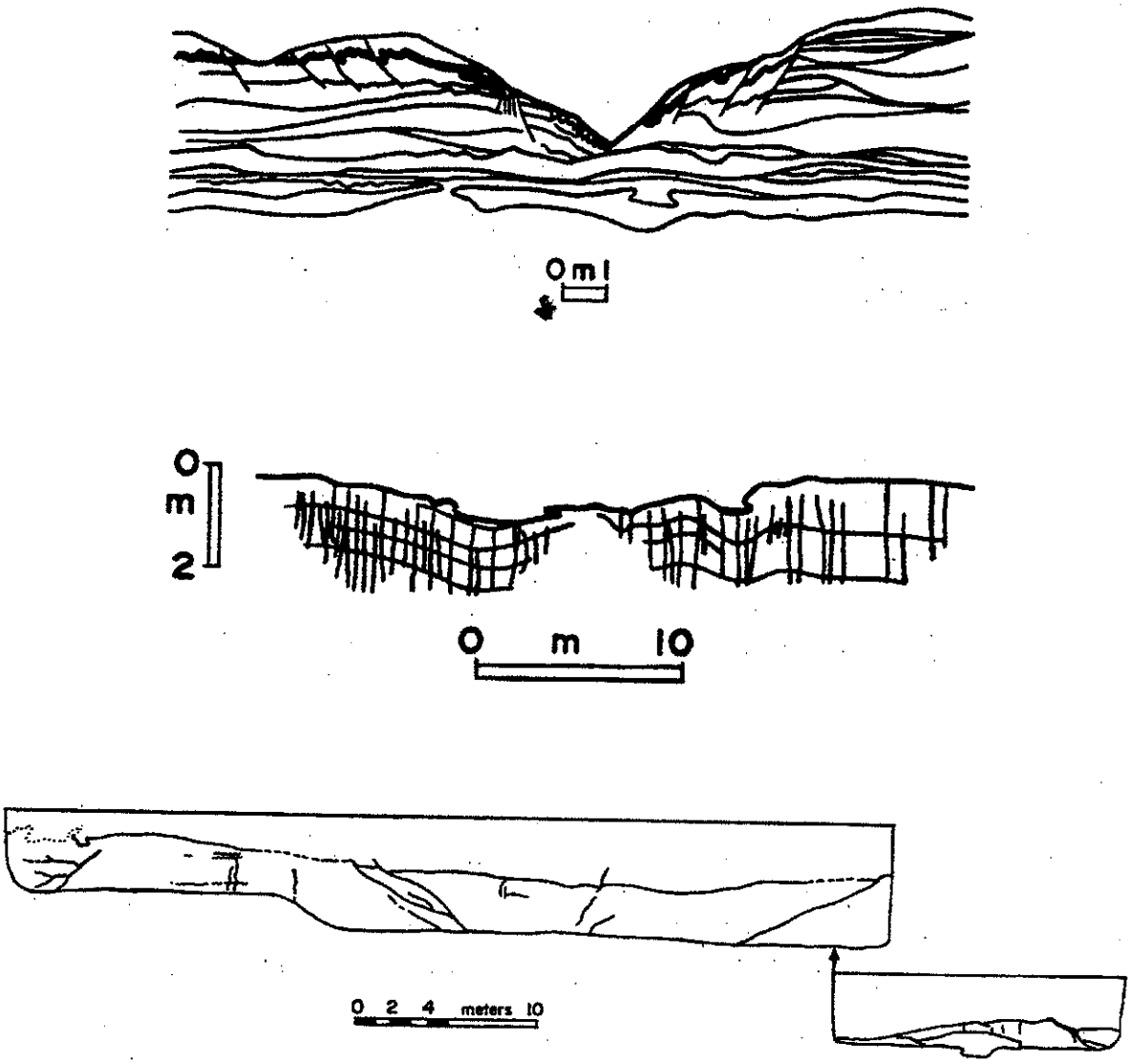

Figure 1. Cross-sections of ice keel scour marks reported in the literature. **Top**: V-shaped lake ice scour mark in sandy sediments, Scarborough Bluffs, Ontario [6]. **Centre**: Scour mark in layered clay, southeastern Norway [7]. **Bottom**: Scour mark in clay, southeast Manitoba [5}.

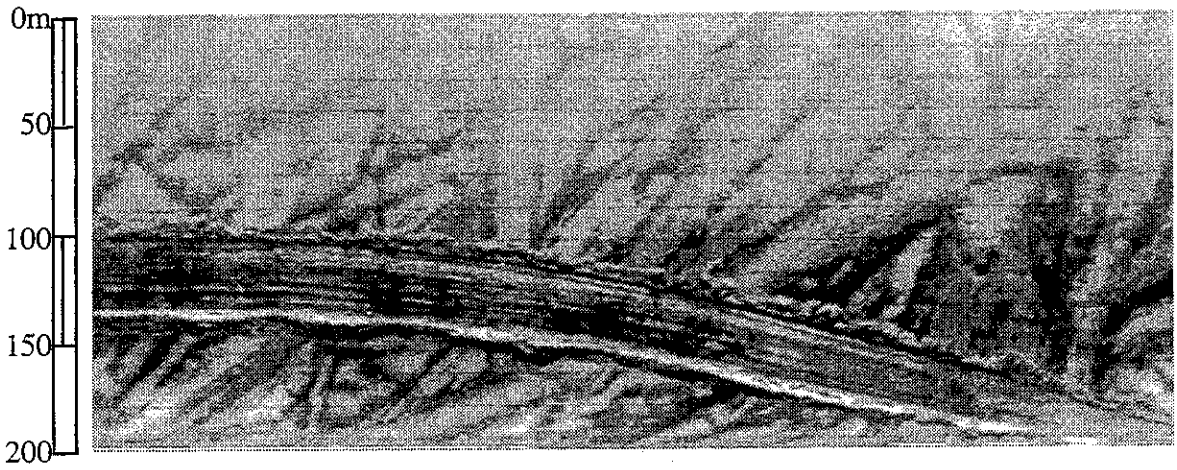

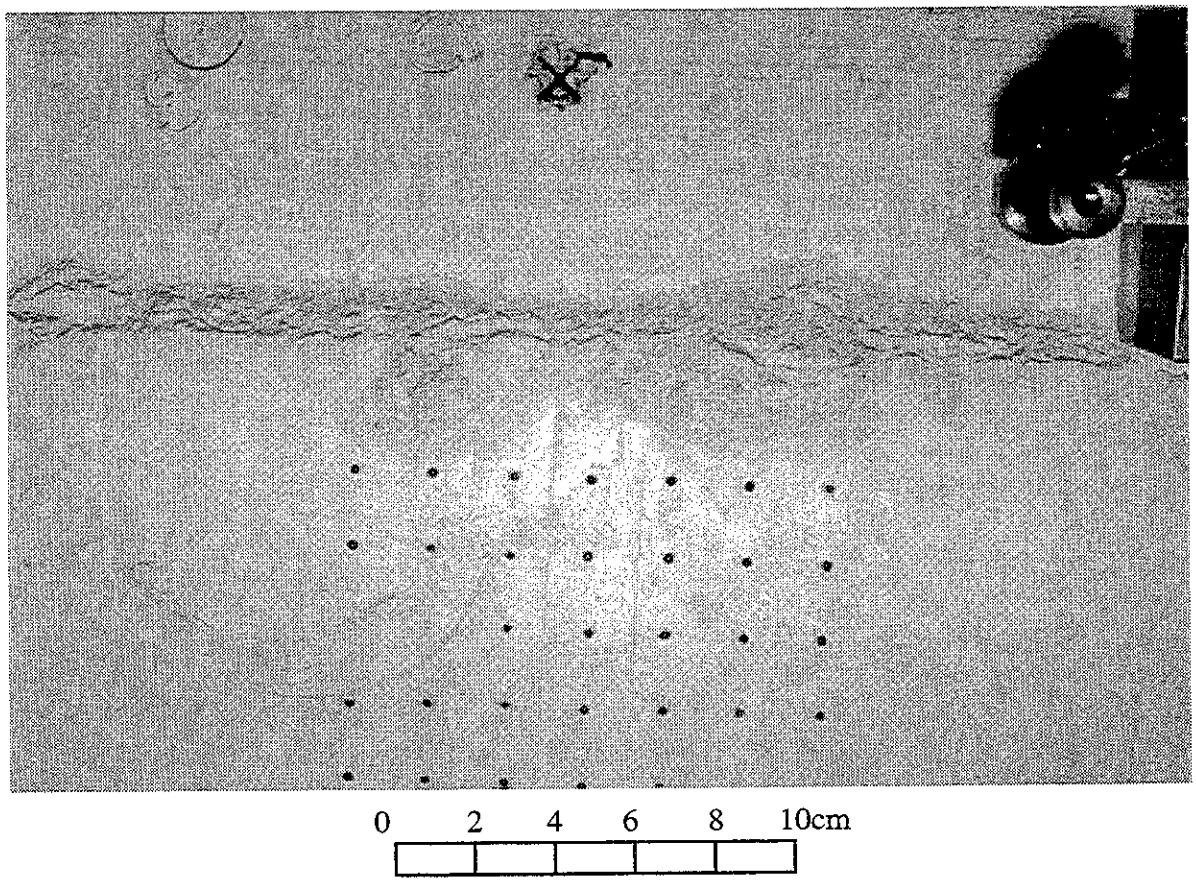

Figure 2. **Top**: Sidescan sonograph of new iceberg scur mark showing berms of variable structure and width. Where berms are wide, soil is generally loose and structureless. Narrow berms are areas of consolidated soils, often fractured into free-standing blocks, (as in Figure 3). **Bottom**: Vertical view of model berm showing variable width and structure (scour mark trough at top, and model keel still *in situ* at right).

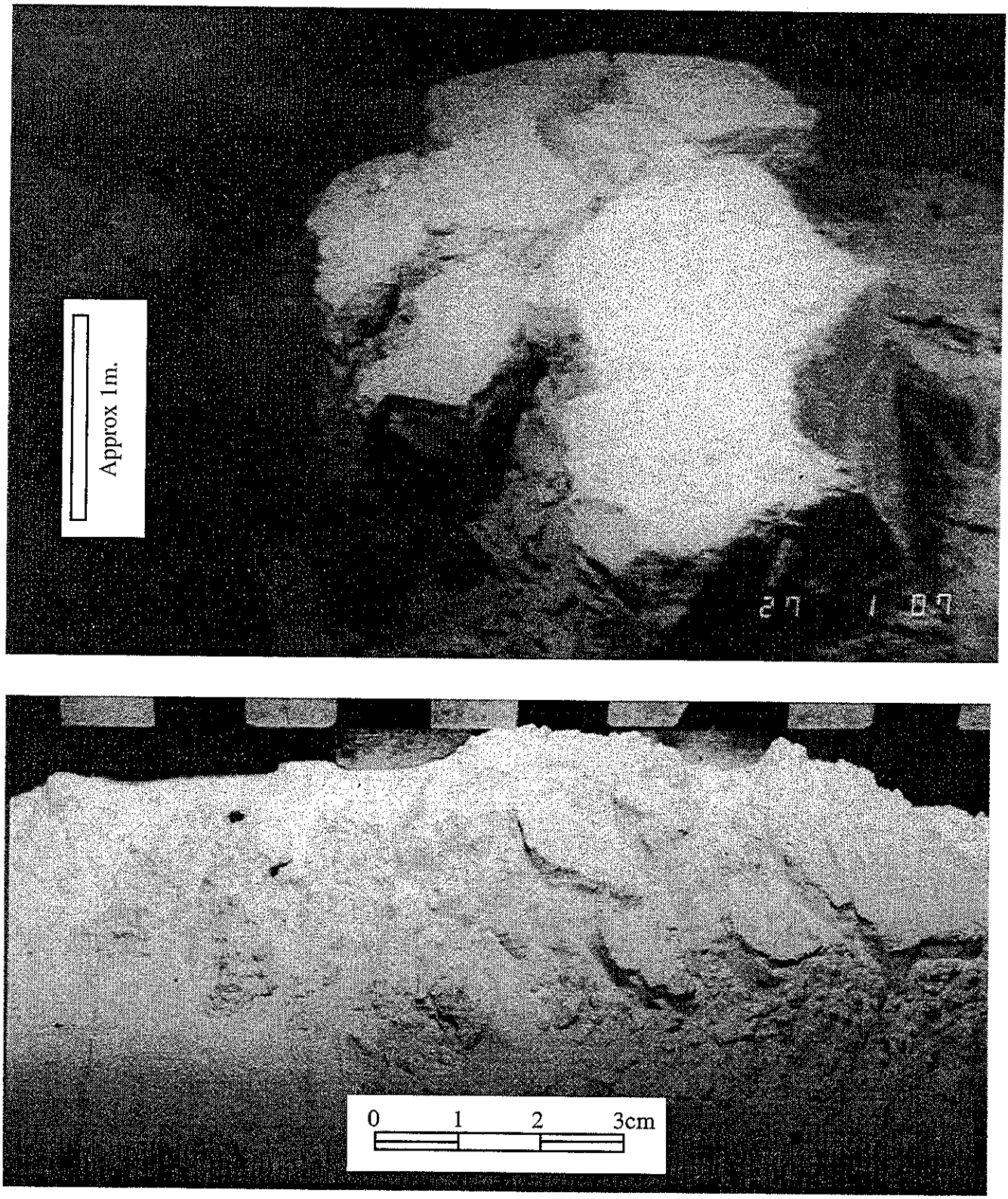

Figure 3. **Top**: Block of cohesive silt on the berm crest of a fresh iceberg scour mark. **Bottom:** Vertical view of centrifuge model scour mark showing fractured clay blocks resting on less cohesive material. The loose clay probably originated from lateral displacement of the leading edge surcharge mound. Outer berm is at the bottom of the picture.

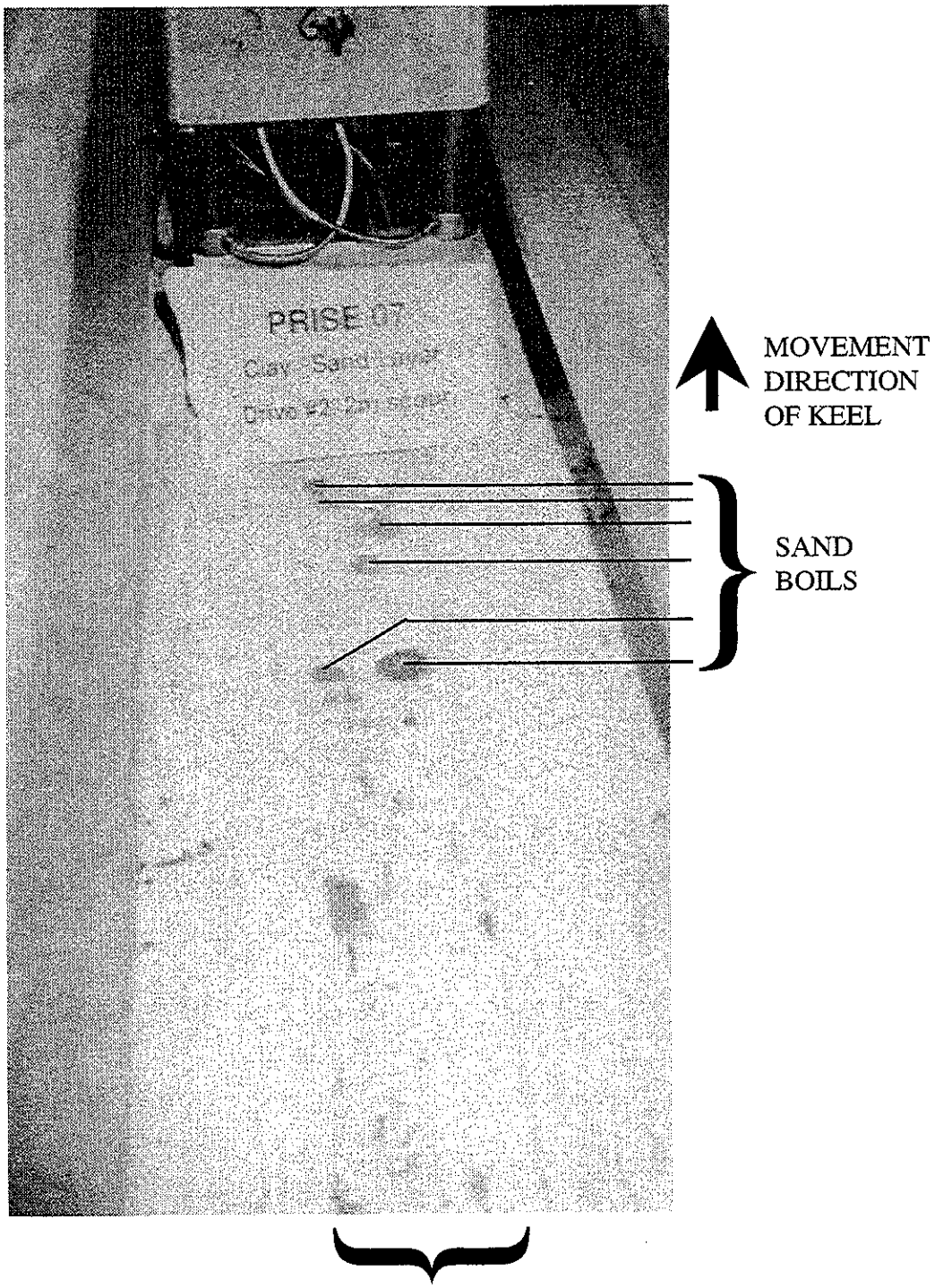

Figure 4. Oblique view of centrifuge model PRISE 07, Drive 2 showing sand boils of blue dyed sand resting above white clay in the scour mark trough. Each boil is characteristically circular and with a central vent through which liquefied sand is extruded. Patches of blue sand elsewhere in the trough probably originated from a pit excavated at the start of the scour mark. This pit was excavated so that, before the scour event, the base of the keel was below the clay surface. Sand from the excavation was dragged forward and deposited from beneath the scouring keel.

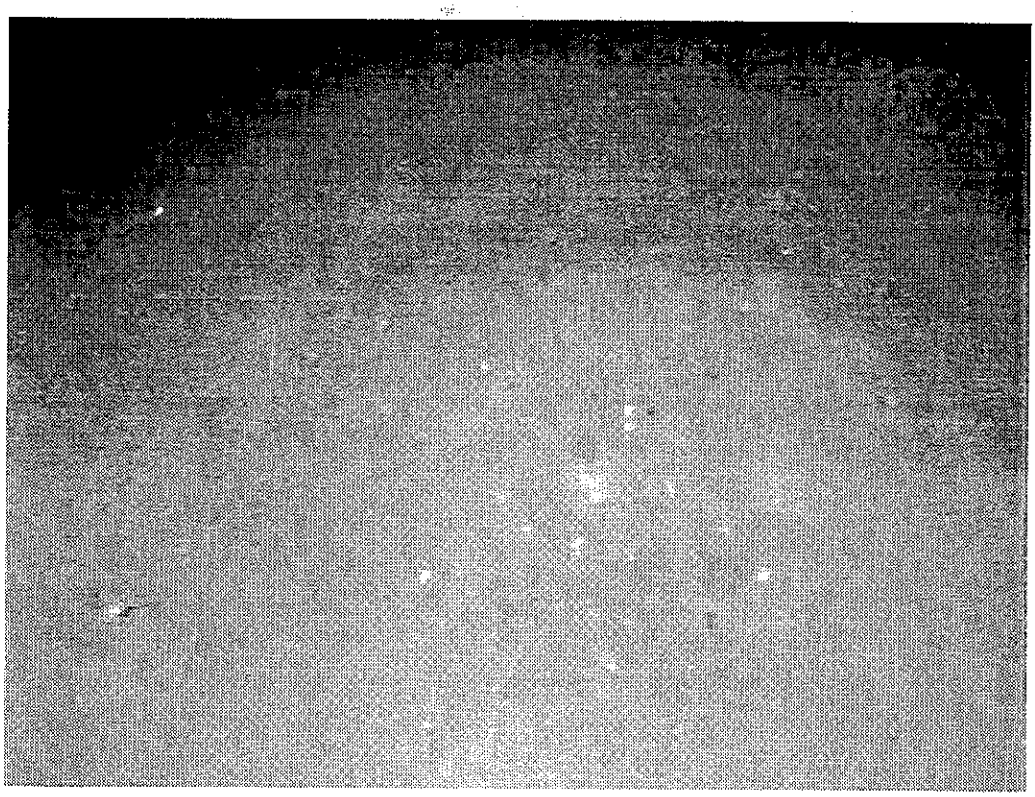

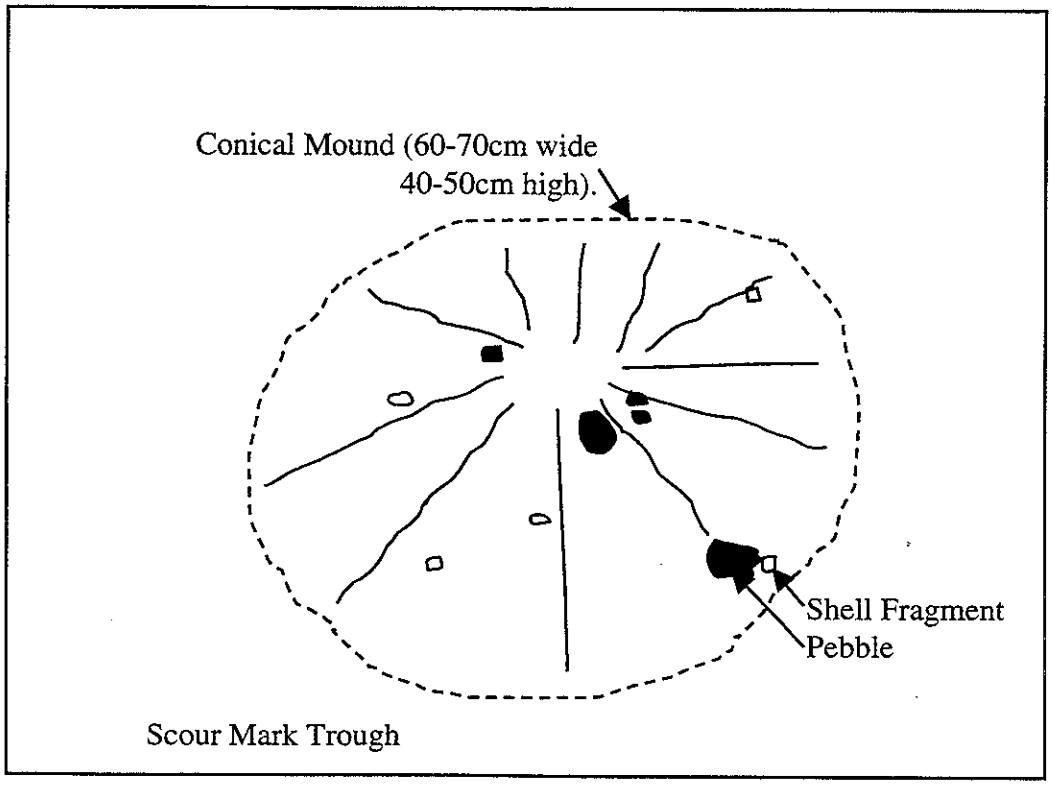

Figure 5. Conical mound in the trough of a fresh iceberg scour mark. The mound consists of loose soil of different colour and texture than the consolidated soil of the scour mark trough, and includes pieces of borken shell and small pebbles. Although no central vent can be seen it is interpretted that this mound, and others (see Figure 6) are of sedimentary extrusive origin related to scour-induced sub-scour liquefaction.

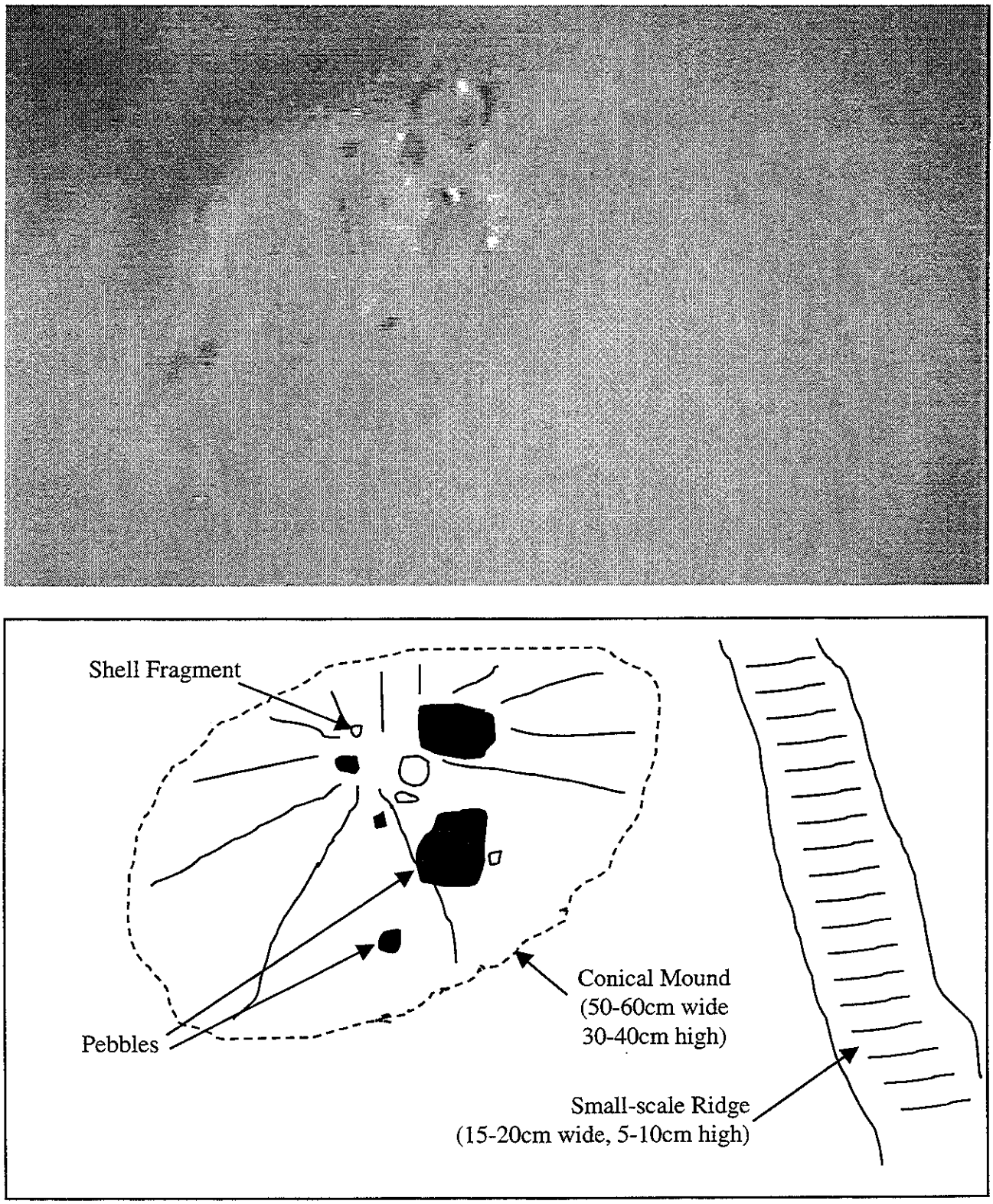

Figure 6. Conical mound in the trough of the same fresh iceberg scour mark as the one shown in Figure 5.

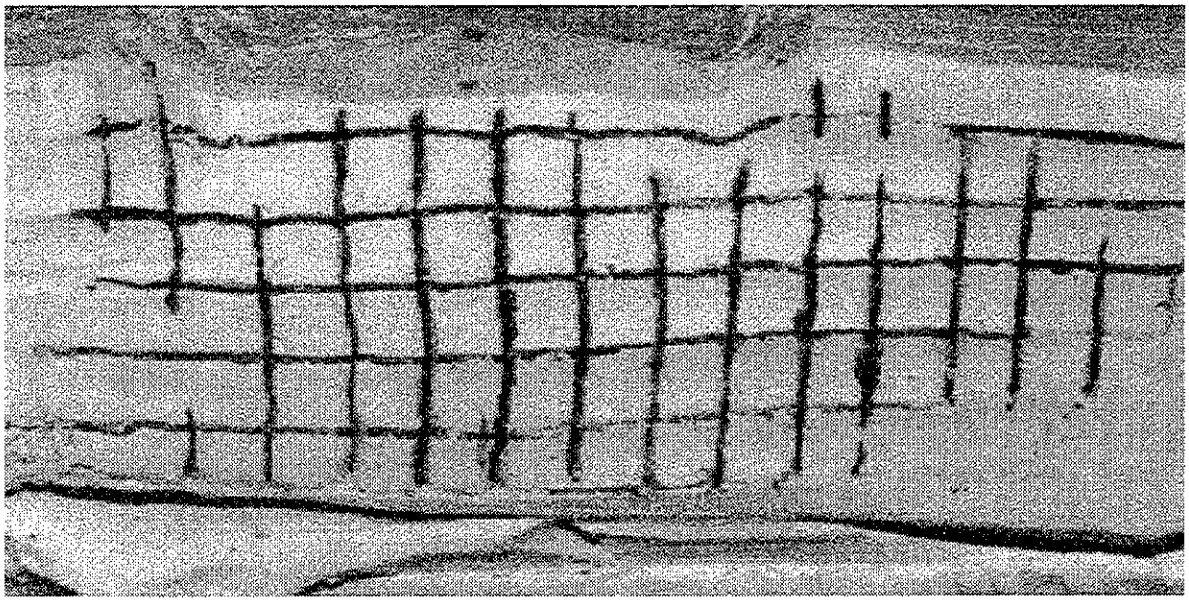

PRISE 03, Aug 25, 1994
Medium CLAY
150g Scour Depth 2m
Width 15m, Keel angle 15 deg.

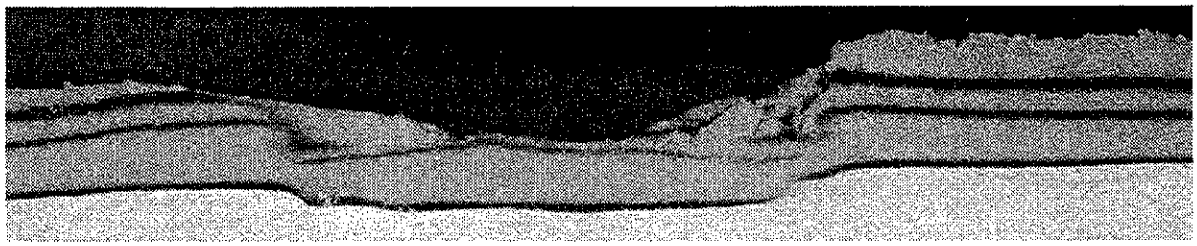

PRISE 08, Drive 2
SAND over CLAY
150g Scour Depth 2m
Width 15m, Keel angle 15 deg.

Figure 7. Downward-displaced markers are evidence of bearing capacity failure beneath the scour mark troughs of a clay model (PRISE 03) and sand-over-clay model (PRISE 08).

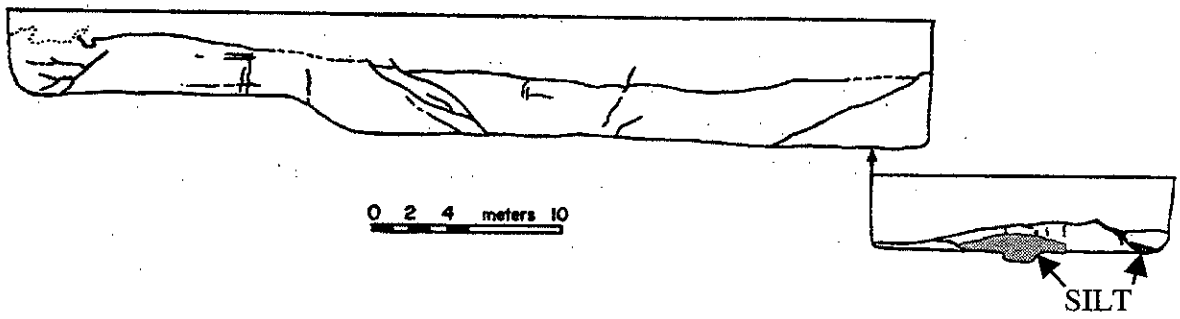

Scour Mark B

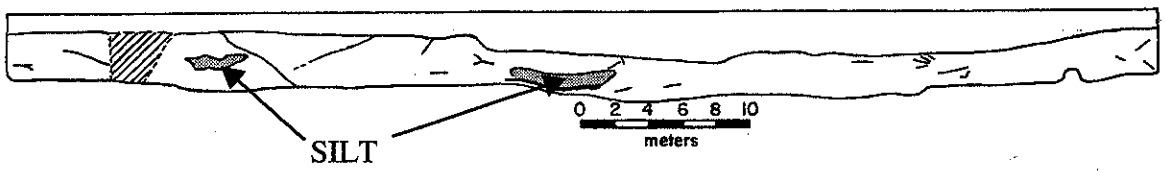

Scour Mark D

Figure 8. Cross-sections (to scale) of scour marks B and D (Manitoba). Thrust faults mark the contact between clay and underlying lenses of silt in the sub-scour soils of both features. It is interpreted that clay slabs were thrust forward and up over a pre-existing surface silt layer. The clay slabs and silt were subsequently overridden by the scouring ice keel and pressed into the lakebed, so that no silt lenses are stratigraphically lower than the original base of the silt unit.

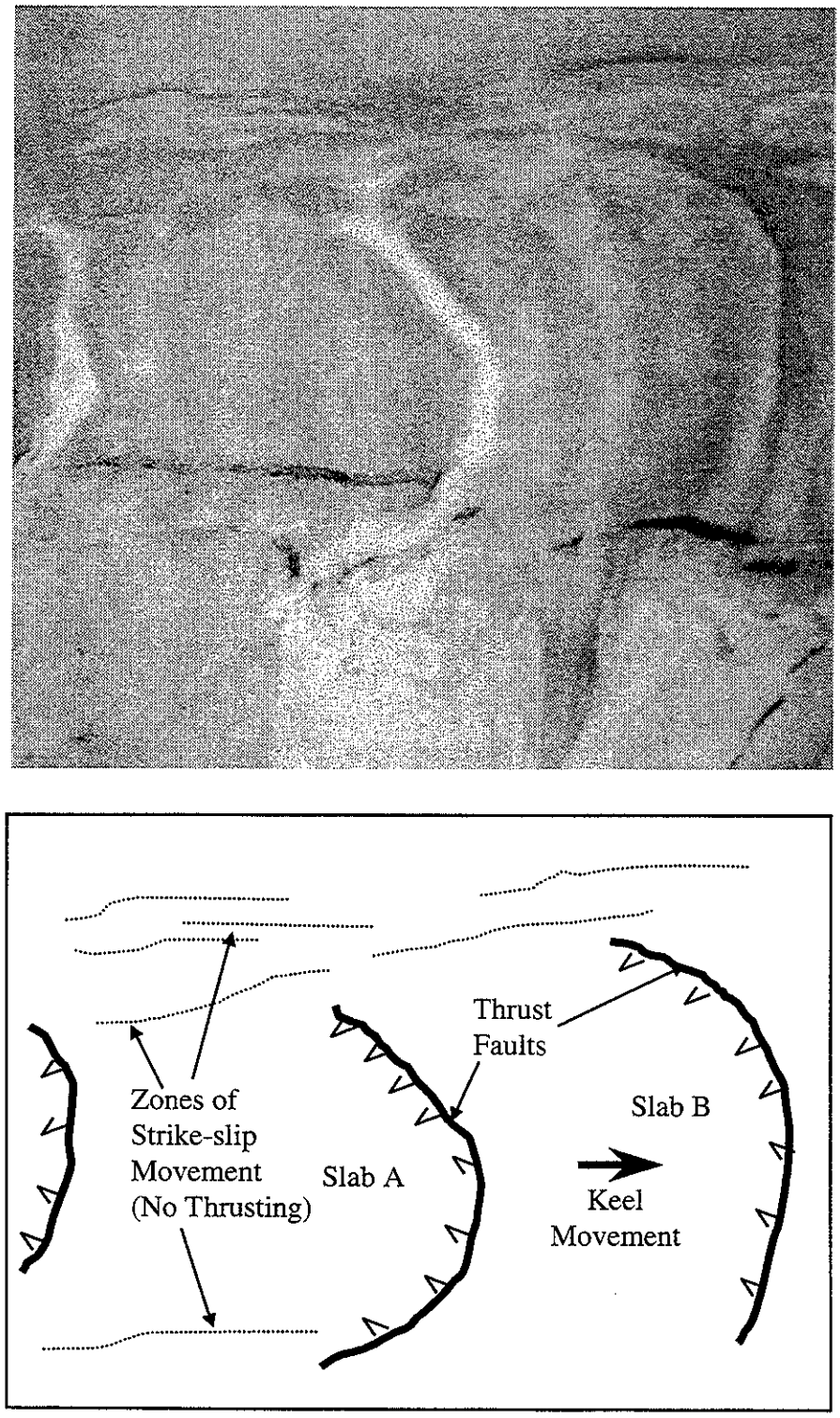

Figure 9. Plan view of PRISE 08, after removal of the sand layer, showing the deformed clay surface that has been pulled forward by shear-dragging to form these three distinct thrust slabs, the leading edges of which are defined by single, prominent thrust faults. Photograph (**Top**) and interpretation (**Bottom**) of the scour-deformed clay surface.

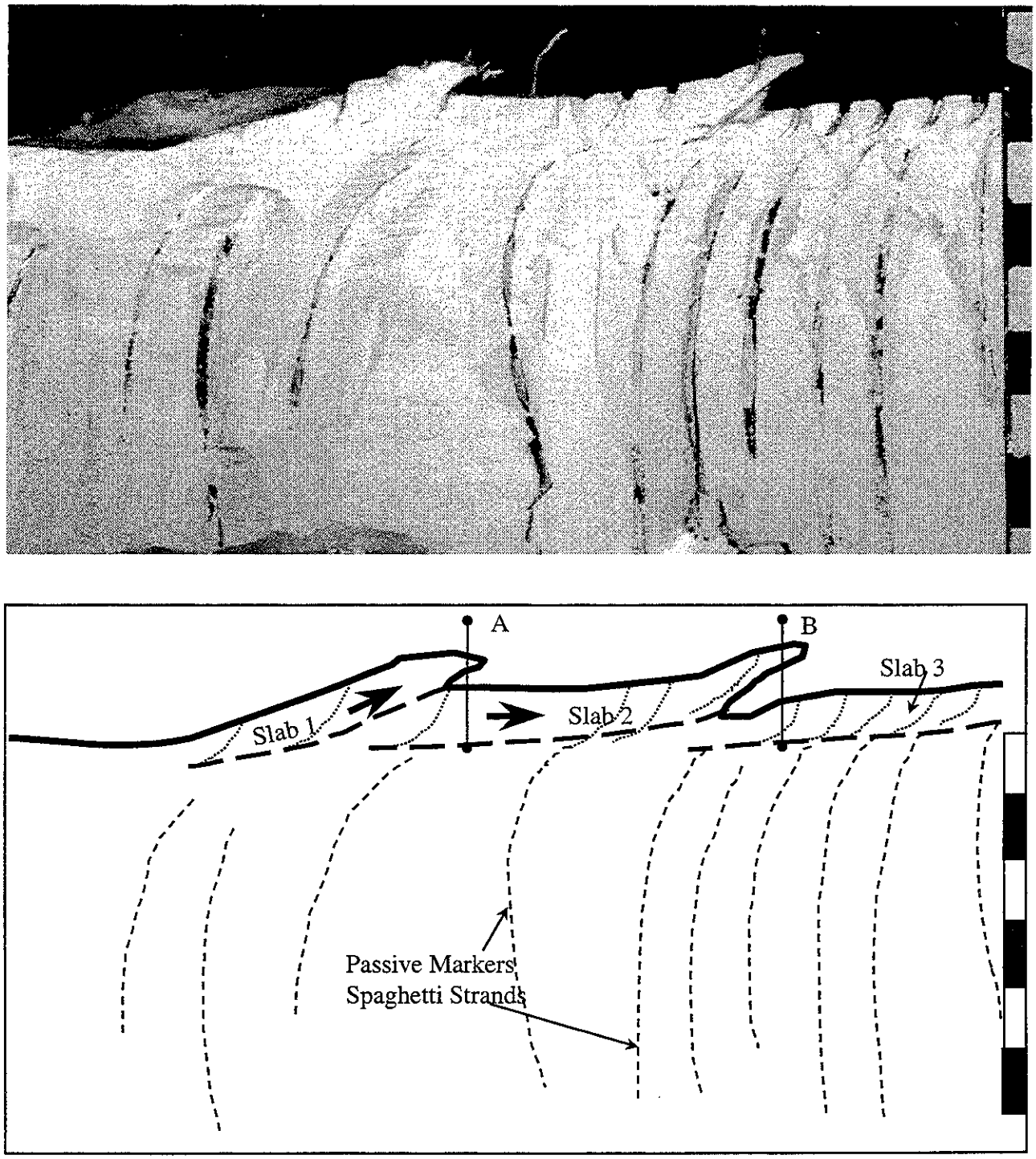

Figure 10. Vertical dissection of the clay along the sour mark centreline of the PRISE 08 model showing the stacked clay slab and sense of displacement. Measuring the horizontal distance between the nose of each thrust slab to where the basal thrust dips below the clay/sand surface it can be shown that Slab 1 has been thrust forward by 1.5m (1cm) and Slab 2 by 2.25m (1.5cm) Photograph of the centreline section (**Top**) and interpretation of structure (**Bottom**). Long dash lines trace approximately the thrust faults.